

1 Reconciling the total carbon budget for boreal forest wildfire emissions using airborne
2 observations

3
4 Katherine L. Hayden^{1*}, Shao-Meng Li², John Liggio¹, Michael J. Wheeler¹, Jeremy J.B. Wentzell¹, Amy
5 Leithead¹, Peter Brickell¹, Richard L. Mittermeier¹, Zachary Oldham^{1,6}, Cris Mihele¹, Ralf M. Staebler¹,
6 Samar G. Moussa¹, Andrea Darlington¹, Mengistu Wolde³, Daniel Thompson⁴, Jack Chen¹, Debora
7 Griffin¹, Ellen Eckert¹, Jenna C. Ditto⁵, Megan He⁵ and Drew R. Gentner⁵

8 [1]{Air Quality Research Division, Environment Canada, Toronto, ON, Canada}
9 [2]{College of Environmental Sciences and Engineering, Peking University, Beijing, China}
10 [3]{National Research Council of Canada, Ottawa, ON, Canada}
11 [4]{Canadian Forest Service, Natural Resources Canada, Edmonton, AB, Canada}
12 [5]{Yale University, New Haven, CT, USA}
13 [6]{University of Waterloo, Waterloo, ON, Canada}

14
15 *Correspondence to: Katherine Hayden (katherine.hayden@ec.gc.ca)
16

17 **Abstract**

18 Wildfire impacts on air quality and climate are expected to be exacerbated by climate change with the
19 most pronounced impacts in the boreal biome. Despite the large geographic coverage, there is limited
20 information on boreal forest wildfire emissions, particularly for organic compounds, which are critical
21 inputs for air quality model predictions of downwind impacts. In this study, airborne measurements of
22 193 compounds from 15 instruments, including 173 non-methane organics compounds (NMOG), were
23 used to provide the most detailed characterization, to date, of boreal forest wildfire emissions. Highly
24 speciated measurements showed a large diversity of chemical classes highlighting the complexity of
25 emissions. Using measurements of the total NMOG carbon (NMOG_T), the ΣNMOG was found to be
26 50±3 to 53±3 % of NMOG_T, of which, the intermediate- and semi-volatile organic compounds (I/SVOCs)
27 were estimated to account for 7 to 10 %. These estimates of I/SVOC emission factors expand the
28 volatility range of NMOG typically reported. Despite extensive speciation, a substantial portion of
29 NMOG_T remained unidentified (47±15 to 50±15 %), with expected contributions from more highly-

30 functionalized VOCs and I/SVOCs. The emission factors derived in this study improve wildfire chemical
31 speciation profiles and are especially relevant for air quality modelling of boreal forest wildfires. These
32 aircraft-derived emission estimates were further linked with those derived from satellite observations
33 demonstrating their combined value in assessing variability in modelled emissions. These results
34 contribute to the verification and improvement of models that are essential for reliable predictions of
35 near-source and downwind pollution resulting from boreal forest wildfires.

36

37

38

39

40

41

42 **1 Introduction**

43 Wildfires play a natural role in maintaining forest health and diversity through the release of
44 nutrients, seed germination, removal of aging vegetation, and reducing the spread of forest diseases.
45 Wildfires are, however, one of the largest global sources of trace gases and aerosols to the atmosphere
46 (Andreae, 2019; Yu et al., 2019) and can have deleterious impacts on human health (Cascio, 2018; Cherry
47 and Haynes, 2017; Reid et al., 2016; Finlay et al., 2012), air quality (Landis et al., 2018; Miller et al.,
48 2011; Rogers et al., 2020), ecosystems (Kou-Giesbrecht et al., 2019; Campos et al., 2019; Kallenborn et
49 al., 2012; Johnstone et al., 2010) and climate (Randerson et al., 2006). Not only can wildfire pollutants
50 fumigate local source areas, they can be transported over long distances resulting in degraded air quality
51 in locations far from fire sources (Miller et al., 2011; Rogers et al., 2020), and pose threats to downwind
52 ecosystems through wet and dry deposition processes (Kou-Giesbrecht et al., 2019; Kallenborn et al.,
53 2012; Campos et al., 2019).

54 The severity and frequency of wildfires is expected to increase in response to climate change
55 (Bush and Lemmen, 2019; Seidl et al., 2017; Whitman et al., 2019) with evidence to suggest that such
56 impacts are expected to be most pronounced in the boreal biome (Seidl et al., 2017; Whitman et al.,
57 2019). The boreal forest zone is the most northerly of all forest biomes accounting for 1.2 billion ha of
58 mostly coniferous forest and comprising about 33 % of the global forest area, or 14 % of the earth's land
59 surface ([https://www.nrcan.gc.ca/our-natural-resources/forests/sustainable-forest-management/boreal-](https://www.nrcan.gc.ca/our-natural-resources/forests/sustainable-forest-management/boreal-forest/8-facts-about-canadas-boreal-forest/17394)
60 [forest/8-facts-about-canadas-boreal-forest/17394](https://www.nrcan.gc.ca/our-natural-resources/forests/sustainable-forest-management/boreal-forest/8-facts-about-canadas-boreal-forest/17394)). On a global basis, boreal forest wildfires are
61 responsible for an estimated 20 % of yearly global biomass burning emissions (van der Werf et al., 2006).
62 Canada's boreal forests account for ~28 % of the global boreal zone area and encompasses 75 % of
63 Canada's 347 million ha of forested land (Fig. S1) ([https://www.nrcan.gc.ca/our-natural-](https://www.nrcan.gc.ca/our-natural-resources/forests/sustainable-forest-management/boreal-forest/8-facts-about-canadas-boreal-forest/17394)
64 [resources/forests/sustainable-forest-management/boreal-forest/8-facts-about-canadas-boreal-forest/17394](https://www.nrcan.gc.ca/our-natural-resources/forests/sustainable-forest-management/boreal-forest/8-facts-about-canadas-boreal-forest/17394)).
65 In the past decade, Canada has experienced unprecedented fire seasons, with large numbers of
66 evacuations, major property damage, poor air quality and significant economic impacts (NRCan, 2018;

67 Landis et al., 2018; McGee et al., 2015). Model predictions have suggested that Canadian fire
68 occurrences will increase by 25 % by 2030 from a 1975 to 1990 baseline scenario (Wotton et al., 2010).

69 To adequately assess and mitigate the risks of wildfire emissions to human and ecosystem health,
70 reliable pollutant predictions are required which depend on accurate and detailed fire emissions data.
71 Such emissions data are developed by multiplying emission factors with the mass of biomass burned
72 (Chen et al., 2019). In Canada, Environment and Climate Change Canada (ECCC) provides predictions
73 of particulate matter (PM) (<2.5 μm in diameter) from wildfire smoke to the public using the FireWork
74 modelling system that combines forecast meteorology, emissions inputs (e.g. emission factors), forest fire
75 and fuel data (e.g. fuel maps, plume height parameterization), and a regional air quality model, GEM-
76 MACH (details in Chen et al., 2019). FireWork is also used for air quality research studies with
77 significantly more complex chemical mechanisms for emissions characterization and detailed physical
78 processes. Wildfire field studies, as well as prescribed burns and laboratory work, have resulted in
79 valuable global databases of fire emission factors covering a broad range of ecosystems and geographic
80 areas (e.g. Andreae, 2019; Akagi et al., 2011), however, they are primarily concentrated on the temperate
81 forests of the American mid-west and savannah/grasslands of Africa (e.g. Andreae 2019; Permar et al.,
82 2021; Palm et al., 2020; Lindaas et al., 2020; Roberts et al., 2020; Juncosa-Calaharrano et al., 2021;
83 Coggon et al., 2019; Koss et al., 2018; Hatch et al., 2017). Until now, the most complete characterization
84 of boreal forest wildfire emissions in Canada was provided by Simpson et al. (2011) which relied on
85 whole air canisters with offline analysis for organic compounds. Due to limited comprehensive emission
86 data specific for boreal wildfires, air quality models for northern regions face significant challenges
87 resulting in uncertain predictions of emissions, exposure and associated impacts.

88 In the summer 2018, a research aircraft was deployed to measure emissions and subsequent
89 transformation processes from a boreal forest wildfire in western Canada (Fig. 1; Fig. S1). In this paper,
90 measurements of a comprehensive suite of gas- and particle-phase compounds are used to provide a
91 detailed characterization of smoldering wildfire emissions. The highly speciated non-methane organic
92 gas (NMOG) measurements are described by broad chemical classes and across a range of volatilities

93 extending from VOCs to SVOCs. The wide range of measured NMOGs, along with concurrent total
94 NMOG carbon (NMOG_T) measurements, provides a unique opportunity to reconcile the total carbon
95 budget. Emission factors are derived for 193 compounds which represents the most extensive chemical
96 speciation of wildfire emissions to date, almost tripling the number of reported values for the boreal forest
97 ecosystem in the Andreae (2019) compilation paper. Emission estimates are also combined with those
98 from satellite observations to evaluate modelled diurnal variability. The purpose of this work is to
99 provide relevant emissions information for boreal forest wildfires to ultimately contribute towards
100 improved emissions quantification and chemical speciation representations in air quality models.

101

102 **2 Methods**

103 **2.1 Aircraft measurements**

104 The NRC's Convair-580 research aircraft was deployed on June 25, 2018 to sample a wildfire
105 detected to the east of the Alberta/Saskatchewan border (56.4°N, 109.7°W) (Fig. 1). Measurements of a
106 comprehensive suite of trace gases, particles and meteorology were made with high time resolution.
107 Meteorological measurements including relative humidity, temperature, wind direction and speed, as well
108 as aircraft state parameters such as altitude (masl) and geographic coordinates were conducted at 1 sec
109 time resolution. A detailed description of the various measurement methods with references is provided
110 in the supporting information (SI Sect. 1.1, Table S1, S2), with only a brief description provided here.

111 **2.1.1 Trace gas measurements** In-situ measurements of NO, NO₂, NO_y, O₃ and SO₂ were conducted
112 using commercial instruments (Thermo Scientific Inc.) modified to measure at 1 sec time resolution.
113 Ammonia (NH₃) measurements were made at 1 sec time resolution using a Los Gatos Research (LGR)
114 NH₃/H₂S Analyzer, model 911-0039. Gas phase elemental Hg (GEM) was measured with a Tekran
115 237X instrument (Tekran Instruments Corporation) modified to allow a reduced sampling time of 2 min
116 (McLagan et al., 2021; Cole et al., 2014). CO, CO₂ and CH₄ were measured with a Cavity Ring Down
117 spectroscopy instrument (Picarro G2401-m). A second Picarro G2401-m instrument was used to measure
118 Total Carbon (TC, in units of ppm C) by passing the sample air through a catalyst to convert all carbon

119 species to CO₂. Total non-methane organic gases (NMOG_T), in mixing ratios units of ppm C, was
120 quantified by subtracting the ambient CH₄, CO and CO₂ measurements (instrument without the catalyst)
121 from the TC measurements (see SI Methods for more details).

122 Individually speciated NMOGs (as well as some inorganic species) were measured with a
123 Chemical Ionization Mass Spectrometer (CIMS), a Proton Transfer Time-of-Flight Mass Spectrometer
124 (PTRMS), and through whole air sampling using canisters (Advanced Whole Air Sampler; AWAS). In
125 addition, integrated cartridge-based samples were taken. The CIMS (a modified ToFwerk/Aerodyne Api-
126 ToF) was operated using iodide as the reagent ion providing 1 sec time resolved measurements for 30
127 compounds (Table S2). The PTRMS (Ionicon Analytik GmbH, Austria) used chemical ionization with
128 H₃O⁺ as the primary reagent ion providing 1 sec measurements for a suite of organic compounds. For
129 those compounds with no available gas standard, a relative response factor was calculated with reaction
130 rate constants using the method described in Sekimoto et al. (2017) and guided by the work of Koss et al.
131 (2018) ('calculated' compounds). Integrated 'grab' samples (20-30 sec) were collected from the aircraft
132 using the Advanced Whole Air Sampler (AWAS) with offline analysis. The AWAS provided speciated
133 measurements of hydrocarbons (≤C₁₀), but no oxygenates. Overlapping compounds/isomers that were
134 measured by both the PTRMS and AWAS, as well as between the PTRMS and CIMS, were handled as
135 described in SI Sect. 1.1.4. Integrated gas phase samples were collected using an automated adsorbent
136 tube (i.e. cartridge) sampling assembly with offline analysis (Ditto et al., 2021; Sheu et al., 2018; Khare et
137 al., 2019). These samples provided targeted measurements of gas-phase compounds ranging in volatility
138 from C₁₀ volatile organic compounds (VOCs) to C₂₅ semivolatile organic compounds (SVOCs) including
139 hydrocarbons (CH), and functionalized compounds containing 1 oxygen atom (CHO₁), and 1 sulfur atom
140 (CHS₁).

141 **2.1.2 Particle measurements**

142 Particle chemistry was obtained with a high resolution aerosol mass spectrometer (AMS)
143 (Aerodyne) providing mass concentrations of particle species including total organics (OA), NO₃, SO₄
144 and NH₄ for particles less than ~1 μm. Particle size distributions were measured between 60 and 1000

145 nm at 1 sec time resolution using the Ultra High Sensitivity Aerosol Spectrometer (UHSAS; Droplet
146 Measurement Technologies). Refractory black carbon (rBC) was measured using a single particle soot
147 photometer (SP2; Droplet Measurement Technologies).

148

149 **2.2 Flight and fire description**

150 A wildfire located near Lac La Loche in Saskatchewan (56.40°N 109.90°W) was detected by
151 satellite on June 23 (Fig. 1; Fig. S1). The fire was ignited by lightning on June 23, 2018 at 19:45 UTC
152 and lasted 50 hrs to June 25 21:41 UTC burning an estimated 10,000 ha before being extinguished by
153 rain. The area burned was mostly mature Jack pine and boreal spruce forest with a smaller fraction of
154 boreal mixed-wood forest. Satellite images from the VIIRS spectroradiometer on the Suomi NPP and
155 NOAA-20 satellites taken on June 25 showed merged fire hot spots with a visible smoke plume moving
156 in a north-westerly direction (Fig. 1; see SI Sect. 2.0 for more details). Lagrangian flight tracks were
157 flown downwind of the wildfire to follow the fire plumes. Multiple horizontal transects, vertically
158 stacked and perpendicular to the plume direction were made at different altitudes from 640 to 1460 m asl
159 (~220 – 1040 m agl, based on 420 m asl at Lac La Loche) forming virtual screens. Five screens were
160 completed over two flights with the closest screen ~10 km and the farthest screen 164 km downwind of
161 the fire, with the screens spaced such that the instruments sampled the same air parcels as they were
162 transported downwind. A vertical profile which typically reached ~2500 m asl was conducted in the
163 plume at each screen to gather information on its vertical structure and the height of the plume. As
164 demonstrated by the elevated CO mixing ratios in Fig. 2, two distinct plumes were identified - a south
165 plume (SP) and north plume (NP), that were transported in parallel in a northwesterly direction. The SP
166 is estimated to be ~42 min old based on the measured wind speed at Screen 1 and the distance from the
167 closest edge of the VIIRS fire hot spots (~10 km). The NP is estimated to be an additional 30 min older
168 than the SP (further details in SI Sect. 2.0). For the purposes of this investigation, only data from Screen
169 1 are used to characterize the direct emissions from this fire. There were no significant anthropogenic
170 sources like upwind urban or industrial areas, impacting the Screen 1 measurements. Plume evolution

171 during transport from Screen 1 to downwind Screens 2 to 5 is discussed in other papers (Ditto et al., 2021;
172 McLagan et al., 2021).

173

174 **2.3 Emission ratios**

175 Emission ratios (ERs) were calculated using an integration method (e.g. Yokelson et al., 2009;
176 Garofalo et al., 2019) using the in-plume measurements for the SP and NP. The integration method was
177 carried out for the real-time measurements by first subtracting a background from the in-plume
178 measurements. Background measurements were defined as the average over short time segments (~30
179 sec) outside and at the same altitude as inside the plume, and typically selected at the ends of the
180 horizontal transects. The background-subtracted plume measurements yielded enhanced plume values
181 (e.g. $\Delta X(t)$) which were then integrated using the plume start and end times guided by when CO mixing
182 ratios were above the CO background. Nominal plume time periods are indicated by the vertical grey
183 bars in Fig. 3 which shows time series for CO, NMOG, OA and acetonitrile for the first 4 of 5 transects
184 on Screen 1. Integrated pollutant values were subsequently normalized by the integrated values of CO
185 (Eq. 1) to account for changes due to dilution producing emission ratios (ER) for the SP and NP for each
186 transect on Screen 1.

187

$$188 \quad ER = \frac{\int_{start}^{end} \Delta X(t) (dt)}{\int_{start}^{end} \Delta CO(t) (dt)} \quad (1)$$

189

190 CO is known to be a suitable dilution tracer as it has a long atmospheric lifetime of 1-4 months (Seinfeld
191 and Pandis, 1998), is unreactive on the time scale of the measurements. In this study, ERs were
192 calculated using CO as it was enhanced above a background of $\sim 0.119 \pm 0.005$ ppmv for the plumes
193 measured, there were no other significant CO sources in the study area, and CO is a particularly good
194 tracer for smoldering fires (e.g. Simpson et al., 2011).

195 ERs for the AWAS compounds were determined using the average mixing ratio of 3 samples
 196 taken in the SP and two in the NP, and the average mixing ratio of two background samples. CO mixing
 197 ratios were averaged across the AWAS sample time period. For the integrated cartridges, samples were
 198 collected over the lower set of aircraft transects ('LOW') and higher set of transects ('HIGH'), resulting
 199 in two integrated cartridge samples for each screen. The HIGH sample was used as the background. The
 200 HIGH sample was collected largely outside the wildfire plume, but may have been influenced to some
 201 extent from emissions. However, this impact is expected to be minimal as average CO mixing ratios
 202 during the HIGH sample were at background levels (~0.14 ppmv). Nevertheless, to address the potential
 203 for influence of the plume in the HIGH sample, the ERs are presented as ranges with the lower estimates
 204 derived by subtracting the HIGH background sample, and the upper estimates without subtracting the
 205 HIGH sample. This calculation is described in Eq. 2 where $Cartridge_{LOW}$ represents the LOW cartridge
 206 sample measurements, $Cartridge_{BKGD}$ is the background derived from the HIGH cartridge sample
 207 measurements, and CO_{LOW} , CO_{BKGD} are the average CO concentrations during the respective LOW and
 208 HIGH cartridge integration time periods. The uncertainty with this bounding analysis is acknowledged,
 209 but the I/SVOCs ERs within a plume are likely to vary similar to other work (Hatch et al., 2018).

$$210 \quad ER = \frac{Cartridge_{LOW} - Cartridge_{BKGD}}{CO_{LOW} - CO_{BKGD}} \quad to \quad \frac{Cartridge_{LOW} - 0}{CO_{LOW} - CO_{BKGD}} \quad (2)$$

211

212 **2.4 Emission factors**

213 Emission factors (EFs) were determined as the mass of species X emitted per unit mass of dry
 214 fuel burned in $g \text{ kg}^{-1}$ assuming that all of the carbon in the fuel was released into the atmosphere and
 215 measured (Ward and Radke, 1993; Yokelson et al., 2007), and that the mass fraction of carbon in the fuel
 216 is constant. EFs were determined using Eq. 3 where F_c is the mass fraction of carbon in the fuel and
 217 estimated to be 0.5 (de Groot et al., 2009 and references therein), mm_x is the molar mass of the compound
 218 of interest, and mm_c is the molar mass of carbon, 12 g mol^{-1} , ΔX is the integrated background-subtracted
 219 mixing ratio or concentration of the species of interest, ΔTC is the integrated background-subtracted TC.

220 TC (see Sect. 2.1.1) was directly measured and includes all the carbon mass in CO₂, CO, CH₄, and
221 NMOG_T, as well as that from particulate black carbon (rBC) and particulate organic carbon (OC) (which
222 were added to the TC), for a complete accounting of all the emitted carbon. For species measured in mass
223 concentration units, Eq. 3 was modified by converting TC to mass concentrations using the measured
224 temperature and pressure, and removing the molar mass ratio term. The EFs for the AWAS and the
225 cartridge samples were derived using the average measurements as discussed for the ER, but with TC as
226 the denominator.

227

$$228 \quad EF \left(\frac{g}{kg} \right) = F_c \times 1000 \left(\frac{g}{kg} \right) \times \frac{mm_X}{mm_C} \times \frac{\int_{start}^{end} \Delta X(t) (dt)}{\int_{start}^{end} \Delta TC(t) (dt)} \quad (3)$$

229

230 EFs were determined for the SP and NP for each transect, and then averaged to obtain screen-averaged
231 EFs for the SP and the NP, as well as for both plumes together.

232 **2.5 Emissions Uncertainties**

233 There is the potential for inherent uncertainties using a plume integration method for calculating
234 EFs and ERs as the ratios derived this way represent the average plume composition and ignore the
235 spatial heterogeneity in wildfire plumes (Palm et al., 2021; Decker et al., 2021; Garofalo et al., 2019),
236 chemical transformation processes, and can also be affected by changing background levels. Pollutants
237 released by wildfires can be influenced by photochemical and physical changes that may take place
238 between the time of emission and the time of measurement, particularly for more reactive compounds
239 (e.g. Palm et al., 2021; Lindaas et al., 2020; Peng et al., 2020; Akagi et al., 2011). Although controlled
240 laboratory studies are well suited to examine direct emissions with minimal aging, they cannot reproduce
241 realistic burning conditions. Field measurements are critical to understand emissions that are impacted by
242 factors such as complex burning dynamics, fuel moisture, temperature and winds (Andreae 2019).
243 Recognizing the challenges of measuring primary emissions by aircraft, at 10 km (<1 hr) away from the

244 fire source, Screen 1 measurements represent some of the freshest emissions measured under wildfire
245 conditions, thus providing best estimates of initial conditions.

246 Uncertainties in the EFs and ERs are estimated by summing in quadrature the standard error of
247 the average EF (or ER) and the propagated measurement uncertainties. The standard error is used as
248 description of the uncertainty on the average EF (and ER) characterizing repeated transects across the SP
249 and NP for a total of 20 min of in-plume sampling. The standard error is expected to at least partially
250 capture uncertainties associated with plume aging and vertical plume heterogeneity. As many compounds
251 exhibited significant in-plume enhancements above background levels, uncertainties in the integrated ΔX ,
252 ΔCO and ΔTC values were assumed to be dominated by instrumental (measurement) uncertainties (Table
253 S1, S2). Emissions are not reported for compounds where the average mixing ratios were within 1σ of
254 the background average. The low and high I/SVOCs EFs (and ERs) are provided as estimates of their
255 uncertainties (as described in Sect. 2.3). The derivation of AWAS and cartridge EFs (and ERs) may have
256 potential limitations as they rely on a limited number of samples, with the potential of the AWAS discrete
257 samples capturing only part of a plume.

258 **2.6 Combustion efficiency**

259 Combustion efficiency (CE) is a useful indicator of the relative proportion of flaming vs
260 smoldering stages of combustion which has a significant influence on the chemical composition of the
261 smoke (see SI Sect. 3.0 for further details). Flaming fires have $CE > 0.90$ (Yokelson et al., 1996) and
262 smoldering fires are typically ~ 0.8 with a range of 0.65 to 0.85 reported in the literature (Akagi et al.,
263 2011; Yokelson et al., 2003). A modified combustion efficiency (MCE) is commonly calculated
264 assuming that $CO_2 + CO$ adequately represents all of the fuel carbon that has been volatilized and detected
265 in ambient air. Here, as the TC in the plume was directly measured, ΔTC was used in Eq. 4 to improve
266 on the estimation of the CE by accounting for all the sources of carbon. ΔCO_2 and ΔTC in Eq. 4 are the
267 integrated, background-subtracted mixing ratios.

268

269 $CE = \frac{\Delta CO_2}{\Delta TC}$ (4)

270

271 **3 Results and Discussion**

272 **3.1 Fire combustion state**

273 The plume-averaged CE for the SP (transects 1 to 4) was 0.84 ± 0.04 and for the NP (transects 1 to
274 3) 0.82 ± 0.01 . Transect 4 was excluded from the calculations for the NP because only a portion of the
275 plume was detectable at this altitude (Fig. 3). The derived CE indicates that the fire was predominantly in
276 a low intensity smoldering phase which is consistent with the satellite-derived fire intensities during the
277 flight (see Fig. 10) and ground-based meteorological observations, and may reflect some residual
278 smoldering combustion (RSC). It is estimated that emissions from this fire were sampled 14 hrs post
279 flaming. Other chemical measurements from this flight also support that the fire was largely smoldering
280 including the detection of elevated $C_2H_4O_2^+$ (levoglucosan fragment from the AMS; Fig. S4), and no
281 detectable K^+ (from the AMS) (Lee et al., 2010). Significant spatial variability in the concentrations of
282 many of the measured species were observed closest to the fire source, while the plumes became more
283 well-mixed as they were transported downwind (Fig. S5). This highlights the complexities of assessing
284 wildfire combustion processes (Ward and Radke, 1993), and in particular, boreal forests have been
285 observed to exhibit greater variability in combustion efficiencies than for other vegetation types
286 (Urbanski et al., 2009).

287 **3.2 General plume features**

288 Table A1 shows mixing ratios (or concentrations) and background levels of 193 pollutants that
289 were enhanced in the fire plumes. The quantification of this suite of compounds provides new and
290 additional emission estimates to those reported in Simpson et al. (2011) and compiled in Andreae (2019)
291 for the boreal forest ecosystem. Several sulphur-containing compounds and a few other VOCs were not
292 detected (Table S6), and although not part of the measurement suite in the present study, Simpson et al.
293 (2011) did not observe emissions of anthropogenic halocarbons from wildfires in the same boreal forest

294 ecosystem. In Fig. 3, the in-plume portions are highlighted by the grey vertical bars and the SP and NP
295 are indicated as the aircraft flew at increasing altitudes to complete five horizontal transects. The lowest 4
296 transects showed enhanced pollutant levels while the 5th transect (not shown) was predominantly above
297 the height of the plumes. Higher concentrations were generally observed in the SP compared to the NP,
298 possibly because of some plume dilution in the NP resulting from a change in wind direction prior to
299 sampling. The SP and NP were distinctly separated from each other, with pollutants typically dropping to
300 background levels between the plumes. NMOG_T mixing ratios varied between background levels of ~375
301 ppbv to near 10 ppmv in-plume. CO and acetonitrile, often used as tracers of biomass burning (e.g.
302 Wiggins et al., 2021; Landis et al., 2018; Simpson et al., 2011; de Gouw et al., 2006), reached 6.6 ppmv
303 and 20 ppbv, respectively in the SP, while maximum OA concentrations reached 276 $\mu\text{g m}^{-3}$, above a
304 background level of $\sim 12.5 \pm 0.83 \mu\text{g m}^{-3}$. OA was the largest contributor to particulate mass (PM)
305 comprising over 90 % of the measured submicron mass with remaining portion comprised of BC, NO₃,
306 NH₄, and SO₄ (Fig. S6). Integrated filter samples taken from the aircraft across Screen 1 also showed the
307 presence of a diverse set of functionalized particle-phase organic compounds (Ditto et al., 2021).

308 The most abundant reactive nitrogen compounds (N_r) were in the forms of reduced nitrogen (79 %)
309 with NH₃ comprising 42 % of ΣN_r (Fig. 4) and substantially lower nitrogen oxides i.e. NO_x < 1 ppbv.
310 Dominant proportions of reduced nitrogen in biomass burning emissions were also reported previously
311 (Lindaas et al., 2020; Burling et al., 2011; Yokelson et al., 1996). Nitrogen-containing organics were
312 detected in the present study totalling 3.9 ppbv and 18 % of ΣN_r (Fig. 4), however, other such compounds
313 that were not included with the instrument suite used in this study were also likely emitted. Such
314 compounds could include organic nitrates, amines, amides, heterocyclic compounds, nitriles and nitro
315 compounds that have been found in biomass burning emissions (Roberts et al., 2020; Lindaas et al., 2020;
316 Andreae 2019; Koss et al., 2018; Tomaz et al., 2018; Stockwell et al., 2015). Alkyl nitrates have been
317 identified in biomass burning emissions, but their contributions to total N_r appeared to be small (Juncosa-
318 Calahorrano et al., 2021; Roberts et al., 2020; Lindaas et al., 2020; Simpson et al., 2011; Alvarado et al.,
319 2010; Singh et al., 2010).

320 3.3 Total carbon budget

321 3.3.1 NMOG chemical classes – PTRMS, CIMS, AWAS

322 In-plume mixing ratios and the relative contribution of individually measured NMOG species to
323 the sum of those species (Σ NMOG) are shown for 13 chemical classes in Fig. 5. (See Fig. S7 for separate
324 SP and NP chemical classes). The largest chemical classes include carbonyls (acids, aldehydes and
325 ketones), alcohols, hydrocarbons (alkanes, alkenes, alkynes), aromatics (including furans, phenol,
326 benzene and toluene), and nitriles. Hydrocarbons (i.e. C_xH_y , including some aromatics) were responsible
327 for just over half of the Σ NMOG (53 %) (Fig. S8), with 29 % identified as alkenes such as ethene,
328 propadiene, and propene, 19 % alkanes, predominantly ethane, and 3 % alkynes, almost entirely
329 acetylene. Non-aromatic oxygenates accounted for an additional 36 % of the Σ NMOG with roughly
330 equal contributions (9 to 12 %) from acids, aldehydes and alcohols, and a smaller fraction from ketones (5
331 %). Including other oxygenated compounds such as furanoids and phenol/phenol derivatives, all
332 oxygenates ($C_xH_yO_z$) comprised 42 % (Fig. S8), of the Σ NMOG.

333 A similar range of compound classes has been observed in previous field and laboratory studies,
334 noting that the measured compound suite between studies varies to some extent. For example, Simpson
335 et al. (2011) found a similar distribution of compound classes with 57 measured NMOG species, based on
336 discrete canister samples, in boreal forest wildfires. In that study, oxygenates (non-aromatic) comprised a
337 smaller portion of NMOG (29 %) as major emitted species like acetaldehyde and acetic acid (Fig. 8) were
338 not included. Other studies have also found oxygenates to be a large portion of NMOG emissions across
339 multiple fuel types, including those similar to the current study, ranging from 51 – 68 % (Permar et al.,
340 2021; Koss et al., 2018; Gilman et al., 2015; Akagi et al., 2011) with a range of 25 – 55 % reported in
341 Hatch et al. (2017). The fraction of NMOG oxygenates in the present study (42 %) was closer to those
342 reported in Hatch et al. (2017) when only the most relevant fuel types of pine and spruce were considered
343 (55 % and 43 %, respectively). Similar to previous work (Koss et al., 2018, Stockwell et al., 2015; Hatch
344 et al., 2015), emissions of substituted oxygenates like furanoids (furans+derivatives) and phenolic
345 compounds were observed. Furanoids contributed 4 % of the Σ NMOG mostly due to furfural, furan and

346 methyl furan while phenolic compounds eg. guaiacol, methyl guaiacol, contributed 0.5 % of the Σ NMOG
347 (Fig. S9). Although these emissions were less abundant in the present study, they represent important OH
348 reactants (Coggon et al., 2019; Koss et al., 2018; Gilman et al., 2015) with phenols being implicated as
349 precursors to brown carbon formation in secondary organic aerosol (SOA) (Palm et al., 2020).

350 Biogenic emissions of terpenoids including isoprene, monoterpenes, carvone, sesquiterpenes,
351 camphor/isomers and terpine-4-ol/cineole/isomers were elevated in the plumes collectively reaching ~2.4
352 ppbv, and contributing ~2 % to the Σ NMOGs (Fig. S9). Isoprene was ~66 % of these compounds with an
353 additional 32 % from monoterpenes. Emissions of isoprene from biomass burning has been observed
354 from a wide range of fuel types (Hatch et al., 2019). As isoprene is not stored by plants and the
355 measurements were taken ~14 hrs post flaming, it was likely emitted as a combustion product.

356 In this study, furfural was the most abundant oxygenated aromatic compound and a factor of 5
357 times higher than that of phenol. Although Koss et al. (2018) found that phenol and furfural emissions
358 were similar for most fuels tested in the laboratory, furfural emissions derived from multiple wildfires
359 sampled in Permar et al. (2021) were similar to those in the present study, and a factor of 1.6 higher for
360 phenol. As phenol emissions are associated with lignin pyrolysis (Stockwell et al., 2015; Simoneit et al.,
361 1999), the lower emissions in the current study could be because the lignin content in the fuel mixture
362 was lower than fuels used in previous laboratory studies or that most of the phenolic compounds were
363 emitted during the earlier phases of the fire. Several modelling studies have indicated that aromatics and
364 terpenes are insufficient to explain SOA formation in biomass burning plumes (e.g. Hodshire et al., 2019)
365 suggesting the importance of inclusion of other aromatic species such as phenolics and furanoid
366 compounds. However, models typically do not include reactions involving phenolic and furanoids
367 species, especially substituted compounds like furfural, guaiacol, and methyl guaiacol. Box model
368 simulations have also shown that incorporation of OH oxidation of furan, 2-methylfuran, 2,5-
369 dimethylfuran, furfural, 5-methylfurfural, and guaiacol, leads to 10 % more O₃ formed (Coggon et al.,
370 2019).

371

372 3.3.2 Intermediate-volatility and semivolatile organic compounds (I/SVOCs)

373 Offline analysis of cartridge samples showed a wider range of hydrocarbons and functionalized
374 gas-phase organic compounds not observed in the PTRMS, CIMS, and AWAS measurements, including
375 I/SVOC compounds in the wildfire plume. ERs (Table S7) for species containing carbon and hydrogen,
376 and with either sulfur or oxygen (i.e. CH (hydrocarbons), CHS₁ and CHO₁ type molecules)) accounted for
377 a sizeable fraction of carbon in the C₁₀ to C₂₅ range. Additional contributions are expected from more
378 highly functionalized organics in the gas (and particle) phase not reflected in the CH, CHO₁, and CHS₁
379 compound classes (e.g., gas-phase species with multiple oxygen atoms like vanillic acid or
380 acetovanillone, and gas-phase species containing combinations of oxygen and nitrogen atoms (CHON)
381 (Ditto et al., 2021; 2022)). ERs in the plume varied across the carbon number range; in general, the
382 highest ratios were observed for the complex mixture of hydrocarbons (i.e. CH compounds) broadly
383 peaking at C₂₀-C₂₃ in the SVOC range, with a larger contribution from C₁₀ compounds including
384 monoterpenes. By comparison, the complex mixture of CHO₁ compounds was slightly lower in
385 abundance than CH with contributions from C₁₀ monoterpene emissions or monoterpene oxidation
386 products. CHS₁ IVOC-SVOCs were the lowest abundance species quantified. CHN₁ compounds
387 represent another observed contributor of IVOCs-SVOCs; the sum of all CHN₁ compound ion
388 abundances was two orders of magnitude smaller than the sum of all CHO₁ species. We note that for
389 CHN₁, this qualitative comparison is in terms of ion abundances only, given a lack of appropriate
390 standards to calibrate for the mass spectrometer's response to the complex mixture of reduced nitrogen-
391 containing I/SVOCs.

392 EFs were estimated to be $1.4 \pm 0.037 - 2.4 \pm 0.063$ g kg⁻¹ for CH, $0.81 \pm 0.078 - 0.81 \pm 0.079$ g kg⁻¹
393 for CHO₁, and $0.21 \pm 0.0033 - 0.22 \pm 0.0060$ g kg⁻¹ for CHS₁ species, for a total EF of $2.4 \pm 0.12 - 3.5 \pm 0.15$
394 g kg⁻¹ (Table A1). Here, the uncertainty represents measurement uncertainty associated with the
395 conversion from signal to mass, and the reported ranges show lower and upper limit EF values that
396 account for a contaminated background and that assume no background concentrations, respectively (as
397 described above). These estimates accounted for C₁₁-C₂₅ species and focused on I/SVOCs to avoid

398 double counting the monoterpenes and C₁₀ monoterpene species, as they were already accounted for in
399 the PTRMS data. It is noted that the concentrations estimated for the cartridge samples may be sensitive
400 to variations in sampling efficiency within the under-wing sampling pod across C₁₀-C₂₅ though these
401 effects are expected to be minimal for the adsorbent tubes used in this study (Ditto et al., 2021; Sheu et al.
402 2018). These emission estimates expanded the characterized spectrum of organic species to include
403 IVOC/SVOCs in boreal forest fire emissions, which until now, had only been available from laboratory
404 measurements (Hatch et al., 2018). However, the observed emissions of the complex mixture of
405 hydrocarbons and functionalized species may include contributions from the re-volatilization of
406 compounds previously emitted from upwind oil sands operations and deposited in the forest ecosystem, as
407 noted in Ditto et al. (2021).

408

409 **3.3.3 Accounting for the observed carbon**

410 Measurements of TC, along with the speciated measurements from the PTRMS, CIMS, AWAS
411 and cartridges, provided a unique opportunity to reconcile the TC budget in a wildfire. Fig. 6 shows the
412 TC partitioning based on derived EFs (Sect. 3.4); overlapping compounds from the individual
413 measurement methods were handled as described in SI Sect. 1.1.4. The total EF for all carbon-containing
414 compounds was 1652 g kg⁻¹ and, as expected, CO₂ was the dominant contributor comprising >90 % of
415 TC. CO contributed 7.0 % followed by a contribution from NMOG_T of 1.9 % with even smaller
416 contributions observed from CH₄ (0.5 %) followed by OC and BC (not shown) at <0.5 %. The two
417 magnified pie charts (right side), representing the low and high I/SVOC EF estimates, show the percent
418 breakdown of the measured NMOGs, and the remaining unidentified portion of NMOG_T. The EF values
419 (g C kg⁻¹) are identified in the box below. The ΣNMOG EFs (for PTRMS+CIMS+AWAS measurements),
420 totalling 13.6±0.9 g C kg⁻¹, accounted for 43±3 % of the NMOG_T EF of 31.2±4.7 g C kg⁻¹ (refer to Fig.
421 S10 for the individual SP and NP breakdowns). The ΣNMOG uncertainties were estimated by summing
422 in quadrature the individual compound EF uncertainties for the SP and NP separately, with these
423 uncertainties subsequently summed in quadrature to derive the average ΣNMOG uncertainty (Fig. 6).

424 The cartridge data showed the presence of a range of larger molecular weight I/SVOC compounds
425 between C₁₀ and C₂₅ with an additional 2.1 to 3.0 g C kg⁻¹ representing 7 to 10 % of NMOG_T. Together,
426 all of the speciated NMOG measurements in this study accounted for 50±3 % to 53±3 % of NMOG_T. The
427 remaining carbon mass was unidentified comprising 47±15 % to 50±15 % of NMOG_T. Despite using
428 four state-of-the-art measurement techniques resulting in an extensive measurement suite, almost half of
429 NMOG_T remained unidentified. This is consistent with previous work estimating ~50 % of NMOG_T by
430 mass as unidentified (Akagi et al., 2011). It is noted, however, that the magnitude of the unidentified
431 portion is partly affected by uncertainties in the speciated measurements. For example, many of the
432 ‘calculated’ PTRMS compounds are uncertain by an estimated factor of ~2 (SI Sect. 1.1.1, Table S1).
433 Nevertheless, a portion of the unidentified species likely consisted of challenging-to-measure-VOCs and
434 larger I/SVOCs that were highly functionalized or contained molecular features like reduced nitrogen
435 groups (e.g. amines) that have been observed in the gas and particle phase at various sites (Ditto et al.,
436 2020; Ditto et al., 2022). The presence of I/SVOCs in biomass burning emissions has been previously
437 observed in laboratory experiments (e.g. Koss et al., 2018; Hatch et al., 2018; Hatch et al., 2017; Bruns et
438 al., 2016) with smoldering more likely to emit a higher fraction of compounds with low volatility than
439 higher temperature processes (Koss et al., 2018). The unidentified portion may also have been comprised
440 of nitrogen-containing organics (Sect. 3.1). Studies that included measurements of a larger range of
441 nitrogen-containing organics in biomass burning emissions estimated that they comprised < 5-6 % of the
442 total nitrogen budget (Lindaas et al. 2020; Gilman et al., 2015), and thus, an even smaller fraction of
443 NMOG_T. Advancing analytical techniques to expand the suite of NMOG speciation will enable further
444 reconciliation of the TC budget which is important for assessing secondary formation processes in the
445 atmosphere.

446 **3.3.4 Volatility distribution of NMOG**

447 Volatility distributions can help track the full range of organic species to assess their partitioning
448 between the condensed and gas phases (Donahue et al., 2011). Fig. 7 shows the fractional sum of all
449 NMOG EFs within each volatility bin in terms of saturation concentration ranges ($\log_{10}C_0$, $\mu\text{g m}^{-3}$) for the

450 low I/SVOC EF estimate. C_o values were estimated using the parameterization developed by Li et al.
451 (2016). NMOG emissions from this fire spanned a large range of volatilities from $\log_{10}C_o$ of -2 to $10 \mu\text{g}$
452 m^{-3} across SVOC to VOC categories. The bin-averaged O/C ratio based on the measurements increased
453 with reduced volatility reflecting the presence of compounds with additional oxygen-containing
454 functional groups. The highest fraction of emissions was present as VOCs with 81 % having $\log_{10}C_o > 6$
455 $\mu\text{g m}^{-3}$, 9 % as IVOCs having $4 < \log_{10}C_o \mu\text{g m}^{-3} < 6 \mu\text{g m}^{-3}$ and 10 % as SVOCs having $\log_{10}C_o < 3 \mu\text{g m}^{-3}$.
456 ³. These results align with laboratory studies showing that oxygenates comprised more than > 75 % of
457 IVOCs across a range of biomass types with IVOCs accounting for ~11 % of the Σ NMOG (Hatch et al.;
458 2018). Fig. 7 encompasses the range of volatilities based on all the identified NMOGs in this study that is
459 expected to represent initial emission conditions for modelling downwind chemistry. However, improved
460 speciation, particularly of lower volatility compounds, is needed to further expand the range of volatilities
461 and advance knowledge in gas to particle partitioning processes.

462

463 **3.4 Emission factors and comparisons with other studies**

464 EFs (and ERs) in this study are derived for 193 compounds from 15 instruments of which 173 are
465 NMOG species (Table A1). This dataset represents the most extensive range of field-based EFs ever
466 determined for a wildfire in the boreal forest ecosystem. In Fig. 8 average EFs are shown for compounds
467 grouped by a) particles, b) gas-phase inorganics, and c) gas-phase organics. Separate EFs and ERs for the
468 SP and NP are shown in the SI (Figs. S11 to S13). In Fig. 9a-c, EFs are compared with those from other
469 relevant studies. Fig. 9a shows a comparison with boreal forest field measurements largely taken from a
470 compilation by Andreae (2019) referred to as BFF19, as well as values from Akagi et al. (2011) and Liu
471 et al. (2017). This results in a comparison for 50 compounds (35 organics and 15 inorganics/particulate
472 species) with the largest suite of EFs from one study conducted in a similar boreal region as the present
473 study (Simpson et al., 2011). EFs are also compared with laboratory-derived EFs for lodgepole pine Koss
474 et al. (2018; referred to as LAB18) (Fig. 9b), a similar fuel type in the current study, with a total of 99
475 NMOGs and 3 inorganics in common. In Fig. 9c, EFs are compared with those recently reported in

476 Permar et al. (2021) (referred to as TFF21) based on aircraft measurements of temperate forest wildfires
477 in areas mostly dominated by pine, fir and spruce trees, which provides the closest suitable comparison
478 with similar speciated NMOGs under wildfire conditions. Comparisons include 111 NMOGs, and 4
479 inorganics/black carbon. While the Permar et al. (2021) study was conducted in a temperate forest
480 region, it was at high elevation locations with similar vegetation types as the current study.

481

482 **3.4.1 Particle species** The PM_{10} EF ($6.8 \pm 0.8 \text{ g kg}^{-1}$) represents the total of all particle component species
483 as measured by the AMS. The PM_{10} EF of $6.8 \pm 1.1 \text{ g kg}^{-1}$ (Fig. 8a) (accounting for estimated mass
484 differences due to particle diameters (SI Sect. 1.1.2)) falls in the lower end of the large range previously
485 observed for boreal forest wildfires ($18.7 \pm 15.9 \text{ g kg}^{-1}$; Fig. 9a). The few PM EFs for BFF19 ($n=5$) over a
486 limited range of MCEs (i.e. 0.89 to 0.93) shows significant variability consistent with previous work
487 (Jolleys et al., 2015; Akagi et al., 2011; Cubison et al., 2011; Hosseini et al., 2013). OA, accounting for
488 90 % of PM_{10} , has the largest EF, with comparatively lower EFs for NO_3 , BC, NH_4 , and SO_4 (Fig. 8a, Fig.
489 S6). This reflects the dominant particle-phase organic carbon content of the burned fuel and
490 correspondingly lower fractions of nitrogen and sulphur-containing compounds. Similar high organic
491 fractions have been previously observed in biomass burning emissions (Liu et al., 2017; May et al., 2014;
492 Hecobian et al., 2011). ERs similarly highlight the dominant OA emissions. Although the magnitude of
493 EFs between the SP and NP are within their derived uncertainties, the ERs showed differences by up to
494 70 % for NH_4 (Fig. S12) suggesting some differences in photochemistry between the two plumes. EFs
495 and ERs for chemically-speciated particle species derived in this study represent the first such
496 measurements under boreal forest wildfire conditions. EFs for chemically speciated compounds are not
497 found in BFF19 (except BC), but when compared with available values for U.S. temperate forest wildfires
498 (Liu et al., 2017) are found to be lower for OA (Fig. 9a), SO_4 , NO_3 and NH_4 by factors of 3.7, 5.0, 5.3,
499 and 3.0, respectively. Although differences in fuel type burned between the present study (mature Jack
500 pine, boreal spruce, boreal mixed-wood) and Liu et al. (2017) (mixed conifer, grass, brush and chaparral)
501 may influence the chemical composition of emissions, these large differences suggest the importance of

502 other factors in controlling OA emissions. The lower OA emissions under smoldering conditions in the
503 current study compared to Liu et al. (2017) with higher combustion efficiencies (0.877 to 0.935) conflicts
504 with some findings showing increased OA emissions with lower fire intensities (Liu et al., 2017, Burling
505 et al., 2011). However, the relationship between EF_{OA} and combustion efficiency can be impacted by
506 multiple factors such as OA loading, gas-particle partitioning related to dilution, and fuel moisture content
507 (May et al., 2014). The EF_{OA} in the current study ($6.6 \pm 2.6 \text{ g kg}^{-1}$) lies in the range of EF_{OA} reported for
508 prescribed burns across three temperate ecosystems (2.8 ± 1.6 to $11.2 \pm 2.7 \text{ g kg}^{-1}$) (May et al., 2014). This
509 may imply that the low intensity, surface, smoldering wildfire conditions in the present study (Sect. 3.1)
510 may be similar to prescribed burn conditions which are typically low intensity fires that are restricted to
511 the forest floor and understory, and conducted under controlled and consistent meteorological and fuel
512 moisture conditions (Yokelson et al., 2013; Carter and Foster, 2004). Inorganic PM emissions, however,
513 are likely more dependent on fuel elemental composition than combustion efficiency (Liu et al., 2017).
514 Differences in fuel composition between boreal and temperate forest ecosystems are inferred through
515 comparisons of NO_x and SO_2 emissions. For example, the average NO_x and SO_2 EFs for boreal forests,
516 are lower than the average EFs for temperate forests by factors of 2.5 and 3.0, respectively. The lower
517 NO_x and SO_2 emissions from boreal vs temperate forest wildfires are likely reflective of the reduced S
518 and N content in boreal biomass (Bond-Lamberty et al., 2006) relative to conifer (Misel, 2012) fuels in
519 the western U.S., as well as the possible influence of lower anthropogenic sources of nitrogen and sulphur
520 atmospheric deposition in boreal forests (Jia et al., 2016).

521
522 **3.4.2 Gas-phase inorganic species** The largest average EFs for inorganic gases (Fig. 8b; separate NP
523 and SP Fig. S11) were from reduced nitrogen compounds dominated by NH_3 ($0.63 \pm 0.14 \text{ g kg}^{-1}$) and
524 followed by HCN ($0.31 \pm 0.07 \text{ g kg}^{-1}$), with lower EFs for oxidized nitrogen compounds such as NO_2
525 ($0.15 \pm 0.04 \text{ g kg}^{-1}$) and HONO ($0.02 \pm 0.012 \text{ g kg}^{-1}$). This is consistent with previous work identifying
526 elevated emissions of NH_3 and HCN during smoldering conditions, whereas emissions of HONO and
527 NO_x are primarily associated with flaming combustion (e.g. Roberts et al., 2020; Akagi et al., 2013;

528 Yokelson et al., 1997; Griffith et al., 1991). The EFs for CO₂ and CO from the present study are
529 comparable within uncertainties of that previously reported for BFF19 (Table A1). However, EFs for
530 most other gaseous inorganic species were lower than the BFF19 EF average including NH₃, HONO, and
531 NO_x by factors of 4.0, 20, and 7.1, respectively (Fig. 9a). There are only a limited number of studies
532 reporting EFs for these compounds in the BFF19 category. For example, there are only 4 previously
533 reported BFF19 EFs for NH₃ (2.5±1.8 g kg⁻¹) showing a large range of values. Although these
534 comparisons are limited by the few reported values in the literature, the differences indicate a strong
535 sensitivity towards factors like fire intensity, chemical reactivity, fuel type and moisture, and
536 meteorology. In contrast, EFs for HCN derived in the current study (0.31±0.07 g kg⁻¹) lie within the
537 range of BFF19, LAB18 and TFF21 values (0.28±0.06 to 0.53±0.30 g kg⁻¹), (Figs 9a, b, c, respectively)
538 and does not vary widely suggesting that HCN may be less sensitive to burning characteristics. HCN is
539 of concern due to its impacts on human health particularly since biomass burning emissions are
540 responsible for the majority of the global HCN (Moussa et al., 2016 and references therein).

541
542 **3.4.3 Gas-phase organic species** In Fig. 8c, the top 25 average EFs for gas-phase organic species are
543 shown in decreasing order of magnitude. The most abundant emissions were from the lower molecular
544 weight compounds; such trends are generally in agreement with previous field-based measurements for a
545 range of fuel types (e.g. Permar et al., 2021; Andreae, 2019; Liu et al., 2017; Simpson et al., 2011;
546 Urbanski et al., 2009). Excluding CH₄, the largest EFs were associated with methanol, followed by
547 ethene, ethane, acetic acid, acetaldehyde, formaldehyde, and acetone ranging from 1.9±0.4 g kg⁻¹ to
548 0.82±0.22 g kg⁻¹ for these compounds. Noting some variations related to differences in measurement
549 methods, other studies have identified many of these same species as dominating biomass burning
550 emissions (e.g. Permar et al., 2021; Simpson et al., 2011; Akagi et al., 2011). For example, Simpson et al.
551 (2011) found that 5 of the same compounds in the present study including formaldehyde, methanol,
552 ethene, ethane and acetone were in the top 10 NMOG EFs from aircraft-based measurements made of
553 boreal forest wildfires in northern Saskatchewan, Canada, and within ~300 km of the current study. In

554 the present study, the top 24 NMOG compounds accounted for 81 % of the Σ NMOG by total molecular
555 mass with lower emissions from the remaining 149 measured compounds. In western U.S. wildfires,
556 small emissions from 151 species were found to account for almost half of Σ NMOG (Permar et al.,
557 2021).EFs for the NP and SP generally agreed within their uncertainties with larger differences for some
558 of the more reactive species like isoprene, monoterpenes, and furan. For example, the SP EF for isoprene
559 was a factor of 3.4 lower than that for the NP ($0.64 \pm 0.34 \text{ g kg}^{-1}$) (Fig. S13). Although the reasons for
560 these differences are not yet known, observations of higher O_3 in the SP ($52.4 \pm 3.0 \text{ ppbv}$) compared to the
561 NP ($44.7 \pm 3.6 \text{ ppbv}$) suggest the influence of higher oxidant chemistry in the SP emissions compared to
562 the NP.

563 To compare the total NMOG derived in the present study with those from previous studies that
564 typically sum up their speciated measurements i.e. Σ NMOG, estimates were made using two methods: 1.
565 increasing the Σ NMOG to account for the unidentified portion of NMOG_T ; and 2. adjusting the NMOG_T
566 to reflect the total molecular mass (not just the carbon portion). For method 1, the Σ NMOG EF
567 (including the I/SVOCs) in this study (24.5 ± 1.6 to $25.6 \pm 1.6 \text{ g kg}^{-1}$) was increased by 50 and 47 % (Fig.
568 6), respectively, equalling 36.8 ± 11.3 to $37.6 \pm 12.2 \text{ g kg}^{-1}$. This estimate assumes that the carbon
569 distribution is the same as the identified, speciated measurements. For method 2, based on the speciated
570 measurements, the average molecular mass was 100 g mol^{-1} and the average carbon number was 6
571 resulting in $\sim 28 \pm 24$ % of the molecular fraction represented by atoms other than carbon. Adjusting the
572 NMOG_T of $31.2 \pm 3.8 \text{ g C kg}^{-1}$ upwards by 28 ± 24 % to reflect the additional molecular mass results in a
573 Σ NMOG of $39.9 \pm 5.8 \text{ g kg}^{-1}$. The resulting estimated NMOG in this study of 36.8 ± 11.3 to $39.9 \pm 5.8 \text{ g kg}^{-1}$
574 lies between the estimated average of 58.7 g kg^{-1} for the BFF19 (Fig. 9a) and those estimated from the
575 Σ NMOG EFs of 25.0 g kg^{-1} (LAB18) (Fig. 9b), and $26.1 \pm 6.9 \text{ g kg}^{-1}$ (TFF21) (Fig. 9c) derived from
576 laboratory- and field-based studies (Table A1). In contrast to the current work, previous estimates of
577 NMOG_T are likely to underestimate total NMOG emissions as they typically represent the sum of
578 measured species only. Some studies have attempted to account for NMOG_T by including the sum of
579 measured plus estimates of ‘unknown’ portions of NMOGs (Σ NMOGs) (Permar et al., 2021; Koss et al.,

580 2018; Stockwell et al., 2015; Gilman et al., 2015). The BFF19 EF was recently doubled from 29.3 ± 10.1 g
581 kg^{-1} to 58.7 g kg^{-1} to account for unidentified NMOGs where the Σ NMOGs were measured by FTIR, GC
582 and PTRMS (Andreae, 2019; Akagi et al., 2011). These results support that doubling the Σ NMOG
583 provides a reasonable estimate the NMOG_T . It is noted that the average BFF19 NMOG EF is ~ 1.5 times
584 higher than that derived in the present study, however, this may reflect variability in NMOG emissions
585 even within the same boreal biome.

586 Although it is known that acidic compounds are emitted from biomass burning, few studies have
587 quantified their emissions, particularly under field conditions (Andreae, 2019; Veres et al., 2010;
588 Yokelson et al., 2009; Goode et al.; 2000). In this study, EFs for 22 organic acidic compounds were
589 derived (Table A1) representing the most detailed set of organic acid EFs from biomass burning for any
590 ecosystem (Andreae, 2019). The largest EFs for these compounds include acetic acid, C4 oxo-carboxylic
591 acids, and pyruvic acid, all of which are found among the top 24 NMOGs (Fig. 8c). For those
592 measurements that are available for comparison, EFs in the present study were lower for formic acid and
593 acetic acid compared to BFF19, and were also lower than in LAB18, and TFF21, ranging from factors of
594 1.7 to 8.8 (Figs. 9a, b, c). Organic acids that were in common with TFF21 and LAB18 (Table A1) had
595 lower EFs, with the exception of pyruvic acid, which was substantially higher ($>$ factor of 37) in the
596 present study. Differences in fuel type may be an important factor in the variability of these comparisons.
597 Based on laboratory experiments, Veres et al. (2010) found a large range (factor of 5 to 13) of organic
598 acid emissions with different fuel types suggesting that the lignin content of the fuel could be a source of
599 biomass burning organic acid emissions. Emissions for 10 organic acids that have not previously been
600 reported, as well as several inorganic acids including nitrous acid, isocyanic acid, and peroxyacetic acid,
601 are included in Table A1. These acids, representing 9 % of the Σ NMOGs (Fig. 5), are an important class
602 of oxygenates as they can form additional PM (Reid et al., 2005) and influence the hygroscopicity of
603 smoke particles (Rogers et al., 1991; Kotchenruther and Hobbs, 1998).

604 Isoprene and monoterpenes, with similar EFs $\sim 0.41 \pm 0.19$ g kg^{-1} , represented 16th and 18th,
605 respectively, of the top 24 NMOG EFs in this study. Terpenes are known to be emitted from a range of

606 biomass burning fuels (Andreae, 2019 and references therein), but there have been few measurements in
607 boreal forest wildfire plumes (Simpson et al., 2011; Andreae, 2019). It is noted that PTRMS
608 measurements of IVOCs like sesquiterpenes likely represent lower limits as they tend to be easily lost to
609 sample inlet lines due to their low volatility. The isoprene average EF of $0.42 \pm 0.26 \text{ g kg}^{-1}$ was more than
610 a factor of 5 higher, while the monoterpenes EF, $0.41 \pm 0.19 \text{ g kg}^{-1}$, was substantially lower than the only
611 reported EF for boreal forest wildfires (Simpson et al., 2011). The difference in EFs for isoprene would
612 be even greater if only the NP EF ($0.64 \pm 0.34 \text{ g kg}^{-1}$) is compared (if it is assumed that isoprene emissions
613 were influenced by photochemical losses in the SP). As the present study and the Simpson et al. (2011)
614 study were conducted in similar locations (i.e. boreal forest region within ~300 km of each other), and
615 comparable background levels, these differences are likely driven by fire combustion state, despite having
616 similar study-averaged MCEs. The majority of monoterpenes are stored in plant tissues (resin stores) for
617 long periods of time, but isoprene is synthesized and immediately released by plants, and can also be
618 emitted as a combustion product (Ciccioli et al., 2014; Akagi et al., 2013). Hatch et al. (2019) found that
619 a wide range of terpenoids are released across a variety of biomass types with variable emissions that
620 were dependent on plant species, and specifically related to their fuel resin stores. In the present study,
621 monoterpenes may have ‘boiled-off’ through distillation processes in the early stages of the fire resulting
622 in lower monoterpene emissions at the aircraft sampling time, ~14 hrs post-flaming. In contrast, the
623 Simpson et al. (2011) study sampled comparatively earlier and more intense fire stages where higher
624 monoterpene emissions were likely released from live or recently fallen trees that still contained
625 significant resin stores. The monoterpenes EF reported by Simpson et al. (2011) was likely even higher
626 given only two monoterpenes were speciated and emissions of other terpenes were likely (Hatch et al.,
627 2019). Higher isoprene emissions in the present study compared to Simpson et al. (2011) could be related
628 to the comparatively larger smoldering component. Although limited data exist on the release of isoprene
629 as a function of fire intensity, negative relationships between isoprene and MCE were observed in
630 Australian temperate forest fires (Guérette et al., 2018) and wheat fields (Kumar et al., 2018).

631 Several furanoid compounds also exhibited significant emissions (Fig. 8c) including furfural,
632 furan, and methyl furan ranking 12th, 19th, and 22nd of the top 24 organic compounds, respectively.
633 Emissions of furanoids have been observed for a wide range of fuel types (Hatch et al., 2017; Simpson et
634 al., 2011). Agreement within uncertainties was found with BFF19 for furfural, and furan (Fig 9a). The
635 EFs for furan ($0.39 \pm 0.19 \text{ g kg}^{-1}$) and furfural ($0.65 \pm 0.31 \text{ g kg}^{-1}$) were also similar to that in LAB18 (Fig.
636 9b), and TFF21 (Fig. 9c), as well as other ecosystems (Andreae, 2019) suggesting their emissions were
637 relatively insensitive to fire intensity and fuel mixture. The comparisons in Fig. 9 indicate that for the
638 higher emitting species, the current results are fairly similar, but for the lower emitting species, these
639 results are lower than previous reported values. These comparisons provide context for the emissions
640 reported in the present study and moves towards improved statistics to better constrain wildfire emissions.
641 Additional factors are considered to explain variability in emissions between this study and other reported
642 values, as well as within this study (NP vs SP). Differences and variability in burn conditions (e.g. fire
643 intensity, winds, fuel density, flame dynamics, fuel moisture) likely influence these comparisons; the
644 Screen 1 measurements in the present study were taken from 9-10 am LT when the fire was in a low
645 intensity, smoldering state, while those in Permar et al. (2021) and Simpson et al. (2011) took place
646 during mid-day under active wildfire conditions. Aircraft measurements in general have a higher
647 probability of sampling variable burn conditions compared to laboratory studies (Hodshire et al., 2019),
648 and as such, aircraft-derived EFs are likely to reflect variability for reactive species as speculated earlier
649 with isoprene. Particularly for reactive species that can exhibit complex variation across plumes, EFs
650 (and ERs) derived by integrating across plumes can be biased low, (Sect. 2.5; Peng et al., 2021; Decker et
651 al., 2021). Also, EFs derived using TC in this study may result in lower, albeit small, EFs compared to
652 reported values that do not account for all the carbon (estimated to be 1-2 % (Akagi et al., 2011)).

653 **3.5 Evaluation of emissions models**

654 **3.5.1 Comparison of EFs with the model emissions speciation profile**

655 EFs derived in the present study are compared with those that are currently incorporated into the
656 emissions component of the FireWork modelling system using the Forest Fire Emissions Prediction
657

658 System (CFFEPS). CFFEPS uses EFs allocated for 3 combustion states (flaming, smoldering and
659 residual) and for 8 species including lumped non-methane hydrocarbons (NMHC) based on United States
660 vegetation data compiled in Urbanski et al. (2014) (Table 3 in Chen et al., 2019). Fig. 9d (bolded
661 compounds) shows that the smoldering EFs in the present study were comparable for CO, CH₄ and
662 NMOG, but lower for PM₁ (PM_{2.5}), NH₃, SO₂ and NO_x by factors of 3.4, 2.4, 6.6 and 17, respectively.
663 The lower EFs for these species implies that the CFFEPS EFs would not adequately capture their total
664 emissions under smoldering conditions for the boreal fuel in the current measurement study.

665 For incorporation into numerical air quality models, total organic gas (TOG=NMOG+CH₄)
666 emissions are typically split into detailed chemical components using chemical mass speciation profiles,
667 and converted to lumped chemical mechanism species. In the FireWork modelling system, the
668 smoldering combustion TOG is split into components based on EPA's SPECIATEv4.5 profile (#95428)
669 (US EPA 2016, Urbanski et al.; 2014 - supplement Table A.2, Boreal Forest Duff/Organic soil). This
670 profile is ultimately compiled using laboratory data from Yokelson et al. (2013), Bertsch et al. (2003),
671 and Yokelson et al. (1997) based entirely on U.S. fuel types. EFs in the present study were found to be
672 generally lower than the laboratory-based EFs for 74 species in common ranging from factors of 1.7 to
673 8.5 including for monoterpenes, formic acid, phenol, and furan (Fig. 9d). A few species including
674 furfural, propane nitrile and ethyl styrene are comparable, while isoprene and pyruvic acid are notably
675 higher by factors 2 to 5.3.

676 For a research version of the FireWork system, the component speciation is mapped to the
677 SAPRC-11 chemical mechanism species (Carter and Heo, 2013) with detailed oxygenated compounds
678 and aromatic species, largely to better represent SOA formation processes. For comparison with the
679 measurement derived speciation profile in this study, EFs were first mapped to SAPRC-11 species and
680 normalized by the total identified mass species fraction without unknowns to obtain mass fractions of
681 relevant model mechanism species (Table S9). Comparing the normalized mass fractions for similar
682 mechanism species (Fig. S14) showed a substantially lower fraction of reactive alkanes (ALK5) with an
683 estimated 5 % in this study compared to 28 % in the SPECIATEv4.5 wildfire smoldering profile. Mass

684 fractions in this study are notably higher for the ACYL, ETHE, and ISOP lumped model species by
685 factors of 13, 7 and 51. The mass fraction of CH₄ is also different with 24 % of TOG in this study
686 compared to 4 % from the SPECIATE4.5 profile. The measurement derived chemical speciation profile
687 is expected to be different from the average speciation profile from EPA's SPECIATEv4.5 due to
688 differences in chemical species identification, fuel type, fire and measurement conditions, and
689 uncertainties on how measured compounds are mapped to lumped mechanism species. The emissions
690 profile developed in the present study can be used to improve predictions of wildfire smoldering
691 emissions specific to the Canadian boreal forest.

692

693 **3.5.2 Linking aircraft and satellite observations to evaluate modelled emissions diurnal variability**

694 Wildfires generally exhibit a diurnal cycle with fire intensities maximizing late afternoon and
695 diminishing at night having important implications for fire emissions (Chen et al., 2019). Evaluating
696 modelled emissions throughout the diurnal cycle with observations is a critical step in verifying smoke
697 predictions. Emissions models mostly parameterize diurnal fire emissions with prescribed profiles that
698 distribute daily total emissions to hourly. In CFFEPS, a diurnal profile is applied to allocate daily burn
699 area to hourly intervals, with highest activity in the late afternoon. The actual fuel consumed, and thus,
700 hourly emissions, is then calculated with depth of burn estimates driven by hourly meteorology (Chen et
701 al., 2019). In Fig. 10, for the wildfire in the present study, the hourly CFFEPS-predicted emissions
702 (orange dots) for selected compounds are shown between 2018-06-24 17:00 UTC and 2018-06-25 21:00
703 UTC, spanning the aircraft sample time (red arrow at 15:00 UTC). After 21:00 UTC, the discrepancy
704 between the CFFEPS-predicted emissions and FRP increased as a result of rain that passed through the
705 area that is not considered in the model bottom-up emission estimates (not shown in the figure). The
706 burning phases are outlined in the figure where flaming (light pink background) is assumed to occur when
707 the atmospheric conditions alongside fire behaviour and emissions model outputs infer a fireline intensity
708 >4,000 kW m⁻¹ (Forestry Canada Fire Danger Rating Group, 1992), and a smoldering fire (blue
709 background) for intensity <4000 kW m⁻¹. The fire intensity distinction between flaming and smoldering

710 roughly aligns with the observed minimum for this particular fire with the fire radiative power (FRP, grey
711 dots) retrieval from the GOES-16 satellite sensor of 500 MW where smoldering occurs <500 MW and
712 flaming for >500 MW. The 500 MW threshold over the approximately 1,700 ha of actively smoldering
713 area observed by overnight VIIRS thermal detections gives an estimated energy density of 0.29 MW ha⁻¹.
714 This energy density threshold for smoldering <0.29 MW ha⁻¹ found in this study is in agreement with
715 O'Brien et al. (2015) who found flaming combustion at >0.4 MW ha⁻¹ for lower intensity flaming fires
716 and smoldering combustion at lower energy densities. The FRP represents the sum over all hotspots of
717 this fire for each 15-min observation period. Emission rates in metric tonnes per hour (t h⁻¹) were derived
718 from selected aircraft measurements using a mass balance method that was designed to estimate pollutant
719 transfer rates through virtual screens using aircraft flight data (Gordon et al., 2015) (see SI Methods).
720 Emission rates were estimated to be 29±2.1 t h⁻¹ for PM₁, 433±26.7 t h⁻¹ for CO, 0.65± 0.03 t h⁻¹ for NO_x
721 (as NO), and 2.7±0.16 t h⁻¹ for NH₃ (red arrows). Emission rates were also derived from satellite
722 observations (black arrows) for CO, NO_x, and NH₃. Emissions of CO were estimated using a flux method
723 as described in Stockwell et al. (2021) using TROPOMI satellite observations yielding 1670±670 t h⁻¹ at
724 19:06 UTC and 4050±1620 t h⁻¹ at 20:48 UTC. NO_x emissions (9.1±3.4; scaled to t NO h⁻¹ at 19:06 UTC
725 (not enough high-quality observations for the 20:48 UTC overpass) were derived from the TROPOMI
726 NO₂ dataset using an Exponentially Modified Gaussian approach (Griffin et al., 2021). NH₃ emission
727 rates (5.6±3.9 t h⁻¹) were derived from CRIS satellite observations at the satellite overpass time of 19:00
728 UTC by applying a flux method (Adams et al., 2019).

729 The aircraft measurements were taken when the FRP was low reflecting a smoldering surface
730 fire. However, the satellite overpass occurred ~4 hrs later than the aircraft measurements close to the
731 FRP daily maximum, after which rain passed through the area. The CFFEPS model, exhibiting a
732 prescribed diurnal pattern, captures the increase in NO_x and NH₃ emissions between that derived from the
733 aircraft and satellites transitioning from a smoldering to predominantly flaming fire; NO_x emissions
734 increased by a factor >10, whereas the NH₃ emissions increased by a factor of approximately 2. This is in
735 agreement with recent laboratory measurements that found that the release of NO_x is favoured during the

736 flaming stage and the release of reduced forms of nitrogen, such as NH_3 , is favoured during the
737 smoldering phase (Roberts et al., 2020) (also see Fig. 4). However, the CFFEPS CO emission rates do
738 not track the increase in CO emissions between the aircraft-derived value and the two TROPOMI values,
739 indicating that the CO EF for flaming is low in the model. This highlights the need to validate model
740 emission rates with measurements to adjust and update the EFs accordingly.

741 The aircraft- and satellite-derived emission rates for CO, NO_x and NH_3 were each ratioed to FRP
742 (in units of $\text{t h}^{-1} \text{MW}^{-1}$, referred to as $R_{\text{species}/\text{FRP}}$) to represent the two end burning states ie. smoldering and
743 flaming conditions. $R_{\text{species}/\text{FRP}}$ values were estimated for the flaming and smoldering phases of the fire and
744 it was assumed that flaming occurred for $\text{FRP} > 500 \text{ MW}$ and smoldering for $\text{FRP} < 500 \text{ MW}$. The CO
745 $R_{\text{species}/\text{FRP}}$ values were roughly twice as large during smoldering compared to flaming. For the two
746 satellite overpasses during the flaming phase of the fire, the $R_{\text{CO}/\text{FRP}}$ values were within the uncertainties
747 (19:06 UTC $R_{\text{CO}/\text{FRP}} = 0.47 \pm 0.25 \text{ t h}^{-1} \text{MW}^{-1}$; 20:48 UTC $R_{\text{CO}/\text{FRP}} = 0.43 \pm 0.23 \text{ t h}^{-1} \text{MW}^{-1}$). The $R_{\text{NO}_x/\text{FRP}}$
748 value for NO_x is also twice as large for flaming compared to smoldering, and for NH_3 , the $R_{\text{NH}_3/\text{FRP}}$ value
749 is ~5 times larger for smoldering than flaming. Total emissions were then estimated by integrating the
750 GOES FRP over the period 2018-06-24 17:00 UTC to 2018-06-25 23:00 UTC (after which no more hot
751 spots were detected by GOES and the fire presumably extinguished), and applying the derived smoldering
752 and flaming $R_{\text{species}/\text{FRP}}$ values. Assuming that the fire went out when GOES did not observe any hot spots,
753 total emissions for this fire of CO, NO_x and NH_3 are estimated at $22,000 \pm 8700$, 104 ± 42 , and 84 ± 33
754 tonnes, respectively. If the fire is assumed to have continued burning when GOES did not detect any fire
755 hot spots (between 22:00 - 04:00 UTC and 07:00 - 15:00 UTC, with an FRP of 150 MW (~GOES
756 detection limit; Roberts et al., 2015), the emissions increase to $24,000 \pm 9600$, 106 ± 43 and 98 ± 39 tonnes,
757 respectively, providing an upper limit of emissions. The combination of aircraft and satellite-derived
758 emission estimates for multiple species helps to obtain the diurnal variability of emissions and to obtain
759 more complete details on the emission information across different burning stages.

760

761

762 **4. Summary and Implications**

763 This study provides detailed emissions information for boreal forest wildfires under smoldering
764 combustion conditions. Consistent with previous results, highly speciated airborne measurements showed
765 a large diversity of chemical classes highlighting the complexity of emissions. Despite extensive
766 speciation across a range of NMOG volatilities, a substantial portion of NMOG_T remained unidentified
767 (47 ± 15 to 50 ± 15 %) and is expected to be comprised of more highly functionalized VOCs and I/SVOCs.
768 Although these compounds are challenging to measure, their characterization is necessary to more fully
769 understand particle-gas partitioning processes related to the formation of SOA. Methodological
770 advancements to achieve higher time resolution speciated measurements of I/SVOCs would move
771 towards further NMOG_T closure and span a more complete range of volatilities. A detailed suite of EFs
772 that were derived in this study builds on previous work (e.g. Simpson et al., 2011; Andreae 2019) and can
773 be used to improve chemical speciation profiles that are relevant for air quality modelling of boreal forest
774 wildfires. Aircraft-derived emission estimates were paired with those from satellite observations
775 demonstrating their combined usefulness in assessing modelled emissions diurnal variability. As satellite
776 instrumentation and methodologies advance, linking emissions derived from aircraft (and ground)
777 observations for additional compounds will improve the ability to simulate and predict the diurnal
778 variation in wildfire emissions.

779 The results presented here represent only one smoldering boreal forest wildfire with limited in-plume
780 sampling times. Additional measurements are needed under a variety of fire conditions (combustion
781 state, fire stage, biomass mixtures, time of day, etc) in order to elucidate the major controlling factors and
782 improve statistical representation for constraining and modelling these sources. For example,
783 measurements are needed to assess dark chemistry reactions in biomass burning emissions which have
784 been shown to be important in the formation of OA (Kodros et al., 2020) and brown carbon (Palm et al.;
785 2020). In addition, reduced actinic flux associated with high particle loadings in biomass burning
786 emissions can influence plume chemistry (e.g. Juncosa-Calahorrano et al., 2021; Parrington et al., 2013).

787 The emissions information in this work can be used for evaluation and improvements of models that are
788 essential for reliable predictions of boreal forest wildfire pollutants and their downwind chemistry.

789

790 **Acknowledgements**

791 The authors acknowledge the significant technical and scientific contributions towards the success of this
792 study from the AQRD technical and data teams, the NRC team, and excellent program management by
793 Stewart Cober. The authors would like to thank Mark Shephard for his work on the CRIS NH₃ retrievals
794 and making those available. JCD, MH, and DRG acknowledge support from the National Science
795 Foundation (AGS1764126) and GERSTEL for their collaboration with the thermal desorption unit used
796 as part of this study, and MH also acknowledges the Goldwater Scholarship Foundation. S.-M.L.
797 acknowledges the support of the Ministry of Science and Technology of China (Grant
798 2019YFC0214700).

799

800 **Author contribution**

801 KH, SML, JL, MJW, JJBW, AL, PB, RLM, CM, AS, RMS, SM, AD, and MW all contributed to the
802 collection and analyses of the aircraft observations in the field. JCD, MH, and DRG analysed the
803 cartridge samples. ZO contributed to the analyses and created many of the figures. DT contributed to the
804 analyses of the physical and combustion state of the wildfire fire. DG and EE provided the satellite
805 observations and DG wrote the satellite comparison section. JC contributed to the comparisons with the
806 model emission speciation profile. KH wrote the paper with input from all co-authors.

807

808 **Competing interests**

809 The authors declare that they have no substantive conflicts of interest, but acknowledge that
810 DRG and JL are associate editors with Atmospheric Chemistry and Physics.

811

812 **Data availability**

813 All data used in this publication are available upon request.

814

815 **References**

- 816 Adams, C., McLinden, C. A., Shephard, M. W., Dickson, N., Dammers, E., Chen, J., Makar, P., Cady-
817 Pereira, K. E., Tam, N., Kharol, S. K., Lamsal, L. N., and Krotkov, N. A.: Satellite-derived emissions of
818 carbon monoxide, ammonia, and nitrogen dioxide from the 2016 Horse River wildfire in the Fort
819 McMurray area, *Atmos. Chem. Phys.*, 19, 2577-2599, <https://doi.org/10.5194/acp-19-2577-2019>, 2019.
820
- 821 Ahern, A. T., Robinson, E. S., Tkacik, D. S., Saleh, R., Hatch, L. E., Barsanti, K. C., Stockwell, C. E.,
822 Yokelson, R. J., Presto, A. A., Robinson, A. L., Sullivan, R. C., and Donahue, N. M.: Production of
823 secondary organic aerosol during aging of biomass burning smoke from fresh fuels and its relationship to
824 VOC Precursors, *J. Geophys. Res.-Atmos*, 124, 3583-3606, <https://doi.org/10.1029/2018JD029068>, 2019.
825
- 826 Akagi, S. K., Yokelson, R. J., Wiedinmyer, C., Alvarado, M. J., Reid, J. S., Karl, T., Crounse, J. D., and
827 Wennberg, P. O.: Emission factors for open and domestic biomass burning for use in atmospheric models,
828 *Atmos. Chem. Phys.*, 11, 4039-4072, <https://doi.org/10.5194/acp-11-4039-2011>, 2011.
829
- 830 Akagi, S. K., Craven, J. S., Taylor, J. W., McMeeking, G. R., Yokelson, R. J., Burling, I. R., Urbanski, S.
831 P., Wold, C. E., Seinfeld, J. H., Coe, H., Alvarado, M. J., and Weise, D. R.: Evolution of trace gases and
832 particles emitted by a chaparral fire in California, *Atmos. Chem. Phys.*, 12, 1397-1421,
833 <https://doi.org/10.5194/acp-12-1397-2012>, 2012.
834
- 835 Akagi, S. K., Yokelson, R. J., Burling, I. R., Meinardi, S., Simpson, I., Blake, D. R., McMeeking, G. R.,
836 Sullivan, A., Lee, T., Kreidenweis, S., Urbanski, S., Reardon, J., Griffith, D. W. T., Johnson, T. J., and
837 Weise, D. R.: Measurements of reactive trace gases and variable O₃ formation rates in some South
838 Carolina biomass burning plumes, *Atmos. Chem. Phys.*, 13, 1141-1165, <https://doi.org/10.5194/acp-13-1141-2013>, 2013.
839
- 840
- 841 Alvarado, M. J., Logan, J. A., Mao, J., Apel, E., Riemer, D., Blake, D., Cohen, R. C., Min, K. E., Perring,
842 A. E., Browne, E. C., Wooldridge, P. J., Diskin, G. S., Sachse, G. W., Fuelberg, H., Sessions, W. R.,
843 Harrigan, D. L., Huey, G., Liao, J., Case-Hanks, A., Jimenez, J. L., Cubison, M. J., Vay, S. A.,
844 Weinheimer, A. J., Knapp, D. J., Montzka, D. D., Flocke, F. M., Pollack, I. B., Wennberg, P. O., Kurten,
845 A., Crounse, J., Clair, J. M. S., Wisthaler, A., Mikoviny, T., Yantosca, R. M., Carouge, C. C., and Le
846 Sager, P.: Nitrogen oxides and PAN in plumes from boreal fires during ARCTAS-B and their impact on
847 ozone: an integrated analysis of aircraft and satellite observations, *Atmos. Chem. Phys.*, 10, 9739-9760,
848 <https://doi.org/10.5194/acp-10-9739-2010>, 2010.
849
- 850 Andreae, M. O.: Emission of trace gases and aerosols from biomass burning – an updated assessment,
851 *Atmos. Chem. Phys.*, 19, 8523-8546, <https://doi.org/10.5194/acp-19-8523-2019>, 2019. Biomass burning
852 emission factors https://edmond.mpdl.mpg.de/imeji/collection/op2vVE8m0us_gcGC, ver 14 Apr 2021.
853
- 854 Andreae, M. O. and Merlet, P.: Emission of trace gases and aerosols from biomass burning, *Global*
855 *Biogeochem. Cy.*, 15, 955-966, <https://doi.org/10.1029/2000GB001382>, 2001.
856
- 857 Baumgardner, D., Kok, G., and Raga, G.: Warming of the Arctic lower stratosphere by light absorbing
858 particles, *Geophys. Res. Lett.*, 31, L06117, <https://doi.org/10.1029/2003GL018883>, 2004.
859
- 860 Bertschi, I., Yokelson, R. J., Ward, D. E., Babbitt, R. E., Susott, R. A., Goode, J. G., and Hao, W. M.:
861 Trace gas and particle emissions from fires in large diameter and belowground biomass fuels, *J. Geophys.*
862 *Res.-Atmos*, 108, 8472, <https://doi.org/10.1029/2002JD002100>, 2003.
863

864 Bond-Lamberty, B., Gower, S. T., Wang, C., Cyr, P., and Veldhuis, H.: Nitrogen dynamics of a boreal
865 black spruce wildfire chronosequence, *Biogeochemistry*, 81, 1-16, [https://doi.org/10.1007/s10533-006-](https://doi.org/10.1007/s10533-006-9025-7)
866 9025-7, 2006.

867

868 Bruns, E. A., El Haddad, I., Slowik, J. G., Kilic, D., Klein, F., Baltensperger, U., and Prevot, A. S. H.:
869 Identification of significant precursor gases of secondary organic aerosols from residential wood
870 combustion, *Sci. Rep.*, 6, <https://doi.org/10.1038/srep27881>, 2016.

871

872 Burling, I. R., Yokelson, R. J., Akagi, S. K., Urbanski, S. P., Wold, C. E., Griffith, D. W. T., Johnson, T.
873 J., Reardon, J., and Weise, D. R.: Airborne and ground-based measurements of the trace gases and
874 particles emitted by prescribed fires in the United States, *Atmos. Chem. Phys.*, 11, 12197-12216,
875 <https://doi.org/10.5194/acp-11-12197-2011>, 2011.

876

877 Bush, E. and Lemmen, D. S.: Canada's changing climate report, Government of Canada, Ottawa, ON.,
878 444 pp., www.ChangingClimate.ca/CCCR2019, 2019.

879

880 Campos, I., Abrantes, N., Pereira, P., Micaelo, A. C., Vale, C., and Keizer, J. J.: Forest fires as potential
881 triggers for production and mobilization of polycyclic aromatic hydrocarbons to the terrestrial ecosystem,
882 *Land Degrad. Dev.*, 30, 2360-2370, <https://doi.org/10.1002/ldr.3427>, 2019.

883

884 Carter, W. P. L. and Heo, G.: Development of revised SAPRC aromatics mechanisms, *Atmos. Environ.*,
885 77, 404-414, <https://doi.org/10.1016/j.atmosenv.2013.05.021>, 2013.

886

887 Carter, M.C., and Foster, C.D., Prescribed burning and productivity in southern pine forests: a review:
888 *Forest Ecol. Mgmt.*, 191, 93-109, 2004.

889

890 Cascio, W. E.: Wildland fire smoke and human health, *Sci. Total Environ.*, 624, 586-595,
891 <https://doi.org/10.1016/j.scitotenv.2017.12.086>, 2018.

892

893 Chen, J., Anderson, K., Pavlovic, R., Moran, M. D., Englefield, P., Thompson, D. K., Munoz-Alpizar, R.,
894 and Landry, H.: The FireWork v2.0 air quality forecast system with biomass burning emissions from the
895 Canadian Forest Fire Emissions Prediction System v2.03, *Geosci. Model Dev.*, 12, 3283-3310,
896 <https://doi.org/10.5194/gmd-12-3283-2019>, 2019.

897

898 Cherry, N. and Haynes, W.: Effects of the Fort McMurray wildfires on the health of evacuated workers:
899 follow-up of 2 cohorts, *Can. Med. Assoc. J.*, 5, E638-E645, <https://doi.org/10.9778/cmajo.20170047>,
900 2017.

901

902 Ciccioli, P., Centritto, M., and Loreto, F.: Biogenic volatile organic compound emissions from vegetation
903 fires, *Plant, Cell Environ.*, 37, 1810-1825, <https://doi.org/10.1111/pce.12336>, 2014.

904

905 Coggon, M. M., Lim, C. Y., Koss, A. R., Sekimoto, K., Yuan, B., Gilman, J. B., Hagan, D. H., Selimovic,
906 V., Zarzana, K. J., Brown, S. S., Roberts, J. M., Müller, M., Yokelson, R., Wisthaler, A., Krechmer, J. E.,
907 Jimenez, J. L., Cappa, C., Kroll, J. H., de Gouw, J., and Warneke, C.: OH chemistry of non-methane
908 organic gases (NMOGs) emitted from laboratory and ambient biomass burning smoke: evaluating the
909 influence of furans and oxygenated aromatics on ozone and secondary NMOG formation, *Atmos. Chem.*
910 *Phys.*, 19, 14875-14899, <https://doi.org/10.5194/acp-19-14875-2019>, 2019.

911

912 Cole, A. S., Steffen, A., Eckley, C. S., Narayan, J., Pilote, M., Tordon, R., Graydon, J. A., St. Louis, V.
913 L., Xu, X., and Branfireun, B. A.: A survey of mercury in air and precipitation across Canada: Patterns
914 and trends, *Atmosphere*, 5, 635-668, <https://doi.org/10.3390/atmos5030635>, 2014.

915 Cubison, M.J., Ortega, A.M., Haves, P.L., Farmer, D.K., Day, D., Lechner, M.J., Brune, W.H., Apel, E.,
916 Diskin, G.S., Fisher, J.A., Fuelberg, H.E., Hecobian, A., Knapp, D.J., Mikoviny, T., Riemer, D., Sachse,
917 G.W., Sessions, W., Weber, R.J., Weinheimer, A.J., Wisthaler, A., and J.L. Jimenez: Effects of aging on
918 organic aerosol from open biomass burning smoke in aircraft and laboratory studies, *Atmos. Chem. Phys.*,
919 11, 12049-12064, doi:10.5194/acp-11-12049-2011, 2011.
920
921 de Gouw, J. A., Warneke, C., Stohl, A., Wollny, A. G., Brock, C. A., Cooper, O. R., Holloway, J. S.,
922 Trainer, M., Fehsenfeld, F. C., Atlas, E. L., Donnelly, S. G., Stroud, V., and Lueb, A.: The VOC
923 composition of merged and aged forest fire plumes from Alaska and Western Canada, *J. Geophys. Res.-*
924 *Atmos*, 111, D10303, <https://doi.org/10.1029/2005JD006175>, 2006.
925
926 de Groot, W. J., Pritchard, J. M., and Lynham, T. J.: Forest floor fuel consumption and carbon emissions
927 in Canadian boreal forest fires, *Can. J. Forest Res.*, 39, 367-382, <https://doi.org/10.1139/x08-192>, 2009.
928
929 Decker, Z. C. J., Zarzana, K. J., Coggon, M., Min, K.-E., Pollack, I., Ryerson, T. B., Peischl, J., Edwards,
930 P., Dubé, W. P., Markovic, M. Z., Roberts, J. M., Veres, P. R., Graus, M., Warneke, C., de Gouw, J.,
931 Hatch, L. E., Barsanti, K. C., and Brown, S. S.: Nighttime chemical transformation in biomass burning
932 plumes: A box model analysis Initialized with aircraft observations, *Environ. Sci. Technol.*, 53, 2529-
933 2538, <https://doi.org/10.1021/acs.est.8b05359>, 2019.
934
935 Decker, Z.C., Wang, S., Novel analysis to quantify plume crosswind heterogeneity applied to biomass
936 burning smoke, *EST*, 2021.
937
938 Ditto, J. C., Joo, T., Slade, J. H., Shepson, P. B., Ng, N. L., and Gentner, D. R.: Nontargeted Tandem
939 Mass Spectrometry Analysis Reveals Diversity and Variability in Aerosol Functional Groups across
940 Multiple Sites, Seasons, and Times of Day, *Environmental Science and Technology Letters*, 7, 60-
941 69, <https://doi.org/10.1021/acs.estlett.9b00702>, 2020.
942
943 Ditto, J. C., He, M., Hass-Mitchell, T. N., Moussa, S. G., Hayden, K., Li, S. M., Liggio, J., Leithead, A.,
944 Lee, P., Wheeler, M. J., Wentzell, J. J. B., and Gentner, D. R.: Atmospheric evolution of emissions from a
945 boreal forest fire: the formation of highly functionalized oxygen-, nitrogen-, and sulfur-containing organic
946 compounds, *Atmos. Chem. Phys.*, 21, 255-267, <https://doi.org/10.5194/acp-21-255-2021>, 2021.
947
948 Ditto, J. C., Machesky, J., and Gentner, D. R.: Analysis of reduced and oxidized nitrogen-containing
949 organic compounds at a coastal site in summer and winter, *Atmos. Chem. Phys.*, 22, 3045-
950 3065, <https://doi.org/10.5194/acp-22-3045-2022>, 2022.
951
952 Donahue, N. M., Epstein, S. A., Pandis, S. N., and Robinson, A. L.: A two-dimensional volatility basis
953 set: 1. organic-aerosol mixing thermodynamics, *Atmos. Chem. Phys.*, 11, 3303-3318,
954 <https://doi.org/10.5194/acp-11-3303-2011>, 2011.
955
956 EPA: Air method, toxic organics-15 (TO-15): Compendium of methods for the determination of toxic
957 organic compounds in ambient air, second edition: Determination of volatile organic compounds (VOCs)
958 in air collected in specially-prepared canisters and analyzed by gas chromatography/mass spectrometry
959 (GC/MS)." EPA 625/R-96/010b, 1999.
960
961 Finlay, S. E., Moffat, A., Gazzard, R., Baker, D., and Murray, V.: Health impacts of wildfires, *PLoS*
962 *Curr.*, 4, e4f959951cce959952c, <https://doi.org/10.1371/4f959951cce2c>, 2012.
963

964 Forestry Canada Fire Danger Rating Group: Development and structure of the Canadian Forest Fire
965 Behaviour Prediction System, Forestry Canada, Headquarters, Fire Danger Group and Science and
966 Sustainable Development Directorate, Ottawa, Information Report ST-X-3, 64 p., 992.
967

968 Garofalo, L. A., Pothier, M. A., Levin, E. J. T., Campos, T., Kreidenweis, S. M., and Farmer, D. K.:
969 Emission and evolution of submicron organic aerosol in smoke from wildfires in the Western United
970 States, *ACS Earth Space Chem.*, 3, 1237-1247, <https://doi.org/10.1021/acsearthspacechem.9b00125>,
971 2019.
972

973 Gilman, J. B., Lerner, B. M., Kuster, W. C., Goldan, P. D., Warneke, C., Veres, P. R., Roberts, J. M., de
974 Gouw, J. A., Burling, I. R., and Yokelson, R. J.: Biomass burning emissions and potential air quality
975 impacts of volatile organic compounds and other trace gases from fuels common in the US, *Atmos.*
976 *Chem. Phys.*, 15, 13915-13938, <https://doi.org/10.5194/acp-15-13915-2015>, 2015.
977

978 Goode, J. G., Yokelson, R. J., Ward, D. E., Susott, R. A., Babbitt, R. E., Davies, M. A., and Hao, W. M.:
979 Measurements of excess O₃, CO₂, CO, CH₄, C₂H₄, C₂H₂, HCN, NO, NH₃, HCOOH, CH₃COOH, HCHO,
980 and CH₃OH in 1997 Alaskan biomass burning plumes by airborne fourier transform infrared spectroscopy
981 (AFTIR), *J. Geophys. Res.*, 105, 22147-22166, <https://doi.org/10.1029/2000JD900287>, 2000.
982

983 Gordon, M., Li, S. M., Staebler, R., Darlington, A., Hayden, K., O'Brien, J., and Wolde, M.: Determining
984 air pollutant emission rates based on mass balance using airborne measurement data over the Alberta oil
985 sands operations, *Atmos. Meas. Tech.*, 8, 3745-3765, <https://doi.org/10.5194/amt-8-3745-2015>, 2015.
986

987 Griffin, D., McLinden, C. A., Dammers, E., Adams, C., Stockwell, C., Warneke, C., Bourgeois, I.,
988 Peischl, J., Ryerson, T. B., Zarzana, K. J., Rowe, J. P., Volkamer, R., Knote, C., Kille, N., Koenig, T. K.,
989 Lee, C. F., Rollins, D., Rickly, P. S., Chen, J., Fehr, L., Bourassa, A., Degenstein, D., Hayden, K.,
990 Mihele, C., Wren, S. N., Liggio, J., Akingunola, A., and Makar, P.: Biomass burning nitrogen dioxide
991 emissions derived from space with TROPOMI: methodology and validation, *Atmos. Meas. Tech.*
992 *Discuss.* [preprint], <https://doi.org/10.5194/amt-2021-223>, in review, 2021.
993

994 Griffith, D. W. T., Mankin, W. G., Coffey, M. T., Ward, D. E., and Riebau, A.: FTIR remote sensing of
995 biomass burning emissions of CO₂, CO, CH₄, CH₂O, NO, NO₂, NH₃, and N₂O, in: *Global Biomass*
996 *Burning: Atmospheric, Climatic, and Biospheric Implications*, edited by: Levine, J. S., MIT Press,
997 Cambridge, MA, United States, 230-241, 1991.
998

999 Guérette, E. A., Paton-Walsh, C., Desservettaz, M., Smith, T. E. L., Volkova, L., Weston, C. J., and
1000 Meyer, C. P.: Emissions of trace gases from Australian temperate forest fires: Emission factors and
1001 dependence on modified combustion efficiency, *Atmos. Chem. Phys.*, 18, 3717-3735,
1002 <https://doi.org/10.5194/acp-18-3717-2018>, 2018.
1003

1004 Hatch, L. E., Luo, W., Pankow, J. F., Yokelson, R. J., Stockwell, C. E., and Barsanti, K. C.: Identification
1005 and quantification of gaseous organic compounds emitted from biomass burning using two-dimensional
1006 gas chromatography–time-of-flight mass spectrometry, *Atmos. Chem. Phys.*, 15, 1865-1899,
1007 <https://doi.org/10.5194/acp-15-1865-2015>, 2015.
1008

1009 Hatch, L. E., Rivas-Ubach, A., Jen, C. N., Lipton, M., Goldstein, A. H., and Barsanti, K. C.:
1010 Measurements of I/SVOCs in biomass-burning smoke using solid-phase extraction disks and two-
1011 dimensional gas chromatography, *Atmos. Chem. Phys.*, 18, 17801-17817, [https://doi.org/10.5194/acp-18-](https://doi.org/10.5194/acp-18-17801-2018)
1012 [17801-2018](https://doi.org/10.5194/acp-18-17801-2018), 2018.
1013

1014 Hatch, L. E., Yokelson, R. J., Stockwell, C. E., Veres, P. R., Simpson, I. J., Blake, D. R., Orlando, J. J.,
1015 and Barsanti, K. C.: Multi-instrument comparison and compilation of non-methane organic gas emissions
1016 from biomass burning and implications for smoke-derived secondary organic aerosol precursors, *Atmos.*
1017 *Chem. Phys.*, 17, 1471-1489, <https://doi.org/10.5194/acp-17-1471-2017>, 2017.

1018
1019 Hatch, L. E., Jen, C. N., Kreisberg, N. M., Selimovic, V., Yokelson, R. J., Stamatis, C., York, R. A.,
1020 Foster, D., Stephens, S. L., Goldstein, A. H., and Barsanti, K. C.: Highly speciated measurements of
1021 terpenoids emitted from laboratory and mixed-conifer forest prescribed fires, *Environ. Sci. Technol.*, 53,
1022 9418-9428, <https://doi.org/10.1021/acs.est.9b02612>, 2019.

1023
1024 Hecobian, A., Liu, Z., Hennigan, C. J., Huey, L. G., Jimenez, J. L., Cubison, M. J., Vay, S., Diskin, G. S.,
1025 Sachse, G. W., Wisthaler, A., Mikoviny, T., Weinheimer, A. J., Liao, J., Knapp, D. J., Wennberg, P. O.,
1026 Kürten, A., Crounse, J. D., Clair, J. S., Wang, Y., and Weber, R. J.: Comparison of chemical
1027 characteristics of 495 biomass burning plumes intercepted by the NASA DC-8 aircraft during the
1028 ARCTAS/CARB-2008 field campaign, *Atmos. Chem. Phys.*, 11, 13325-13337,
1029 <https://doi.org/10.5194/acp-11-13325-2011>, 2011.

1030
1031 Hodshire, A. L., Akherati, A., Alvarado, M. J., Brown-Steiner, B., Jathar, S. H., Jimenez, J. L.,
1032 Kreidenweis, S. M., Lonsdale, C. R., Onasch, T. B., Ortega, A. M., and Pierce, J. R.: Aging effects on
1033 biomass burning aerosol mass and composition: A critical review of field and laboratory studies, *Environ.*
1034 *Sci. Technol.*, 53, 10007-10022, <https://doi.org/10.1021/acs.est.9b02588>, 2019.

1035
1036 Hosseini, S., Urbanski, S., Dixit, P., Li, Q., Burling, I., Yokelson, R., Johnson, T.E., Sharivastava, M.,
1037 Jung, H., Weise, D.R., Miller, W., and Cocker, D.: Laboratory characterization of PM emissions from
1038 combustion of wildland biomass fuels, *J. Geophys. Res.*, 118, 9914-9929,
1039 <https://doi.org/10.1002/jgrd.50481>, 2013.

1040
1041 Jia, Y., Yu, G., Gao, Y., He, N., Wang, Q., Jiao, C., and Zuo, Y.: Global inorganic nitrogen dry
1042 deposition inferred from ground- and space-based measurements, *Sci. Rep.*, 6, 19810,
1043 <https://doi.org/10.1038/srep19810>, 2016.

1044
1045 Johnstone, J. F., Hollingsworth, T. N., Chapin III, F. S., and Mack, M. C.: Changes in fire regime break
1046 the legacy lock on successional trajectories in Alaskan boreal forest, *Global Change Biol.*, 16, 1281-1295,
1047 <https://doi.org/10.1111/j.1365-2486.2009.02051.x>, 2010.

1048
1049 Jolley, M.D., Coe, H., McFiggans, G., Taylor, J.W., O'Shea, S.J., Le Breton, M., Bauguitte, S.J.-B.,
1050 Moller, S., Di Carlo, P., Aruffo, E., Palmer, P.I., Lee, J.D., Percival, C.J., and Gallagher, M.W.:
1051 Properties and evolution of biomass burning organic aerosol from Canadian boreal forest fires, *Atmos.*
1052 *Chem. Phys.*, 15, 3077-3095, doi:10.5194/acp-15-3077-2015, 2015.

1053
1054 Juncosa Calahorrano, J. F., Lindaas, J., O'Dell, K., Palm, B. B., Peng, Q., Flocke, F., Pollack, I. B.,
1055 Garofalo, L. A., Farmer, D. K., Pierce, J. R., Collett Jr., J. L., Weinheimer, A., Campos, T., Hornbrook,
1056 R. S., Hall, S. R., Ullmann, K., Pothier, M. A., Apel, E. C., Permar, W., Hu, L., Hills, A. J., Montzka, D.,
1057 Tyndall, G., Thornton, J. A., and Fischer, E. V.: Daytime oxidized reactive nitrogen partitioning in
1058 western U.S. wildfire smoke plumes, *J. Geophys. Res.-Atmos*, 126, e2020JD033484,
1059 <https://doi.org/10.1029/2020JD033484>, 2021.

1060
1061 Kaiser, J. W., Heil, A., Andreae, M. O., Benedetti, A., Chubarova, N., Jones, L., Morcrette, J.-J.,
1062 Razinger, M., Schultz, M. G., Suttie, M., and van der Werf, G. R.: Biomass burning emissions estimated
1063 with a global fire assimilation system based on observed fire radiative power, *Biogeosciences*, 9, 527–
1064 554, <https://doi.org/10.5194/bg-9-527-2012>, 2012.

1065 Kallenborn, R., Halsall, C., Dellong, M., and Carlsson, P.: The influence of climate change on the global
1066 distribution and fate processes of anthropogenic persistent organic pollutants, *J. Environ. Monitor.*, 14,
1067 2854-2869, <https://doi.org/10.1039/c2em30519d>, 2012.

1068

1069 Khare, P., Marcotte, A., Sheu, R., Walsh, A. N., Ditto, J. C., and Gentner, D. R.: Advances in offline
1070 approaches for trace measurements of complex organic compound mixtures via soft ionization and high-
1071 resolution tandem mass spectrometry, *J. Chromatogr. A*, 1598, 163-
1072 174, <https://doi.org/10.1016/j.chroma.2019.03.037>, 2019.

1073

1074 Kodros, J. K., Papanastasiou, D. K., Paglione, M., Masiol, M., Squizzato, S., Florou, K., Skyllakou, K.,
1075 Kaltsonoudis, C., Nenes, A., and Pandis, S. N.: Rapid dark aging of biomass burning as an overlooked
1076 source of oxidized organic aerosol, *P. Natl. Acad. Sci. USA*, 117, 33028-33033,
1077 <https://doi.org/10.1073/pnas.2010365117>, 2020.

1078

1079 Kondo, Y., Sahu, L., Moteki, N., Khan, F., Takegawa, N., Liu, X., Koike, M., and Miyakawa, T.:
1080 Consistency and traceability of black carbon measurements made by laser-induced incandescence,
1081 thermal-optical transmittance, and filter-based photo-absorption techniques, *Aerosol Sci. Tech.*, 45, 295-
1082 312, <https://doi.org/10.1080/02786826.2010.533215>, 2011.

1083

1084 Koss, A. R., Sekimoto, K., Gilman, J. B., Selimovic, V., Coggon, M. M., Zarzana, K. J., Yuan, B.,
1085 Lerner, B. M., Brown, S. S., Jimenez, J. L., Krechmer, J., Roberts, J. M., Warneke, C., Yokelson, R. J.,
1086 and de Gouw, J.: Non-methane organic gas emissions from biomass burning: identification,
1087 quantification, and emission factors from PTR-ToF during the FIREX 2016 laboratory experiment,
1088 *Atmos. Chem. Phys.*, 18, 3299-3319, <https://doi.org/10.5194/acp-18-3299-2018>, 2018.

1089

1090 Kotchenruther, R. A. and Hobbs, P. V.: Humidification factors of aerosols from biomass burning in
1091 Brazil, *J. Geophys. Res.-Atmos*, 103, 32081-32089, <https://doi.org/10.1029/98JD00340>, 1998.

1092

1093 Kou-Giesbrecht, S. and Menge, D.: Nitrogen-fixing trees could exacerbate climate change under elevated
1094 nitrogen deposition, *Nat. Commun.*, 10, 1493, <https://doi.org/10.1038/s41467-019-09424-2>, 2019.

1095

1096 Kumar, V., Chandra, B. P., and Sinha, V.: Large unexplained suite of chemically reactive compounds
1097 present in ambient air due to biomass fires, *Sci. Rep.*, 8, 626, <https://doi.org/10.1038/s41598-017-19139-3>, 2018.

1098

1099

1100 Laborde, M., Mertes, P., Zieger, P., Dommen, J., Baltensperger, U., and Gysel, M.: Sensitivity of the
1101 Single Particle Soot Photometer to different black carbon types, *Atmos. Meas. Tech.*, 5, 1031-1043,
1102 <https://doi.org/10.5194/amt-5-1031-2012>, 2012.

1103

1104 Landis, M. S., Edgerton, E. S., White, E. M., Wentworth, G. R., Sullivan, A. P., and Dillner, A. M.: The
1105 impact of the 2016 Fort McMurray Horse River Wildfire on ambient air pollution levels in the Athabasca
1106 Oil Sands Region, Alberta, Canada, *Sci. Total Environ.*, 618, 1665-1676,
1107 <https://doi.org/10.1016/j.scitotenv.2017.10.008>, 2018.

1108

1109 Lee, T., Sullivan, A. P., Mack, L., Jimenez, J. L., Kreidenweis, S. M., Onasch, T. B., Worsnop, D. R.,
1110 Malm, W., Wold, C. E., Hao, W. M., and Collett Jr, J. L.: Chemical smoke marker emissions during
1111 flaming and smoldering phases of laboratory open burning of wildland fuels, *Aerosol Sci. Tech.*, 44, i-v,
1112 <https://doi.org/10.1080/02786826.2010.499884>, 2010.

1113

1114 Leifer, I., Melton, C. Tratt, D.M., Buckland, K.N., Clarisse, L., Coheur, P., Frash, J., Gupta, M., Johnson,
1115 P.D., Leen, J.B., Van Damme, M., Whitburn, S., and Yurganov, L.: Remote sensing and in situ

1116 measurements of methane and ammonia emissions from a megacity dairy complex: Chino, CA, Environ.
 1117 Poll., 221, 37-51, <https://doi.org/10.1016/j.envpol.2016.09.083>, 2017.

1118

1119 Lerner, B. M., Gilman, J. B., Aikin, K. C., Atlas, E. L., Goldan, P. D., Graus, M., Hendershot, R.,
 1120 Isaacman-VanWertz, G. A., Koss, A., Kuster, W. C., Lueb, R. A., McLaughlin, R. J., Peischl, J., Sueper,
 1121 D., Ryerson, T. B., Tokarek, T. W., Warneke, C., Yuan, B., and de Gouw, J. A.: An improved, automated
 1122 whole air sampler and gas chromatography mass spectrometry analysis system for volatile organic
 1123 compounds in the atmosphere, *Atmos. Meas. Tech.*, 10, 291-313, [https://doi.org/10.5194/amt-10-291-](https://doi.org/10.5194/amt-10-291-2017)
 1124 2017, 2017.

1125

1126 Li, Y., Poschl, U., and Shiraiwa, M.: Molecular corridors and parameterizations of volatility in the
 1127 chemical evolution of organic aerosols, *Atmos. Chem. Phys.*, 16, 3327-3344, [https://doi.org/10.5194/acp-](https://doi.org/10.5194/acp-16-3327-2016)
 1128 16-3327-2016, 2016.

1129

1130 Lindaas, J., Pollack, I. B., Garofalo, L. A., Pothier, M. A., Farmer, D. K., Kreidenweis, S. M., Campos, T.
 1131 L., Flocke, F., Weinheimer, A. J., Montzka, D. D., Tyndall, G. S., Palm, B. B., Peng, Q., Thornton, J. A.,
 1132 Permar, W., Wielgasz, C., Hu, L., Ottmar, R. D., Restaino, J. C., Hudak, A. T., Ku, I.-T., Zhou, Y., Sive,
 1133 B. C., Sullivan, A., Collett Jr, J. L., and Fischer, E. V.: Emissions of reactive nitrogen from western U.S.
 1134 wildfires during summer 2018, *J. Geophys. Res.-Atmos*, 125, e2020JD032657,
 1135 <https://doi.org/10.1029/2020JD032657>, 2020.

1136

1137 Liu, X., Huey, L. G., Yokelson, R. J., Selimovic, V., Simpson, I. J., Müller, M., Jimenez, J. L.,
 1138 Campuzano-Jost, P., Beyersdorf, A. J., Blake, D. R., Butterfield, Z., Choi, Y., Crouse, J. D., Day, D. A.,
 1139 Diskin, G. S., Dubey, M. K., Fortner, E., Hanisco, T. F., Hu, W., King, L. E., Kleinman, L., Meinardi, S.,
 1140 Mikoviny, T., Onasch, T. B., Palm, B. B., Peischl, J., Pollack, I. B., Ryerson, T. B., Sachse, G. W.,
 1141 Sedlacek, A. J., Shilling, J. E., Springston, S., St. Clair, J. M., Tanner, D. J., Teng, A. P., Wennberg, P.
 1142 O., Wisthaler, A., and Wolfe, G. M.: Airborne measurements of western U.S. wildfire emissions:
 1143 Comparison with prescribed burning and air quality implications, *J. Geophys. Res.-Atmos.*, 122, 6108-
 1144 6129, <https://doi.org/10.1002/2016JD026315>, 2017.

1145

1146 Loehman, R. A., Reinhardt, E., and Riley, K. L.: Wildland fire emissions, carbon, and climate: Seeing the
 1147 forest and the trees – A cross-scale assessment of wildfire and carbon dynamics in fire-prone, forested
 1148 ecosystems, *For. Ecol. Manag.*, 317, 9-19, <https://doi.org/10.1016/j.foreco.2013.04.014>, 2014.

1149

1150 Matz, C.J., Egyed, M., Xi, G., Racine, J., Pavlovic, R., Rittmaster, R., Henderson, S.B., and Stieb, D.M.:
 1151 Health impact analysis of PM_{2.5} from wildfire smoke in Canada (2013-2015, 2017-2018), *Sci. Total*
 1152 *Environ.*, 725(10), <https://doi.org/10.1016/j.scitotenv.2020.138506>, 2020.

1153

1154 May, A. A., McMeeking, G. R., Lee, T., Taylor, J. W., Craven, J. S., Burling, I., Sullivan, A. P., Akagi,
 1155 S., Collett Jr., J. L., Flynn, M., Coe, H., Urbanski, S. P., Seinfeld, J. H., Yokelson, R. J., and Kreidenweis,
 1156 S. M.: Aerosol emissions from prescribed fires in the United States: A synthesis of laboratory and aircraft
 1157 measurements, *J. Geophys. Res.-Atmos*, 119, 11826-11849, <https://doi.org/10.1002/2014JD021848>,
 1158 2014.

1159

1160 McGee, T., McFarlane, B., and Tymstra, C.: Chapter 3 - Wildfire: A Canadian Perspective, in: *Wildfire*
 1161 *Hazards, Risks and Disasters*, edited by: Shroder, J. F., and Paton, D., Elsevier, Amsterdam, The
 1162 Netherlands, 35-58, <https://doi.org/10.1016/B978-0-12-410434-1.00003-8>, 2015.

1163

1164 McLagan, D. S., Stupple, G. W., Darlington, A., Hayden, K., and Steffen, A.: Where there is smoke there
 1165 is mercury: Assessing boreal forest fire mercury emissions using aircraft and highlighting uncertainties

1166 associated with upscaling emissions estimates, *Atmos. Chem. Phys.*, 21, 5635-5653,
1167 <https://doi.org/10.5194/acp-21-5635-2021>, 2021.

1168

1169 McMeeking, G. R., Kreidenweis, S. M., Baker, S., Carrico, C. M., Chow, J. C., Collett Jr., J. L., Hao, W.
1170 M., Holden, A. S., Kirchstetter, T. W., Malm, W. C., Moosmüller, H., Sullivan, A. P., and Wold, C. E.:
1171 Emissions of trace gases and aerosols during the open combustion of biomass in the laboratory, *J.*
1172 *Geophys. Res.-Atmos.*, 114, D19210, <https://doi.org/10.1029/2009JD011836>, 2009.

1173

1174 Miller, D. J., Sun, K., Zondlo, M. A., Kanter, D., Dubovik, O., Welton, E. J., Winker, D. M., and Ginoux,
1175 P.: Assessing boreal forest fire smoke aerosol impacts on U.S. air quality: A case study using multiple
1176 data sets, *J. Geophys. Res.-Atmos.*, 116, D22209, <https://doi.org/10.1029/2011JD016170>, 2011.

1177

1178 Moteki, N. and Kondo, Y.: Dependence of laser-induced incandescence on physical properties of black
1179 carbon aerosols: Measurements and theoretical interpretation, *Aerosol Sci. Tech.*, 44, 663-675,
1180 <https://doi.org/10.1080/02786826.2010.484450>, 2010.

1181

1182 Moussa, S. G., Leithead, A., Li, S. M., Chan, T. W., Wentzell, J. J. B., Stroud, C., Zhang, J. H., Lee, P.,
1183 Lu, G., Brook, J. R., Hayden, K., Narayan, J., and Liggio, J.: Emissions of hydrogen cyanide from on-
1184 road gasoline and diesel vehicles, *Atmos. Environ.*, 131, 185-195,
1185 <https://doi.org/10.1016/j.atmosenv.2016.01.050>, 2016.

1186

1187 NRCan, Blueprint for wildland fire science in Canada (2019-2029), Sankey, S., Technical
1188 Coordinator. Canadian Forest Service, Northern Forestry Centre, Edmonton, AB, 45p,
1189 <https://cfs.nrcan.gc.ca/publications?id=39429>, 2018.

1190

1191 O'Brien, J. J., Loudermilk, E. L., Hornsby, B. S., Hudak, A. T., Bright, B. C., Dickinson, M. B., Hiers, J.
1192 K., Teske, C., and Ottmar, R. D.: High-resolution infrared thermography for capturing wildland fire
1193 behaviour: RxCADRE 2012, *Int. J. Wildland Fire*, 25, 62-75, <https://doi.org/10.1071/WF14165>, 2015.

1194

1195 Palm, B. B., Peng, Q., Fredrickson, C. D., Lee, B. H., Garofalo, L. A., Pothier, M. A., Kreidenweis, S.
1196 M., Farmer, D. K., Pokhrel, R. P., Shen, Y., Murphy, S. M., Permar, W., Hu, L., Campos, T. L., Hall, S.
1197 R., Ullmann, K., Zhang, X., Flocke, F., Fischer, E. V., and Thornton, J. A.: Quantification of organic
1198 aerosol and brown carbon evolution in fresh wildfire plumes, *P. Natl. Acad. Sci. USA*, 117, 29469-29477,
1199 <https://doi.org/10.1073/pnas.2012218117>, 2020.

1200

1201 Peng, Q., Palm, B. B., Melander, K. E., Lee, B. H., Hall, S. R., Ullmann, K., Campos, T., Weinheimer, A.
1202 J., Apel, E. C., Hornbrook, R. S., Hills, A. J., Montzka, D. D., Flocke, F., Hu, L., Permar, W., Wielgasz,
1203 C., Lindaas, J., Pollack, I. B., Fischer, E. V., Bertram, T. H., and Thornton, J. A.: HONO Emissions from
1204 Western U.S. Wildfires Provide Dominant Radical Source in Fresh Wildfire Smoke, *Environ. Sci.*
1205 *Technol.*, 54, 5954-5963, <https://doi.org/10.1021/acs.est.0c00126>, 2020.

1206

1207 Permar, W., Wang, Q., Selimovic, V., Wielgasz, C., Yokelson, R. J., Hornbrook, R. S., Hills, A. J., Apel,
1208 E. C., Ku, I.-T., Zhou, Y., Sive, B. C., Sullivan, A. P., Collett Jr, J. L., Campos, T. L., Palm, B. B., Peng,
1209 Q., Thornton, J. A., Garofalo, L. A., Farmer, D. K., Kreidenweis, S. M., Levin, E. J. T., DeMott, P. J.,
1210 Flocke, F., Fischer, E. V., and Hu, L.: Emissions of trace organic gases from western U.S. wildfires based
1211 on WE-CAN aircraft measurements, *J. Geophys. Res.-Atmos.*, 126, e2020JD033838,
1212 <https://doi.org/10.1029/2020JD033838>, 2021.

1213

1214 Randerson, J. T., Liu, H., Flanner, M. G., Chambers, S. D., Jin, Y., Hess, P. G., Pfister, G., Mack, M. C.,
1215 Treseder, K. K., Welp, L. R., Chapin, F. S., Harden, J. W., Goulden, M. L., Lyons, E., Neff, J. C., Schuur,

1216 E. A., and Zender, C. S.: The impact of boreal forest fire on climate warming, *Science*, 314, 1130-1132,
1217 <https://doi.org/10.1126/science.1132075>, 2006.
1218
1219 Reid, C. E., Brauer, M., Johnston, F. H., Jerrett, M., Balmes, J. R., and Elliott, C. T.: Critical review of
1220 health impacts of wildfire smoke exposure, *Environ. Health Persp.*, 124, 1334-1343,
1221 <https://doi.org/10.1289/ehp.1409277>, 2016.
1222
1223 Reid, J. S., Koppmann, R., Eck, T. F., and Eleuterio, D. P.: A review of biomass burning emissions part
1224 II: intensive physical properties of biomass burning particles, *Atmos. Chem. Phys.*, 5, 799-825,
1225 <https://doi.org/10.5194/acp-5-799-2005>, 2005.
1226
1227 Roberts, J. M., Stockwell, C. E., Yokelson, R. J., de Gouw, J., Liu, Y., Selimovic, V., Koss, A. R.,
1228 Sekimoto, K., Coggon, M. M., Yuan, B., Zarzana, K. J., Brown, S. S., Santin, C., Doerr, S. H., and
1229 Warneke, C.: The nitrogen budget of laboratory-simulated western US wildfires during the FIREX 2016
1230 Fire Lab study, *Atmos. Chem. Phys.*, 20, 8807-8826, <https://doi.org/10.5194/acp-20-8807-2020>, 2020.
1231
1232 Roberts, G., Wooster, M. J., Xu, W., Freeborn, P. H., Morcrette, J. J., Jones, L., Benedetti, A., Jiangping,
1233 H., Fisher, D., and Kaiser, J. W.: LSA SAF Meteosat FRP products – Part 2: Evaluation and
1234 demonstration for use in the Copernicus Atmosphere Monitoring Service (CAMS), *Atmos. Chem. Phys.*,
1235 15, 13241-13267, <https://doi.org/10.5194/acp-15-13241-2015>, 2015.
1236
1237 Rogers, C. F., Hudson, J. G., Hallett, J., and Penner, J. E.: Cloud Droplet Nucleation by Crude-Oil Smoke
1238 and Coagulated Crude-Oil Wood Smoke Particles, *Atmos. Environ. a-Gen*, 25, 2571-2580,
1239 [https://doi.org/10.1016/0960-1686\(91\)90174-6](https://doi.org/10.1016/0960-1686(91)90174-6), 1991.
1240
1241 Rogers, H. M., Ditto, J. C., and Gentner, D. R.: Evidence for impacts on surface-level air quality in the
1242 northeastern US from long-distance transport of smoke from North American fires during the Long Island
1243 Sound Tropospheric Ozone Study (LISTOS) 2018, *Atmos. Chem. Phys.*, 20, 671-
1244 682, <https://doi.org/10.5194/acp-20-671-2020>, 2020.
1245
1246 Schwarz, J. P., Gao, R. S., Fahey, D. W., Thomson, D. S., Watts, L. A., Wilson, J. C., Reeves, J. M.,
1247 Darbeheshti, M., Baumgardner, D. G., Kok, G. L., Chung, S. H., Schulz, M., Hendricks, J., Lauer, A.,
1248 Kärcher, B., Slowik, J. G., Rosenlof, K. H., Thompson, T. L., Langford, A. O., Loewenstein, M., and
1249 Aikin, K. C.: Single-particle measurements of midlatitude black carbon and light-scattering aerosols from
1250 the boundary layer to the lower stratosphere, *J. Geophys. Res.-Atmos*, 111, D16207,
1251 <https://doi.org/10.1029/2006JD007076>, 2006.
1252
1253 Seidl, R., Thom, D., Kautz, M., Martin-Benito, D., Peltoniemi, M., Vacchiano, G., Wild, J., Ascoli, D.,
1254 Petr, M., Honkaniemi, J., Lexer, M. J., Trotsiuk, V., Mairota, P., Svoboda, M., Fabrika, M., Nagel, T. A.,
1255 and Reyer, C. P. O.: Forest disturbances under climate change, *Nat. Clim. Change*, 7, 395-402,
1256 <https://doi.org/10.1038/nclimate3303>, 2017.
1257
1258 Seinfeld, J. H. and Pandis, S. N.: *Atmospheric chemistry and physics: from air pollution to climate*
1259 *change*, John Wiley & Sons, New York, 1998.
1260
1261 Sekimoto, K., Li, S.-M., Yuan, B., Koss, A., Coggon, M., Warneke, C., and de Gouw, J.: Calculation of
1262 the sensitivity of proton-transfer-reaction mass spectrometry (PTR-MS) for organic trace gases using
1263 molecular properties, *Int. J. Mass Spectrom.*, 421, 71-94, <https://doi.org/10.1016/j.ijms.2017.04.006>,
1264 2017.
1265

1266 Sheu, R., Marcotte, A., Khare, P., Charan, S., Ditto, J. C., and Gentner, D. R.: Advances in offline
1267 approaches for chemically speciated measurements of trace gas-phase organic compounds via adsorbent
1268 tubes in an integrated sampling-to-analysis system, *J. Chromatogr. A*, 1575, 80-
1269 90, <https://doi.org/10.1016/j.chroma.2018.09.014>, 2018.

1270
1271 Simoneit, B. R. T., Schauer, J. J., Nolte, C. G., Oros, D. R., Elias, V. O., Fraser, M. P., Rogge, W. F., and
1272 Cass, G. R.: Levoglucosan, a tracer for cellulose in biomass burning and atmospheric particles, *Atmos.*
1273 *Environ.*, 33, 173-182, [https://doi.org/10.1016/S1352-2310\(98\)00145-9](https://doi.org/10.1016/S1352-2310(98)00145-9), 1999.

1274
1275 Simpson, I. J., Akagi, S. K., Barletta, B., Blake, N. J., Choi, Y., Diskin, G. S., Fried, A., Fuelberg, H. E.,
1276 Meinardi, S., Rowland, F. S., Vay, S. A., Weinheimer, A. J., Wennberg, P. O., Wiebring, P., Wisthaler,
1277 A., Yang, M., Yokelson, R. J., and Blake, D. R.: Boreal forest fire emissions in fresh Canadian smoke
1278 plumes: C₁-C₁₀ volatile organic compounds (VOCs), CO₂, CO, NO₂, NO, HCN and CH₃CN, *Atmos.*
1279 *Chem. Phys.*, 11, 6445-6463, <https://doi.org/10.5194/acp-11-6445-2011>, 2011.

1280
1281 Singh, H. B., Anderson, B. E., Brune, W. H., Cai, C., Cohen, R. C., Crawford, J. H., Cubison, M. J.,
1282 Czech, E. P., Emmons, L., Fuelberg, H. E., Huey, G., Jacob, D. J., Jimenez, J. L., Kadowela, A., Kondo,
1283 Y., Mao, J., Olson, J. R., Sachse, G. W., Vay, S. A., Weinheimer, A., Wennberg, P. O., and Wisthaler, A.:
1284 Pollution influences on atmospheric composition and chemistry at high northern latitudes: Boreal and
1285 California forest fire emissions, *Atmos. Environ.*, 44, 4553-4564,
1286 <https://doi.org/10.1016/j.atmosenv.2010.08.026>, 2010.

1287
1288 Stephens, M., Turner, N., and Sandberg, J.: Particle identification by laser-induced incandescence in a
1289 solid-state laser cavity, *Appl. Optics*, 42, 3726-3736, <https://doi.org/10.1364/ao.42.003726>, 2003.

1290
1291 Stockwell, C. E., Veres, P. R., Williams, J., and Yokelson, R. J.: Characterization of biomass burning
1292 emissions from cooking fires, peat, crop residue, and other fuels with high-resolution proton-transfer-
1293 reaction time-of-flight mass spectrometry, *Atmos. Chem. Phys.*, 15, 845-865, <https://doi.org/10.5194/acp-15-845-2015>, 2015.

1294
1295 Stockwell, C. E., Kupc, A., Witkowski, B., Talukdar, R. K., Liu, Y., Selimovic, V., Zarzana, K. J.,
1296 Sekimoto, K., Warneke, C., Washenfelder, R. A., Yokelson, R. J., Middlebrook, A. M., and Roberts, J.
1297 M.: Characterization of a catalyst-based conversion technique to measure total particulate nitrogen and
1298 organic carbon and comparison to a particle mass measurement instrument, *Atmos. Meas. Tech.*, 11,
1299 2749-2768, <https://doi.org/10.5194/amt-11-2749-2018>, 2018.

1300
1301 Stockwell, C. E., Bela, M., Coggon, M. M., Gkatzelis, G. I., Wiggins, E. B., Gargulinski, E. M., Shingler,
1302 T., Fenn, M., Griffin, D., Holmes, C. D., Ye, X., Saide, P. E., Bourgeois, I., Peischl, J., Womack, C. C.,
1303 Washenfelder, R. A., Veres, P. R., Neuman, J. A., Gilman, J. B., Lamplugh, A., Schwantes, R. H.,
1304 McKeen, S. A., Wisthaler, A., Piel, F., Guo, H., Campuzano-Jost, P., Jimenez, J. L., Fried, A., Hanisco,
1305 T. F., Huey, L. G., Kondragunta, S., Zhang, X., Perring, A., Katich, J. M., Diskin, G. S., Nowak, J. B.,
1306 Bui, T. P., Halliday, H. S., Pereira, G., James, E. P., Ahmadov, R., McLinden, C. A., Soja, A. J., Moore,
1307 R. H., Hair, J. W., and Warneke, C.: Airborne emission rate measurements validate remote sensing
1308 observations and emission inventories of western U.S. wildfires, submitted to *ES&T*, in review, 2021.

1309
1310 Urbanski, S.: Wildland fire emissions, carbon, and climate: Emission factors, *For. Ecol. Manag.*, 317, 51-
1311 60, <https://doi.org/10.1016/j.foreco.2013.05.045>, 2014.

1312
1313 Urbanski, S. P.: Combustion efficiency and emission factors for wildfire-season fires in mixed conifer
1314 forests of the Northern Rocky Mountains, US, *Atmos. Chem. Phys.*, 13, 7241-7262,
1315 <https://doi.org/10.5194/acp-13-7241-2013>, 2013.

1316

1317
1318 Urbanski, S. P., Hao, W. M., and Baker, S.: Chapter 4 Chemical Composition of Wildland Fire
1319 Emissions, in: *Developments in Environmental Science*, edited by: Bytnerowicz, A., Arbaugh, M. J.,
1320 Riebau, A. R., and Andersen, C., Elsevier, Amsterdam, The Netherlands, 79-107,
1321 [https://doi.org/10.1016/S1474-8177\(08\)00004-1](https://doi.org/10.1016/S1474-8177(08)00004-1), 2009.
1322
1323 Uresk, D. W., Cline, J. F., and Rickard, W. H.: Growth rates of a cheatgrass community and some
1324 associated factors, *J. Range Manage.*, 32, 168-170, <https://doi.org/10.2307/3897114>, 1979.
1325
1326 US EPA, SPECIATE Version 4.5 Database Development Documentation, Final Report EPA/600/R-
1327 16/294, September 2016. Available <https://www.epa.gov/air-emissions-modeling/speciate>.
1328
1329 van der Werf, G. R., Randerson, J. T., Giglio, L., Collatz, G. J., Kasibhatla, P. S., and Arellano Jr, A. F.:
1330 Interannual variability in global biomass burning emissions from 1997 to 2004, *Atmos. Chem. Phys.*, 6,
1331 3423-3441, <https://doi.org/10.5194/acp-6-3423-2006>, 2006.
1332
1333 van der Werf, G. R., Randerson, J. T., Giglio, L., van Leeuwen, T. T., Chen, Y., Rogers, B. M., Mu, M.,
1334 van Marle, M. J. E., Morton, D. C., Collatz, G. J., Yokelson, R. J., and Kasibhatla, P. S.: Global fire
1335 emissions estimates during 1997–2016, *Earth Syst. Sci. Data*, 9, 697–720, [https://doi.org/10.5194/essd-9-](https://doi.org/10.5194/essd-9-697-2017)
1336 697-2017, 2017.
1337
1338 Veres, P., Roberts, J. M., Burling, I. R., Warneke, C., de Gouw, J., and Yokelson, R. J.: Measurements of
1339 gas-phase inorganic and organic acids from biomass fires by negative-ion proton-transfer chemical-
1340 ionization mass spectrometry, *J. Geophys. Res.-Atmos.*, 115, D23302,
1341 <https://doi.org/10.1029/2010JD014033>, 2010.
1342
1343 Ward, D. E. and Radke, L. F.: Emissions measurements from vegetation fires: A comparative evaluation
1344 of methods and results, in: *Fire in the Environment: The Ecological, Atmospheric, and Climatic*
1345 *Importance of Vegetation Fires*. Dahlem Workshop Reports: Environmental Sciences Research Report
1346 13, edited by: Crutzen, P. J., and Goldammer, J. G., John Wiley & Sons, Chischester, England, 53-76,
1347 1993.
1348
1349 Whitman, E., Parisien, M. A., Thompson, D. K., and Flannigan, M. D.: Short-interval wildfire and
1350 drought overwhelm boreal forest resilience, *Sci. Rep.*, 9, 18796, [https://doi.org/10.1038/s41598-019-](https://doi.org/10.1038/s41598-019-55036-7)
1351 55036-7, 2019.
1352
1353 Wiggins, E. B., Andrews, A., Sweeney, C., Miller, J. B., Miller, C. E., Veraverbeke, S., Commane, R.,
1354 Wofsy, S., Henderson, J. M., and Randerson, J. T.: Boreal forest fire CO and CH₄ emission factors
1355 derived from tower observations in Alaska during the extreme fire season of 2015, *Atmos. Chem. Phys.*,
1356 21, 8557-8574, <https://doi.org/10.5194/acp-21-8557-2021>, 2021.
1357
1358 Wiggins, E. B., Soja, A. J., Gargulinski, E., Halliday, H. S., Pierce, R. B., Schmidt, C. C., Nowak, J. B.,
1359 DiGangi, J. P., Diskin, G. S., Katich, J. M., Perring, A. E., Schwarz, J. P., Anderson, B. E., Chen, G.,
1360 Crosbie, E. C., Jordan, C., Robinson, C. E., Sanchez, K. J., Shingler, T. J., Shook, M., Thornhill, K. L.,
1361 Winstead, E. L., Ziemba, L. D., and Moore, R. H.: High Temporal Resolution Satellite Observations of
1362 Fire Radiative Power Reveal Link Between Fire Behavior and Aerosol and Gas Emissions, *Geophys. Res.*
1363 *Lett.*, 47, <https://doi.org/10.1029/2020GL090707>, 2020.
1364
1365 Wotton, B. M., Nock, C. A., and Flannigan, M. D.: Forest fire occurrence and climate change in Canada,
1366 *Int. J. Wildland Fire*, 19, 253-271, <https://doi.org/10.1071/WF09002>, 2010.
1367

1368 Yokelson, R. J., Bertschi, I. T., Christian, T. J., Hobbs, P. V., Ward, D. E., and Hao, W. M.: Trace gas
1369 measurements in nascent, aged, and cloud-processed smoke from African savanna fires by airborne
1370 Fourier transform infrared spectroscopy (AFTIR), *J. Geophys. Res.-Atmos*, 108, 8478,
1371 <https://doi.org/10.1029/2002JD002322>, 2003.
1372

1373 Yokelson, R. J., Burling, I. R., Gilman, J. B., Warneke, C., Stockwell, C. E., de Gouw, J., Akagi, S. K.,
1374 Urbanski, S. P., Veres, P., Roberts, J. M., Kuster, W. C., Reardon, J., Griffith, D. W. T., Johnson, T. J.,
1375 Hosseini, S., Miller, J. W., Cocker, D. R., Jung, H., and Weise, D. R.: Coupling field and laboratory
1376 measurements to estimate the emission factors of identified and unidentified trace gases for prescribed
1377 fires, *Atmos. Chem. Phys.*, 13, 89-116, <https://doi.org/10.5194/acp-13-89-2013>, 2013.
1378

1379 Yokelson, R. J., Crounse, J. D., DeCarlo, P. F., Karl, T., Urbanski, S., Atlas, E., Campos, T., Shinozuka,
1380 Y., Kapustin, V., Clarke, A. D., Weinheimer, A., Knapp, D. J., Montzka, D. D., Holloway, J., Weibring,
1381 P., Flocke, F., Zheng, W., Toohey, D., Wennberg, P. O., Wiedinmyer, C., Mauldin, L., Fried, A., Richter,
1382 D., Walega, J., Jimenez, J. L., Adachi, K., Buseck, P. R., Hall, S. R., and Shetter, R.: Emissions from
1383 biomass burning in the Yucatan, *Atmos. Chem. Phys.*, 9, 5785-5812, [https://doi.org/10.5194/acp-9-5785-](https://doi.org/10.5194/acp-9-5785-2009)
1384 2009, 2009.
1385

1386 Yokelson, R. J., Goode, J. G., Ward, D. E., Susott, R. A., Babbitt, R. E., Wade, D. D., Bertschi, I.,
1387 Griffith, D. W. T., and Hao, W. M.: Emissions of formaldehyde, acetic acid, methanol, and other trace
1388 gases from biomass fires in North Carolina measured by airborne Fourier transform infrared
1389 spectroscopy, *J. Geophys. Res.-Atmos*, 104, 30109-30125, <https://doi.org/10.1029/1999JD900817>, 1999.
1390

1391 Yokelson, R. J., Griffith, D. W. T., and Ward, D. E.: Open-path Fourier transform infrared studies of
1392 large-scale laboratory biomass fires, *J. Geophys. Res.-Atmos*, 101, 21067-21080,
1393 <https://doi.org/10.1029/96JD01800>, 1996.
1394

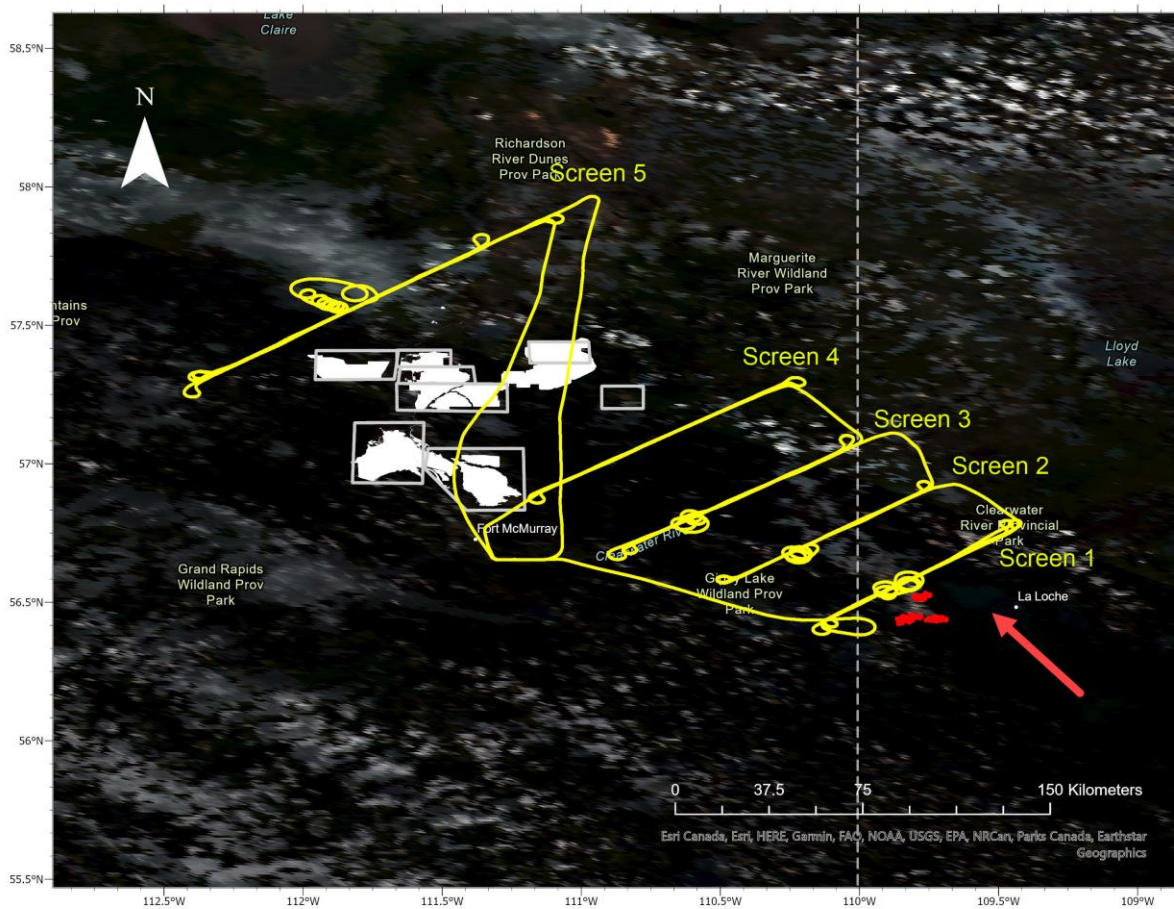
1395 Yokelson, R. J., Karl, T., Artaxo, P., Blake, D. R., Christian, T. J., Griffith, D. W. T., Guenther, A., and
1396 Hao, W. M.: The tropical forest and fire emissions experiment: Overview and airborne fire emission
1397 factor measurements, *Atmos. Chem. Phys.*, 7, 5175-5196, <https://doi.org/10.5194/acp-7-5175-2007>, 2007.
1398

1399 Yokelson, R. J., Susott, R., Ward, D. E., Reardon, J., and Griffith, D. W. T.: Emissions from smoldering
1400 combustion of biomass measured by open-path Fourier transform infrared spectroscopy, *J. Geophys.*
1401 *Res.-Atmos*, 102, 18865-18877, <https://doi.org/10.1029/97JD00852>, 1997.
1402

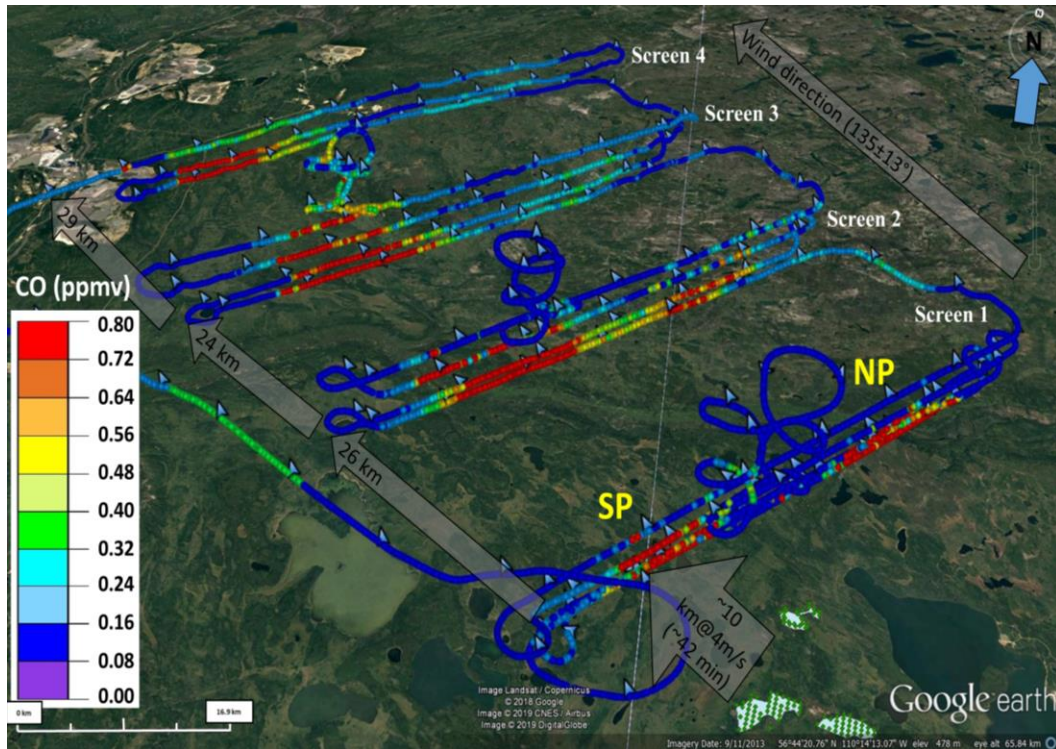
1403 Yu, S.: Role of organic acids (formic, acetic, pyruvic and oxalic) in the formation of cloud condensation
1404 nuclei (CCN): a review, *Atmos. Res.*, 53, 185-217, [https://doi.org/10.1016/S0169-8095\(00\)00037-5](https://doi.org/10.1016/S0169-8095(00)00037-5),
1405 2000.
1406

1407 Yu, P., Toon, O. B., Bardeen, C. G., Zhu, Y., Rosenlof, K. H., Portmann, R. W., Thornberry, T. D., Gao,
1408 R.-S., Davis, S. M., Wolf, E. T., Gouw, J. d., Peterson, D. A., Fromm, M. D., and Robock, A.: Black
1409 carbon lofted wildfire smoke high into the stratosphere to form a persistent plume, *Science*, 365, 587-590,
1410 <https://doi.org/10.1126/science.aax1748>, 2019.
1411

1412 Zhang, R., Suh, I., Zhao, J., Zhang, D., Fortner, E. C., Tie, X., Molina, L. T., and Molina, M. J.:
1413 Atmospheric new particle formation enhanced by organic acids, *Science*, 304, 1487-1490,
1414 <https://doi.org/10.1126/science.1095139>, 2004.
1415

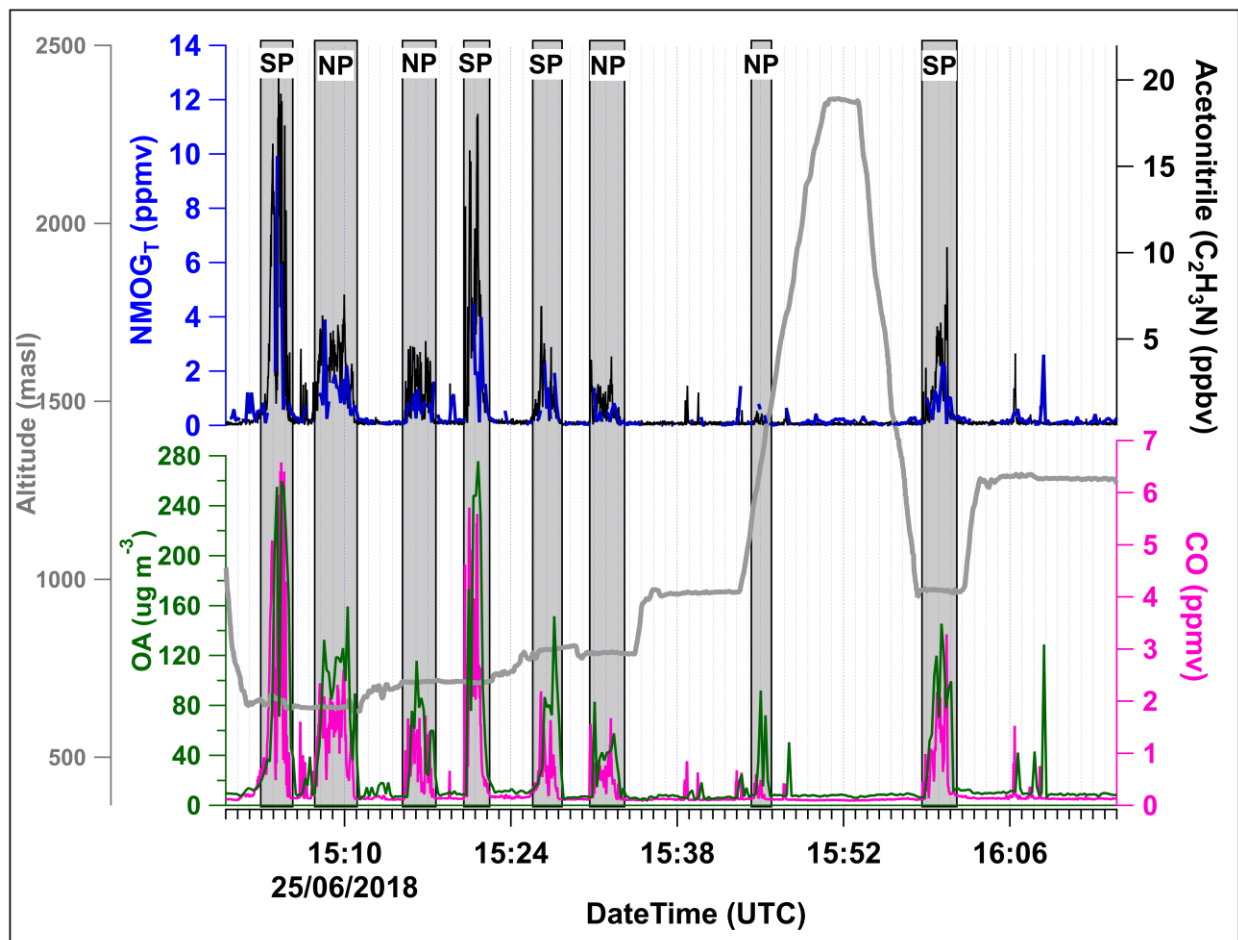


1416
 1417 Figure 1. Corrected reflectance satellite image from the VIIRS spectroradiometer on the Suomi
 1418 NPP and NOAA-20 satellites taken on June 25, 2018. The fire hot spots for the wildfire of
 1419 interest are indicated by the red dots. Flight tracks were flown at Lagrangian distances
 1420 downwind of the wildfire. Multiple transects at varying altitudes perpendicular to the plume
 1421 direction formed 5 virtual screens. Plume direction of travel is indicated by the red arrow. The
 1422 location of the Alberta oil sands mining facilities are shown in white.
 1423

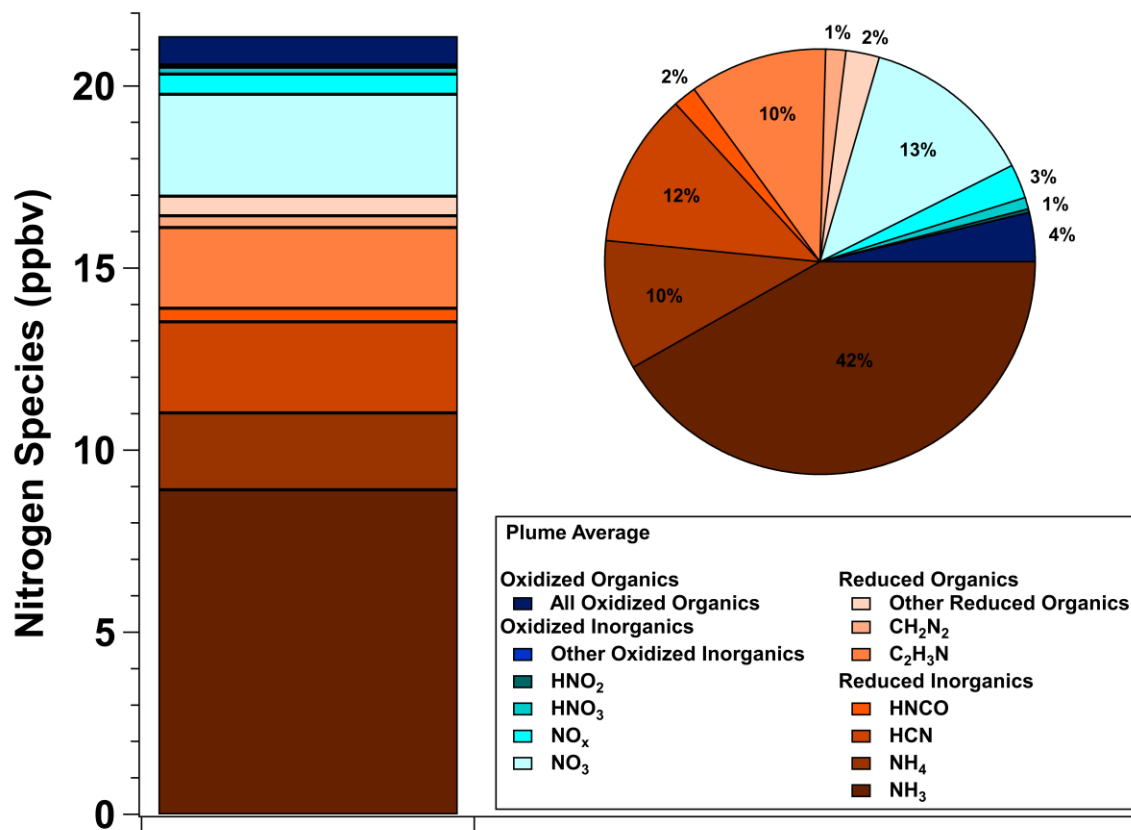


1424
1425

1426 Figure 2. Flight tracks coloured by CO mixing ratio (ppmv) for Screens 1 to 4. The two plumes
1427 are identified as south plume (SP) and north plume (NP). The fire perimeter surrounding the
1428 detected MODIS-derived ‘hot spots’ on June 25, 2018 is shown in the green hatched area. The
1429 source of the NP is expected to be the same hot spots as the SP but ~ 30 min older; see Sect. 2.2.
1430 The small blue arrows along the flight tracks indicate the aircraft measured wind direction with
1431 the average wind direction depicted with the large grey arrow. Distances between screens are
1432 shown in the grey arrows.
1433

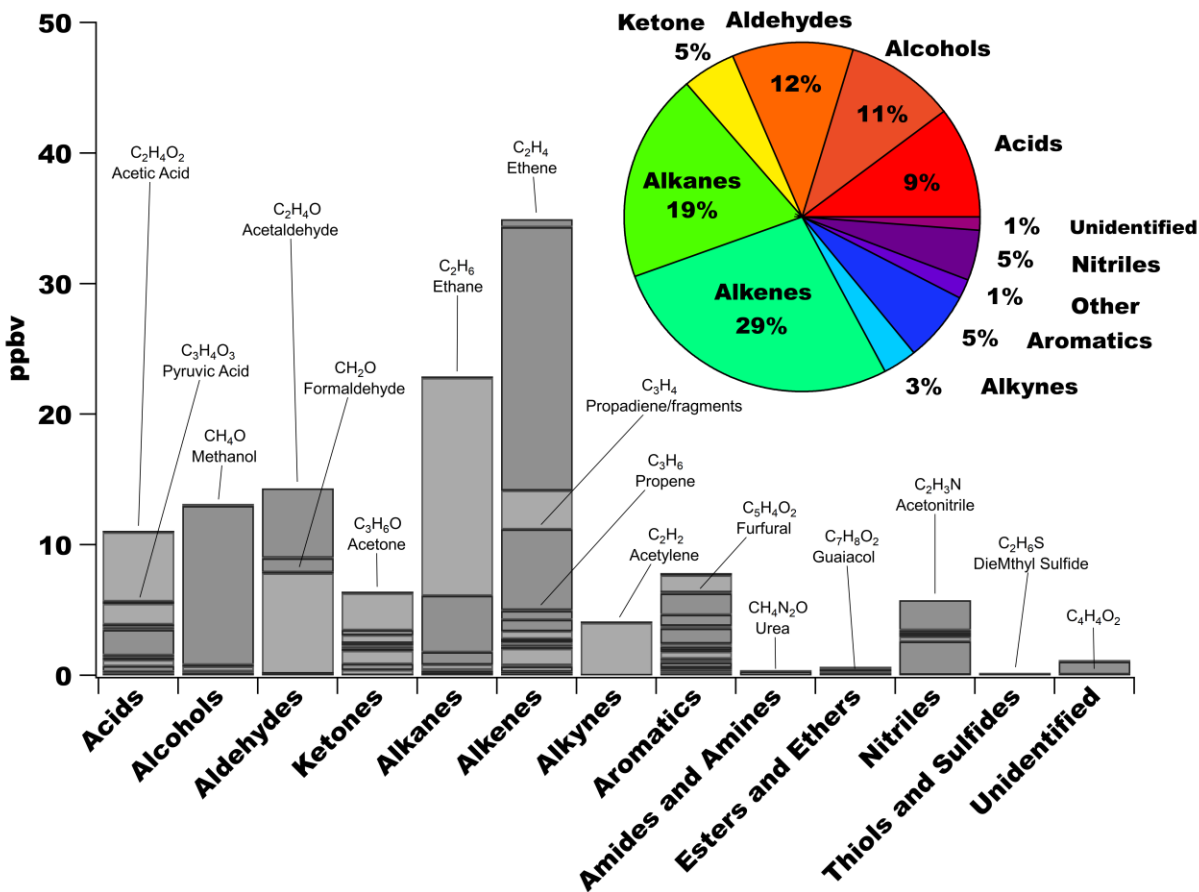


1434
 1435 Figure 3. Time series of NMOGs (ppmv), acetonitrile (C_2H_3N ; ppbv) and CO (ppmv), as well as
 1436 OA concentrations ($\mu g m^{-3}$) and altitude for Screen 1. The in-plume portions are indicated by the
 1437 vertical grey bars. The aircraft flew back and forth across the plumes at increasing altitudes to
 1438 complete five transects; a transect represents one pass across the SP and NP at the same altitude.
 1439
 1440

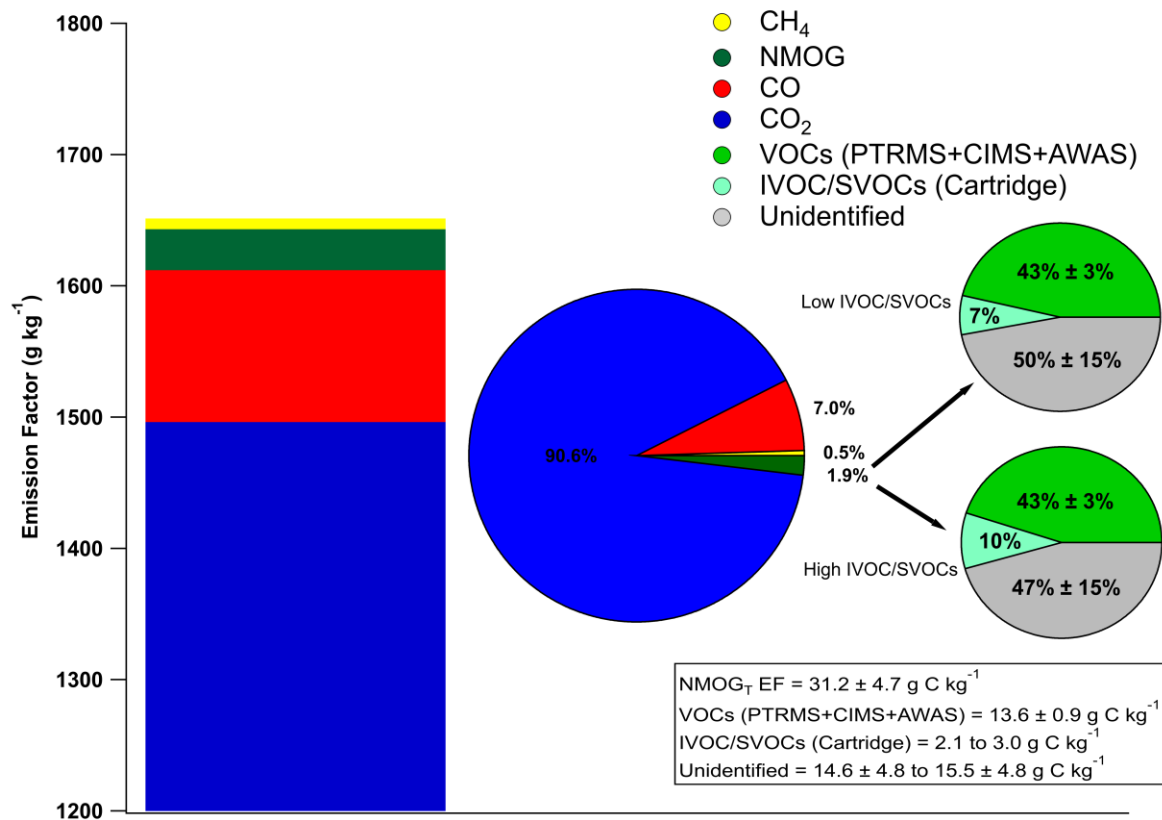


1441
 1442 Figure 4. Background-subtracted average Screen 1 in-plume mixing ratios of measured gas- and
 1443 particle-phase N-containing species (N_r) and their fractional contribution to the total summed N_r
 1444 species. The N_r species are grouped into categories of reduced inorganics, reduced organics,
 1445 oxidized inorganics and oxidized organics with reduced species in shades of red and oxidized
 1446 species in shades of blue.

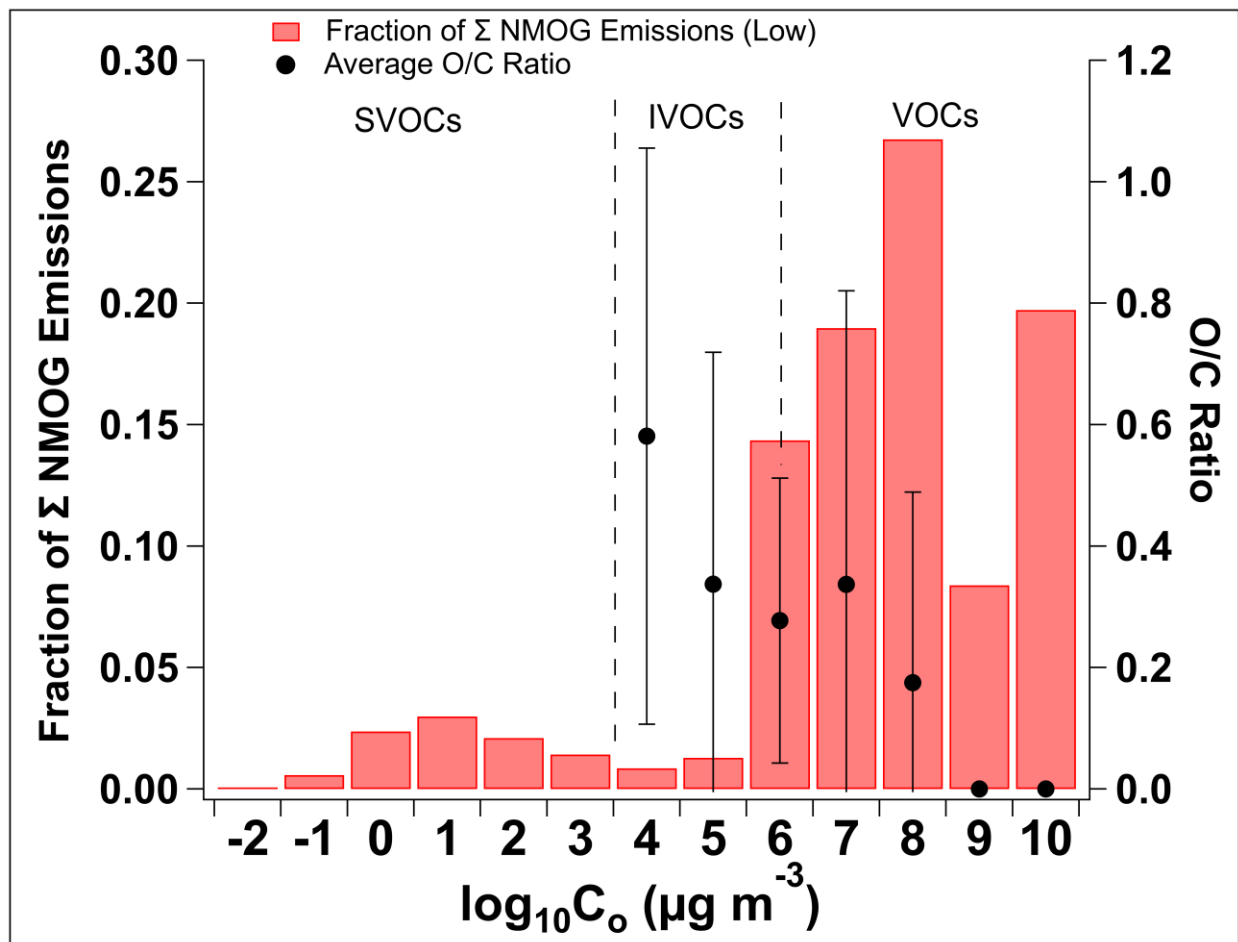
1447
 1448
 1449
 1450
 1451
 1452
 1453
 1454



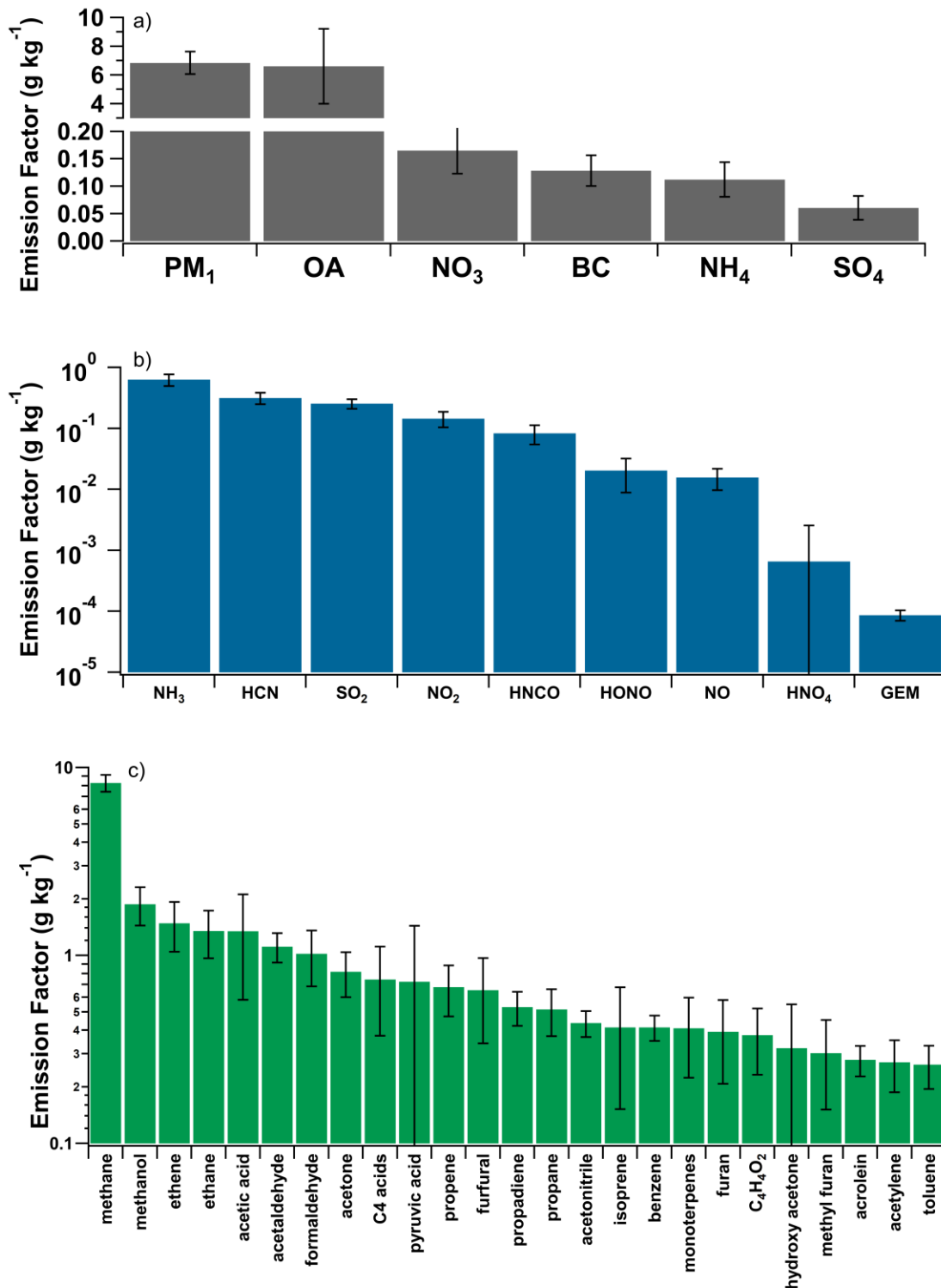
1455
 1456 Figure 5. Background-subtracted average mixing ratios of individually measured NMOGs
 1457 shown for thirteen chemical classes. In some cases, compounds are double- (or triple-) counted if
 1458 they can be identified in more than one category. For example, phenol is an alcohol + an
 1459 aromatic; guaiacol is an alcohol + an ether + an aromatic. In the pie chart, the *Other* category
 1460 includes amides, amines, ethers, thiols and sulfides. The unidentified category contains
 1461 molecular formulas detected, but the compound(s) could not be identified.
 1462
 1463



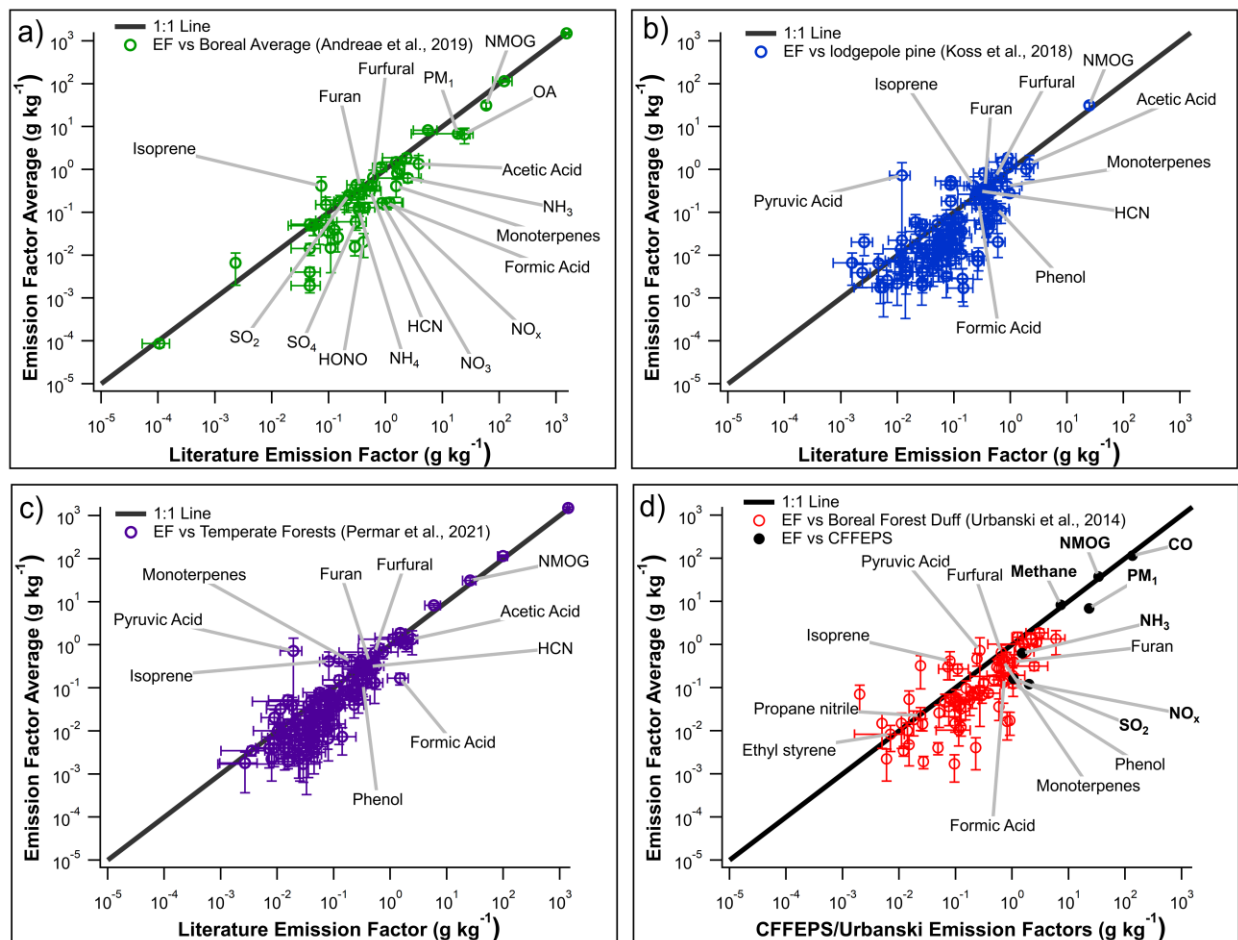
1464
 1465 Figure 6. Total carbon (TC) partitioning based on EFs (carbon fraction). The bar chart shows
 1466 the stacked EFs for carbon-containing compounds with the middle pie chart showing their
 1467 percent contributions to the TC. The two magnified pie charts (right side), representing the low and
 1468 high I/SVOC EF estimates, show the percent breakdown of the measured NMOGs and the
 1469 remaining unidentified portion. The EF values (g C kg⁻¹) are provided in the box. Note that all the
 1470 EFs shown in Table A1 were converted to g C kg⁻¹ for this breakdown
 1471
 1472
 1473



1474
 1475 Figure 7. Fraction of total ΣNMOG emissions in each volatility bin, as well as the bin-averaged
 1476 O/C ratio spanning VOCs, IVOCs and SVOCs. Data is included from PTRMS, CIMS, AWAS
 1477 and cartridge measurements. The O/C ratio is derived for only the PTRMS, CIMS and AWAS
 1478 measurements and the errors bars indicate the standard deviation of the average O/C ratio.
 1479

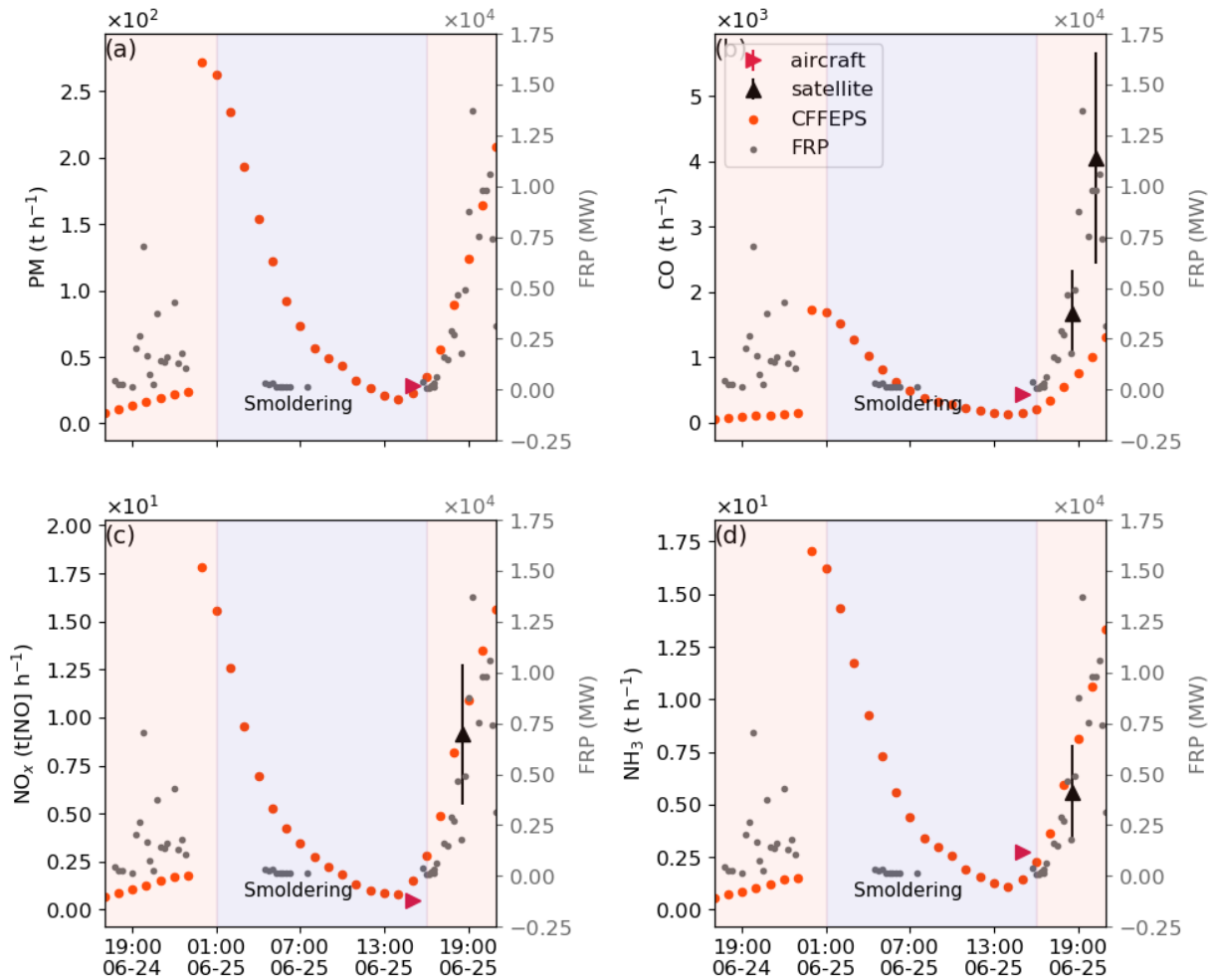


1481
 1482 Figure 8. Average emission factors (g kg⁻¹) of a) particle species; b) inorganic gas-phase species, and c)
 1483 the top 25 measured gas-phase organic species. C4 acids = C4 oxo-carboxylic acids; propadiene =
 1484 fragments/propadiene; hydroxy acetone = hydroxy acetone/ ethyl formate. Organic species
 1485 measurements are from the PTRMS, CIMS and AWAS.



1486
 1487 Figure 9. Comparison of averaged emission factors with a) boreal forest field-based
 1488 measurements (Andreae, 2019; Akagi et al., 2011; Liu et al., 2017), b) laboratory-based
 1489 measurements of lodgepole pine (Koss et al., 2018), c) temperate forest field-based
 1490 measurements (Permar et al., 2021), and d) those used in CFFEPS (Urbanski et al., 2014). See
 1491 Table S8 for compound comparisons that don't have exact matches.

1492
 1493
 1494
 1495
 1496



1497
1498

1499 Figure 10. Fire radiative power (FRP; in MW) from GOES-R (grey dots) and emissions from
 1500 the CFFEPS model (orange dots) from 2018-06-24 17:00 UTC to 2018-06-25 21:00 UTC. Local
 1501 time = UTC – 6 hrs. Aircraft-derived emission rates are shown for a) PM_{10} , b) CO, c) NO_x (as
 1502 NO) and d) NH_3 (in $t\ h^{-1}$; red arrow) at 15:00 UTC when the aircraft flew closest to the fire. The
 1503 corresponding TROPOMI satellite-derived emission rates are also shown (in $t\ h^{-1}$; black arrows).
 1504 Note, the aircraft flight time occurred when the fire intensity reflected a surface, smoldering fire
 1505 and the satellite overpass time took place when the fire had transitioned to a crown (flaming)
 1506 fire. The smoldering and flaming time periods are coloured in blue and pink, respectively.
 1507

1508 **Table A1**

1509
 1510 Summary of in-plume and background average mixing ratios (or concentrations), emission
 1511 factors (g kg^{-1}) (EF) and emission ratios (ppbv ppmv^{-1} except CO_2 which is in units of ppmv
 1512 ppmv^{-1} ; particulates in $\mu\text{g m}^{-3} \text{ppm}^{-1}$ and GEM in $\text{ng m}^{-3} \text{ppmv}^{-1}$) (ER) for the SP, NP, and the EF
 1513 average of the two plumes. In-plume and background averages are in units of $\mu\text{g m}^{-3}$ for
 1514 particulates, ppbv for gas-phase compounds, except GEM which is ng m^{-3} , and CO_2 is ppmv.
 1515 Compounds are grouped by particulate species, and inorganic and organic gas-phase species and
 1516 sorted by increasing molecular weight. PM_1 is the sum of the AMS-derived particulate species.
 1517 The CE was 0.84 ± 0.04 and 0.82 ± 0.01 for the SP and NP, respectively. For comparison, EFs are
 1518 also included from previously published literature including Andreae (2019)¹, Koss et al.
 1519 (2018)², Permar et al. (2021)³, and Liu et al. (2017)⁴. The Andreae (2019) PM EF represents
 1520 $\text{PM}_{2.5}$. See Table S8 for compounds that did not have exact matches for comparison to literature
 1521 values. To derive the EF for species measured in mass concentration units, Eq. 3 was modified
 1522 by converting TC to mass concentrations using the measured temperature and pressure, and
 1523 removing the molar mass ratio term. * Indicates that the compound was ‘calculated’ (SI Sect
 1524 1.1.1) while the remaining compounds were calibrated. Uncertainties were estimated by
 1525 summing in quadrature the standard error of the average EF (or ER) and the measurement
 1526 uncertainties (see Sect. 2.5).
 1527
 1528

Molecular Weight	Compound	Compound Name	Instrument	SP Average	NP Average	Background	Average EF (g kg^{-1})	NP EF (g kg^{-1})	SP EF (g kg^{-1})	Literature EF (g kg^{-1})	NP ER	SP ER
Particulates												
	PM_1	particulate matter (<1 μm)	AMS	112 \pm 35	75.5 \pm 29.3	13.2 \pm 0.9	6.8 \pm 0.8	7.1 \pm 0.3	6.6 \pm 1.1	18.7 \pm 15.9 ¹ 26.0 \pm 6.2 ⁴	58.8 \pm 1.0	65.1 \pm 7.3
	BC	black carbon	SP2	1.3 \pm 0.4	0.74 \pm 0.30	0.11 \pm 0.06	0.13 \pm 0.03	0.11 \pm 0.02	0.14 \pm 0.04	0.43 \pm 0.21 ¹ 0.39 \pm 0.17 ³	0.55 \pm 0.08	0.58 \pm 0.19
	NH_4	p-ammonium	AMS	2.3 \pm 1.0	1.2 \pm 0.4	0.21 \pm 0.03	0.11 \pm 0.03	0.11 \pm 0.03	0.12 \pm 0.04	0.34 \pm 0.15 ⁴	1.1 \pm 0.3	1.9 \pm 0.6
	NO_3	p-nitrate	AMS	3.2 \pm 1.5	1.4 \pm 0.5	0.078 \pm 0.017	0.17 \pm 0.04	0.14 \pm 0.03	0.19 \pm 0.05	0.87 \pm 0.13 ⁴	0.90 \pm 0.16	1.2 \pm 0.3
	SO_4	p-sulphate	AMS	1.7 \pm 0.7	0.98 \pm 0.31	0.39 \pm 0.03	0.060 \pm 0.022	0.066 \pm 0.020	0.055 \pm 0.023	0.30 \pm 0.16 ⁴	0.035 \pm 0.011	0.054 \pm 0.020
	OA	p-total organics	AMS	101 \pm 34	72.6 \pm 27.0	12.5 \pm 0.83	6.6 \pm 2.6	6.9 \pm 2.4	6.3 \pm 2.8	24.3 \pm 0.21 ⁴	57.5 \pm 9.4	61.7 \pm 27.1
Gas												
Inorganic												
17.031	NH_3	ammonia	LGR	15.4 \pm 9.6	5.2 \pm 2.1	0.039 \pm 0.02	0.63 \pm 0.14	0.45 \pm 0.04	0.82 \pm 0.19	2.5 \pm 1.8 ¹ 0.68 \pm 0.19 ²	5.8 \pm 0.6	12.6 \pm 2.5
27.026	HCN	hydrogen cyanide	CIMS	3.2 \pm 1.6	2.3 \pm 1.0	0.18 \pm 0.07	0.31 \pm 0.07	0.34 \pm 0.06	0.29 \pm 0.07	0.53 \pm 0.30 ¹ 0.28 \pm 0.060 ² 0.43 \pm 0.17 ³	2.8 \pm 0.5	2.9 \pm 0.7
28.01	CO	carbon monoxide	Picarro	991 \pm 443	819 \pm 327	119 \pm 5	116 \pm 6	127 \pm 4	104 \pm 7	121 \pm 47 ¹ 99.3 \pm 19.7 ³	108 \pm 39	126 \pm 52
30.006	NO	nitric oxide	TECOs	0.14 \pm 0.05		0.0014 \pm 0.086	0.016 \pm 0.006	0.016 \pm 0.006	0.14 \pm 0.05	0.29 ¹		0.14 \pm 0.046
43.025	HNCO	isocyanic acid	CIMS	0.52 \pm 0.17	0.44 \pm 0.13	0.068 \pm 0.024	0.083 \pm 0.029	0.091 \pm 0.027	0.076 \pm 0.031	0.57 \pm 0.24 ² 0.16 \pm 0.04 ³	0.46 \pm 0.13	0.47 \pm 0.92

Molecular Weight	Compound	Compound Name	Instrument	SP Average	NP Average	Background	Average EF (g kg ⁻¹)	NP EF (g kg ⁻¹)	SP EF (g kg ⁻¹)	Literature EF (g kg ⁻¹)	NP ER	SP ER
44.009	CO ₂	carbon dioxide	Picarro	414±0.4	411±0.2	405±0.4	1496±92	1481±103	1511±80	1529±135 ¹ 1413±61 ³	7.4±0.5	9.4±0.45
46.005	NO ₂	nitrogen dioxide	TECOs	0.88±0.17		0.39±0.19	0.15±0.04	0.15±0.04	0.88±0.17	1.0 ¹		0.83±0.21
46.005	NO _x	sum (NO+NO ₂)	TECOs	1.0±0.2		0.39±0.20	0.17±0.04	0.17±0.04	1.0±0.2	1.2±0.9 ¹		0.97±0.58
47.013	HONO	nitrous acid	CIMS	0.22±0.04		0.098±0.038	0.020±0.012	0.020±0.012	0.22±0.04	0.60±0.20 ²		0.11±0.061
64.064	SO ₂	sulphur dioxide	TECOs	1.3±0.3		0.19±0.46	0.26±0.05	0.26±0.05	1.3±0.3	0.22±0.31 ¹		1.1±0.16
79.011	HNO ₄	pernitric acid	CIMS	0.036±0.0049	0.032±0.0043	0.020±0.007	0.0010±0.0019	0.00047±0.0025	0.00085±0.001		0.00089±0.0068	0.0028±0.0033
200.59	GEM	gaseous elemental mercury	Tekran	1.6±0.2	1.4±0.1	1.2±0.03	0.000087±0.000017	0.000082±0.000017	0.000092±0.000016	0.00023±0.00030 ¹	0.00068±0.0014	0.00091±0.0014
Gas Organic												
	ΣNMOG	non methane organic gases	PTRMS +CIMS +AWAS + cartridges				24.5±1.6 to 25.6±1.6	26.2±2.1	25.4±5.8			
	Estim. NMOG _T (see Sect 3.4.3)	non methane organic gases	PTRMS +CIMS +AWAS + cartridges				36.8±11.3 to 39.9±5.8			58.7 ¹ 25.0 ² 26.1 ³		
	NMOG _T	carbon fraction of NMOG	Picarro	936±341	649±225	375±85	31.2±3.8	36.8±5.1	25.5±5.6		680±111	580±92
16.043	CH ₄	methane	Picarro	2026±54	1982±35	1911±8	8.3±0.9	7.8±0.4	8.7±1.1	5.5±2.5 ¹ 5.9±1.8 ³	107±5	146±16
26.038	C ₂ H ₂	acetylene	AWAS	6.9±2.5	1.8±0.7	0.34±0.041	0.27±0.08	0.20±0.05	0.34±0.11	0.31±0.17 ³	2.2±0.9	4.0±1.1
28.054	C ₂ H ₄	ethene	AWAS	32.4±14.0	9.3±3.8	0.64±0.1	1.5±0.4	1.3±0.3	1.7±0.5	1.5±1.0 ³	12.9±3.5	18.3±5.0
30.026	CH ₂ O	formaldehyde	PTR	13.9±4.9	10.1±2.8	4.4±2.0	1.0±0.3	1.1±0.3	0.93±0.36	1.8±0.4 ¹ 1.9±0.7 ² 1.9±0.4 ³	8.1±2.2	8.9±3.2
30.07	C ₂ H ₆	ethane	AWAS	27.1±12.4	10.1±3.4	1.9±0.016	1.3±0.4	1.3±0.3	1.4±0.5	1.1±0.84 ³	12.5±2.7	13.8±3.8
32.042	CH ₄ O	methanol	PTR	21.9±7.9	15.9±4.9	6.8±0.9	1.9±0.4	2.2±0.4	1.6±0.4	2.3±1.0 ¹ 0.90±0.35 ² 1.5±0.4 ³	14.9±2.9	13.4±3.6
40.065	C ₃ H ₄	fragment s/propadiene*	PTR	3.7±1.6	3.0±1.3	0.39±0.35	0.53±0.11	0.64±0.11	0.42±0.11	0.060±0.030 ¹ 0.088±0.041 ²	3.5±0.6	2.8±0.7
41.053	C ₂ H ₃ N	acetonitrile	PTR	2.8±1.4	2.0±0.8	0.10±0.06	0.44±0.07	0.48±0.06	0.40±0.08	0.31±0.10 ¹ 0.086±0.027 ² 0.31±0.15	2.6±0.3	2.6±0.5
42.041	CH ₂ N ₂	cyanamide*	PTR	0.55±0.22	0.40±0.12	0.10±0.20	0.064±0.042	0.067±0.042	0.061±0.042		1.4±0.9	1.3±0.9
42.081	C ₃ H ₆	propene	AWAS	9.7±4.8	2.9±1.3	0.12±0.01	0.68±0.21	0.62±0.15	0.73±0.25	0.74±0.62 ³	4.2±1.0	5.2±1.5

Molecular Weight	Compound	Compound Name	Instrument	SP Average	NP Average	Background	Average EF (g kg ⁻¹)	NP EF (g kg ⁻¹)	SP EF (g kg ⁻¹)	Literature EF (g kg ⁻¹)	NP ER	SP ER
44.053	C ₂ H ₄ O	acetaldehyde	PTR	7.3±3.2	5.2±2.0	0.96±0.20	1.1±0.2	1.2±0.2	1.0±0.2	0.81±0.23 ¹ 0.92±0.32 ² 1.7±0.4 ³	6.3±0.9	6.3±1.2
44.097	C ₃ H ₈	propane	AWAS	6.7±3.2	2.5±1.0	0.28±0.03	0.52±0.14	0.53±0.12	0.50±0.16	0.46±0.18 ³	3.4±0.7	3.4±1.0
46.025	CH ₂ O ₂	formic acid	CIMS	3.0±1.2	2.8±0.9	2.4±0.1	0.17±0.05	0.17±0.04	0.17±0.06	1.0±0.9 ¹ 0.28±0.14 ² 1.5±0.6 ³	1.2±2.6	0.56±1.3
48.103	CH ₄ S	methanethiol*	PTR	0.074±0.039	0.049±0.022	0.0024±0.028	0.014±0.0086	0.015±0.009	0.013±0.008	0.011±0.006 ²	0.068±0.043	0.073±0.043
50.057	CH ₆ O ₂	methanol hydrate*	PTR	0.25±0.10	0.16±0.06	0.062±0.057	0.028±0.020	0.034±0.023	0.022±0.017		0.15±0.10	0.12±0.09
52.076	C ₄ H ₄	butyne/fragments*	PTR	0.11±0.05	0.080±0.034	0.011±0.044	0.018±0.010	0.020±0.011	0.016±0.010	0.052±0.018 ³	0.086±0.046	0.081±0.050
53.064	C ₃ H ₃ N	acrylonitrile*	PTR	0.17±0.08	0.12±0.06	0.0024±0.013	0.036±0.018	0.040±0.018	0.032±0.018	0.025±0.012 ² 0.044±0.015 ³	0.17±0.07	0.16±0.09
54.048	C ₃ H ₂ O	propynal*	PTR	0.053±0.033	0.023±0.0054	0.013±0.019	0.0087±0.0053	0.0045±0.0031	0.013±0.007	0.034±0.014 ² 0.037±0.015 ³	0.018±0.013	0.062±0.032
54.092	C ₄ H ₆	butadiene/fragments*	PTR	0.74±0.38	0.47±0.24	0.070±0.017	0.15±0.08	0.15±0.08	0.15±0.08	0.089±0.030 ¹ 0.34±0.18 ² 0.27±0.10 ³	0.62±0.30	0.73±0.37
54.092	C ₄ H ₆	1,3-butadiene	AWAS	0.74±0.38	0.20±0.09	0.0041±0.0006	0.065±0.022	0.055±0.016	0.075±0.026	0.089±0.030 ¹ 0.34±0.18 ² 0.27±0.10 ³	0.29±0.09	0.41±0.12
55.08	C ₃ H ₅ N	propane nitrile*	PTR	0.11±0.05	0.080±0.032	0.0097±0.019	0.022±0.012	0.025±0.012	0.019±0.012	0.012±0.005 ² 0.037±0.018 ³	0.10±0.05	0.094±0.057
56.064	C ₃ H ₄ O	acrolein	PTR	1.5±0.6	1.0±0.4	0.17±0.09	0.28±0.05	0.29±0.04	0.26±0.06	0.34 ¹ 0.97±0.50 ² 0.40±0.18 ³	0.82±0.12	0.83±0.15
56.108	C ₄ H ₈	cis-2-butene	AWAS	0.16±0.08		0.016±0.008	0.015±0.006		0.015±0.006			0.078±0.023
56.108	C ₄ H ₈	isobutene	AWAS	0.94±0.49	0.34±0.12	0.062±0.022	0.084±0.023	0.082±0.008	0.086±0.032		0.41±0.03	0.45±0.13
56.108	C ₄ H ₈	t-2-butene	AWAS	0.13±0.07		0.010±0.003	0.012±0.005		0.012±0.005			0.063±0.018
56.108	C ₄ H ₈	1-butene	AWAS	1.4±0.7	0.41±0.17	0.014±0.005	0.13±0.03	0.12±0.01	0.14±0.04		0.60±0.05	0.74±0.12
57.052	C ₂ H ₃ NO	hydroxy acetonitrile	CIMS	0.021±0.029	0.0078±0.014	0.00035±0.00014	0.0035±0.0031	0.0025±0.0028	0.0044±0.0034	0.033±0.009 ³	0.0095±0.011	0.021±0.016
57.052	C ₂ H ₃ NO	methyl isocyanate*	PTR	0.074±0.029		0.0067±0.06	0.0052±0.0032		0.0052±0.0032	0.033±0.009 ³		0.024±0.015
58.08	C ₃ H ₆ O	acetone	PTR	6.0±1.8	4.7±1.2	2.5±0.3	0.82±0.22	0.99±0.25	0.65±0.19	1.6±1.6 ¹ 0.34±0.12 ² 0.84±0.22 ³	0.065±0.018	0.072±0.028
58.124	C ₄ H ₁₀	n-butane	AWAS	1.5±0.7	0.62±0.22	0.098±0.013	0.15±0.04	0.16±0.04	0.14±0.05	0.11±0.06 ¹ 0.12±0.06 ³	0.79±0.17	0.73±0.20
60.052	C ₂ H ₄ O ₂	acetic acid	CIMS	8.8±7.5	6.0±3.9	2.1±0.8	1.3±0.8	1.1±0.5	1.6±0.9	3.8±2.0 ¹ 2.4±0.6 ³	7.4±3.5	8.9±5.2

Molecular Weight	Compound	Compound Name	Instrument	SP Average	NP Average	Background	Average EF (g kg ⁻¹)	NP EF (g kg ⁻¹)	SP EF (g kg ⁻¹)	Literature EF (g kg ⁻¹)	NP ER	SP ER
60.056	CH ₄ N ₂ O	Urea*	PTR	0.44±0.18	0.28±0.08	0.067±0.13	0.078±0.052	0.079±0.054	0.076±0.049		0.29±0.20	0.34±0.21
61.04	CH ₃ NO ₂	nitromethane*	PTR	0.055±0.023	0.038±0.020	0.0051±0.023	0.011±0.007	0.010±0.007	0.011±0.007	0.074±0.030 ² 0.078±0.009 ³	0.036±0.024	0.048±0.030
62.068	C ₂ H ₆ O ₂	ethylene glycol*	PTR	0.023±0.0077		0.0036±0.018	0.0036±0.0023		0.0036±0.0023			0.015±0.010
62.13	C ₂ H ₆ S	dimethyl sulfide	PTR	0.051±0.022		0.011±0.034	0.0067±0.0047		0.0067±0.0047	0.0016±0.008 ² 0.080±0.083 ³ 0.0047 ⁴		0.029±0.020
66.103	C ₅ H ₆	cyclopentadiene*	PTR	0.13±0.05	0.12±0.04	0.025±0.039	0.032±0.019	0.041±0.022	0.023±0.016	0.011±0.005 ³	0.14±0.07	0.096±0.064
67.091	C ₄ H ₅ N	pyrrole*	PTR	0.10±0.06	0.067±0.033	0.00073±0.013	0.026±0.014	0.027±0.014	0.025±0.014	0.054±0.029 ² 0.039±0.021 ³	0.090±0.046	0.098±0.055
68.075	C ₄ H ₄ O	furan*	PTR	1.5±0.8	1.1±0.5	0.0083±0.035	0.39±0.19	0.43±0.17	0.35±0.20	0.36±0.44 ¹ 0.36±0.11 ² 0.43±0.19 ³	1.4±0.6	1.4±0.8
68.119	C ₅ H ₈	isoprene	PTR	1.7±0.7	1.8±0.8	0.52±0.25	0.42±0.26	0.64±0.34	0.19±0.15	0.074 ¹ 0.22±0.11 ² 0.082±0.095 ³	2.1±1.1	0.47±0.47
68.119	C ₅ H ₈	isoprene	AWAS	0.82±0.46	0.35±1.65	1.3±0.4	0.30±0.18	0.40±0.17	0.20±0.19	0.074 ¹ 0.22±0.11 ² 0.082±0.095 ³	2.0±1.0	0.18±0.18
69.083	C ₄ H ₅ O	*	PTR	0.017±0.0064	0.013±0.0063	0.00079±0.01	0.0043±0.0025	0.0047±0.0028	0.0038±0.0022		0.015±0.009	0.015±0.008
69.107	C ₄ H ₇ N	butane nitrile*	PTR	0.030±0.014	0.022±0.009	0.0041±0.011	0.0077±0.0051	0.0088±0.0059	0.0065±0.0042	0.011±0.005 ² 0.020±0.010 ³	0.028±0.019	0.025±0.016
70.091	C ₄ H ₆ O	MVK, methacrolein, crotonaldehyde	PTR	1.3±0.3	1.3±0.3	0.91±0.17	0.19±0.09	0.20±0.08	0.18±0.11	0.11±0.12 ¹ 0.34±0.15 ² 0.39±0.15 ³	0.66±0.26	0.68±0.38
70.135	C ₅ H ₁₀	c-2-pentene	AWAS	0.040±0.017	0.013±0.0034	0.0040±0.0006	0.0040±0.0012	0.0033±0.0007	0.0048±0.0016	0.046±0.025 ¹ 0.015±0.008 ³	0.013±0.004	0.021±0.0057
70.135	C ₅ H ₁₀	cyclopentane	AWAS	0.031±0.013	0.015±0.0022	0.0052±0.0003	0.0035±0.0009	0.0038±0.0009	0.0031±0.0009	0.046±0.025 ¹ 0.015±0.008 ³	0.016±0.004	0.014±0.005
70.135	C ₅ H ₁₀	1-pentene	AWAS	0.42±0.21	0.15±0.06	0.0053±0.0012	0.052±0.015	0.053±0.013	0.052±0.018	0.046±0.025 ¹ 0.015±0.008 ³	0.21±0.05	0.22±0.06
70.135	C ₅ H ₁₀	t-2-pentene	AWAS	0.13±0.12	0.068±0.020	0.0094±0.0058	0.018±0.013	0.0049±0.0040	0.031±0.018	0.046±0.025 ¹ 0.015±0.008 ³	0.013±0.010	0.063±0.035
70.135	C ₅ H ₁₀	2-me-1-butene	AWAS	0.12±0.061	0.047±0.018	0.0088±0.0017	0.014±0.005	0.014±0.004	0.015±0.005	0.046±0.025 ¹	0.056±0.013	0.062±0.018

Molecular Weight	Compound	Compound Name	Instrument	SP Average	NP Average	Background	Average EF (g kg ⁻¹)	NP EF (g kg ⁻¹)	SP EF (g kg ⁻¹)	Literature EF (g kg ⁻¹)	NP ER	SP ER
										0.015±0.008 ³		
70.135	C ₅ H ₁₀	2-me-2-butene	AWAS	0.019±0.0071	0.0077±0.0016	0.0034±0.0006	0.0019±0.0006	0.0017±0.0004	0.0022±0.0008	0.046±0.025 ¹ 0.015±0.008 ³	0.0068±0.0030	0.0095±0.0027
70.135	C ₅ H ₁₀	3-me-1-butene	AWAS	0.10±0.10	0.045±0.032	0.029±0.012	0.016±0.010	0.0078±0.0037	0.025±0.013	0.046±0.025 ¹ 0.015±0.008 ³	0.045±0.018	0.058±0.028
72.063	C ₃ H ₄ O ₂	acrylic acid	CIMS	0.28±0.24	0.21±0.15	0.060±0.046	0.096±0.048	0.13±0.06	0.062±0.035	0.22±0.08 ³	0.25±0.11	0.35±0.20
72.107	C ₄ H ₈ O	MEK, 2-methyl acetate, ethyl formate	PTR	0.80±0.35	0.57±0.23	0.097±0.051	0.18±0.07	0.22±0.08	0.14±0.06		0.67±0.23	0.54±0.20
72.151	C ₅ H ₁₂	n-pentane	AWAS	0.59±0.28	0.26±0.09	0.035±0.005	0.078±0.021	0.086±0.019	0.070±0.023	0.057±0.028 ³	0.34±0.07	0.29±0.08
72.151	C ₅ H ₁₂	2-methylbutane	AWAS	0.21±0.08	0.11±0.01	0.051±0.001	0.022±0.006	0.024±0.0049	0.021±0.007	0.057±0.028 ³	0.097±0.019	0.086±0.027
74.079	C ₃ H ₆ O ₂	propanoic acid	CIMS	0.81±0.24	0.70±0.15	0.49±0.17	0.13±0.08	0.12±0.08	0.14±0.09	0.57±0.20 ³	0.35±0.24	0.51±0.30
74.079	C ₃ H ₆ O ₂	hydroxy acetone/ ethyl formate *	PTR	1.5±0.62	1.1±0.4	0.30±0.11	0.32±0.23	0.35±0.25	0.30±0.20		1.0±0.8	1.1±0.7
78.114	C ₆ H ₆	benzene	PTR	1.4±0.69	1.0±0.5	0.054±0.045	0.41±0.06	0.47±0.06	0.36±0.07	0.57±0.21 ¹ 0.42±0.25 ² 0.50±0.14 ³	1.3±0.2	1.2±0.2
80.086	C ₅ H ₄ O	cyclopentadiene/isomers*	PTR	0.049±0.026	0.024±0.012	- 0.00054±0.0061	0.011±0.006	0.0093±0.0047	0.012±0.007	0.027±0.017 ³	0.026±0.013	0.040±0.023
80.13	C ₆ H ₈	cyclohexadiene/monoterpene fragment *	PTR	0.45±0.18	0.40±0.20	0.040±0.040	0.14±0.07	0.17±0.07	0.10±0.06		0.48±0.19	0.34±0.20
81.118	C ₅ H ₇ N	pentene nitriles/ methyl pyrrole*	PTR	0.018±0.0093	0.013±0.0053	0.0015±0.0055	0.0047±0.0032	0.0050±0.0036	0.0044±0.0028	0.020±0.011 ³	0.014±0.010	0.015±0.009
82.102	C ₅ H ₆ O	methyl furan*	PTR	1.1±0.5	0.69±0.32	0.042±0.065	0.30±0.15	0.31±0.13	0.29±0.17	0.32±0.11 ² 0.28±0.13 ³	0.84±0.34	0.96±0.55
82.146	C ₆ H ₁₀	cyclohexene*	PTR	0.14±0.06	0.093±0.044	0.015±0.035	0.054±0.030	0.075±0.038	0.033±0.020	0.015±0.011 ³	0.20±0.10	0.11±0.07
83.09	C ₄ H ₅ N	methyloxazole*	PTR	0.0096±0.0044		0.00012±0.0083	0.0020±0.0011		0.0020±0.0011			0.0066±0.0037
83.134	C ₅ H ₉ N	pentanenitriles*	PTR	0.049±0.025	0.037±0.017	0.0024±0.0088	0.016±0.008	0.019±0.009	0.013±0.008	0.021±0.011 ³	0.049±0.024	0.042±0.025
84.074	C ₄ H ₄ O ₂	*	CIMS	1.7±0.7	0.79±0.24	0.29±0.13	0.38±0.14	0.23±0.04	0.52±0.20	0.32±0.11 ³	0.61±0.20	1.3±0.6
84.074	C ₄ H ₄ O ₂	furanone *	ptr	0.54±0.25	0.37±0.16	0.0030±0.041	0.16±0.09	0.16±0.09	0.15±0.08		0.42±0.23	0.48±0.26

Molecular Weight	Compound	Compound Name	Instrument	SP Average	NP Average	Background	Average EF (g kg ⁻¹)	NP EF (g kg ⁻¹)	SP EF (g kg ⁻¹)	Literature EF (g kg ⁻¹)	NP ER	SP ER
84.118	C ₅ H ₈ O	cyclopentanone/isomers*	PTR	0.23±0.11	0.16±0.07	0.017±0.026	0.069±0.036	0.073±0.032	0.065±0.039	0.087±0.038 ³	0.19±0.09	0.21±0.12
84.162	C ₆ H ₁₂	hexene*	PTR	0.029±0.013	0.021±0.0065	0.0013±0.015	0.015±0.011	0.020±0.014	0.0098±0.0065	0.008±0.014 ³	0.052±0.037	0.031±0.019
84.162	C ₆ H ₁₂	c-2-hexene	AWAS	0.019±0.012	0.0079±0.0024	0.0031±0.0002	0.0020±0.0014	0.0021±0.0016	0.0020±0.0011	0.008±0.014 ³	0.0069±0.0044	0.0064±0.0055
84.162	C ₆ H ₁₂	cyclohexane	AWAS	0.022±0.0077	0.0089±0.0010	0.0051±0.0008	0.0022±0.0016	0.0019±0.0015	0.0026±0.0016	0.008±0.014 ³	0.0064±0.0053	0.0097±0.0058
86.09	C ₄ H ₆ O ₂	butanediol/isomers	ptr	0.57±0.23	0.39±0.14	0.089±0.077	0.13±0.09	0.13±0.09	0.13±0.09		0.33±0.23	0.41±0.26
86.134	C ₅ H ₁₀ O	pentanone	PTR	0.14±0.07	0.11±0.04	0.013±0.020	0.046±0.025	0.053±0.026	0.038±0.024	0.062±0.023 ³	0.0095±0.0046	0.0080±0.0049
86.178	C ₆ H ₁₄	n-hexane	AWAS	0.31±0.14	0.13±0.05	0.013±0.0012	0.049±0.020	0.053±0.019	0.044±0.021	0.050±0.036 ³	0.17±0.06	0.16±0.07
86.178	C ₆ H ₁₄	2,3-DMB	AWAS	0.017±0.0091	0.013±0.001	0.0048±0.0001	0.0031±0.0012	0.004±0.0012	0.0022±0.0013	0.050±0.036 ³	0.014±0.004	0.0066±0.0039
86.178	C ₆ H ₁₄	2,3-methylpentane	AWAS	0.090±0.047	0.026±0.004	0.011±0.0003	0.010±0.005	0.0089±0.0041	0.011±0.006	0.050±0.036 ³	0.032±0.011	0.039±0.021
88.062	C ₃ H ₄ O ₃	pyruvic acid	CIMS	4.4±2.4	3.4±1.0	2.3±0.3	0.72±0.71	0.56±0.54	0.89±0.85	0.012±0.005 ² 0.019±0.008 ³	0.022±0.022	- 0.0025±0.010
88.106	C ₄ H ₈ O ₂	methyl propanoate *	ptr	0.24±0.11	0.17±0.07	0.021±0.040	0.070±0.043	0.075±0.047	0.065±0.040		0.19±0.12	0.20±0.12
88.168	C ₄ H ₈ OS	oxathiane*	PTR	0.012±0.0049	0.0090±0.0030	0.00061±0.0073	0.0031±0.0024	0.0023±0.0021	0.0040±0.0026		0.0058±0.0053	0.012±0.008
90.125	C ₇ H ₆	*	PTR	0.026±0.014		0.0012±0.018	0.0074±0.0011		0.0074±0.0011			0.022±0.013
90.184	C ₄ H ₁₀ S	diethyl sulfide, butanethiol	PTR	0.31±0.13	0.22±0.10	0.036±0.012	0.077±0.015	0.083±0.014	0.071±0.015		0.20±0.04	0.21±0.05
92.141	C ₇ H ₈	toluene	PTR	0.62±0.30	0.48±0.21	0.034±0.037	0.26±0.07	0.26±0.04	0.26±0.09	0.35±0.11 ¹ 0.25±0.13 ² 0.42±0.16 ³	0.63±0.08	0.71±0.23
93.082	C ₂ H ₇ NO ₃	*	PTR	0.0071±0.0034		0.0012±0.0046	0.0025±0.0012		0.0025±0.0012			0.0070±0.0048
93.085	C ₅ H ₃ NO	furancarboxonitrile*	PTR	0.056±0.031	0.038±0.017	0.00022±0.0040	0.020±0.011	0.022±0.010	0.018±0.011	0.0026±0.010 ² 0.0088±0.037 ³	0.053±0.025	0.053±0.030
94.113	C ₆ H ₆ O	phenol*	PTR	0.42±0.22	0.27±0.13	0.0026±0.030	0.12±0.06	0.12±0.05	0.12±0.07	3.0 ¹ 0.57±0.36 ² 0.33±0.13 ³	0.28±0.11	0.35±0.20
94.157	C ₇ H ₁₀	cycloheptadiene*	PTR	0.080±0.035	0.061±0.028	0.005±0.020	0.021±0.011	0.023±0.011	0.020±0.012		0.053±0.025	0.056±0.033
94.19	C ₂ H ₆ S ₂	dimethyl disulfide*	PTR	0.012±0.0071		0.0012±0.012	0.0039±0.0022		0.0039±0.0022	0.0024±0.009 ²		0.011±0.006
95.077	C ₅ H ₃ O ₂	*	PTR	0.014±0.0085	0.0094±0.0043	0.0012±0.0070	0.0030±0.0021	0.0043±0.0028	0.0038±0.0012		0.0099±0.0063	0.011±0.007

Molecular Weight	Compound	Compound Name	Instrument	SP Average	NP Average	Background	Average EF (g kg ⁻¹)	NP EF (g kg ⁻¹)	SP EF (g kg ⁻¹)	Literature EF (g kg ⁻¹)	NP ER	SP ER
95.101	C ₅ H ₅ N O	pyridinol*	PTR	0.0066 ±0.0026	0.0045±0 .0026	- 0.00087± 0.0041	0.0022±0 .0015	0.0021±0 .0017	0.0023±0 .0012	0.0099±0.0 054 ²	0.0048 ±0.0041	0.0063±0.003 2
95.145	C ₆ H ₉ N	C2 pyrrole*	PTR	0.0068 ±0.0034		- 0.000091 ±0.0054	0.0021±0 .0012		0.0021±0 .0012			0.0060±0.003 3
96.085	C ₅ H ₄ O ₂	furfural*	PTR	2.0±1.0	1.3±0.6	- 0.0040±0 .029	0.65±0.3 1	0.67±0.2 6	0.64±0.3 6	0.61 ¹ 0.54±0.17 ² 0.53±0.21 ³	1.5±0.6	1.8±1.0
96.129	C ₆ H ₈ O	C2-furan*	PTR	0.32±0. 16	0.20±0.0 9	- 0.00016± 0.024	0.087±0. 044	0.086±0. 037	0.087±0. 050	0.20±0.10 ³	0.20±0. 09	0.24±0.14
96.173	C ₇ H ₁₂	cycloheptene*	PTR	0.042± 0.02	0.035±0. 013	0.0049±0 .017	0.022±0. 015	0.033±0. 020	0.011±0. 007		0.076± 0.047	0.031±0.020
97.073	C ₄ H ₃ N O ₂	*	PTR	0.010± 0.005	0.0093±0 .0026	0.0012±0 .0075	0.0030±0 .0021	0.0044±0 .0027	0.0036±0 .0012		0.0098 ±0.007 3	0.0096±0.007 1
97.161	C ₆ H ₁₁ N	hexanenitrile*	PTR	0.011± 0.0053	0.0077±0 .0041	0.00031± 0.0040	0.0040±0 .0026	0.0041±0 .0028	0.0040±0 .0023	0.0088±0.0 047 ³	0.0093 ±0.006 3	0.011±0.006
98.057	C ₄ H ₂ O ₃	maleic anhydride*	PTR	0.21±0. 08	0.16±0.0 5	0.011±0. 032	0.070±0. 036	0.072±0. 031	0.068±0. 040	0.14±0.07 ³	0.16±0. 07	0.18±0.11
98.101	C ₅ H ₆ O ₂	furan methanol/isomers*	PTR	0.28±0. 13	0.20±0.0 8	0.021±0. 047	0.058±0. 030	0.061±0. 025	0.054±0. 034	0.38±0.15 ² 0.090±0.04 3 ³	0.14±0. 06	0.15±0.09
98.145	C ₆ H ₁₀ O	methyl cyclopentanone/isomers*	PTR	0.052± 0.023	0.036±0. 015	0.0027±0 .015	0.015±0. 008	0.017±0. 009	0.013±0. 008	0.022±0.00 9 ² 0.034±0.01 5 ²	0.038± 0.019	0.035±0.020
100.117	C ₅ H ₈ O ₂	unsaturated C5 carboxylic acids	CIMS	0.20±0. 03	0.25±0.0 7	0.078±0. 043	0.072±0. 027	0.10±0.0 3	0.045±0. 021	0.11±0.04 ³	0.22±0. 07	0.13±0.06
100.117	C ₅ H ₈ O ₂	methyl methacrylate/isomers*	ptr	0.15±0. 06	0.12±0.0 4	0.017±0. 041	0.036±0. 023	0.035±0. 022	0.037±0. 024		0.078± 0.049	0.098±0.062
100.161	C ₆ H ₁₂ O	hexanal/hexanone*	PTR	0.022± 0.0077	0.018±0. 008	0.003±0. 010	0.0065±0 .0043	0.0074±0 .0049	0.0057±0 .0035	0.0046±0.0 029 ² 0.013±0.00 6 ³	0.016± 0.011	0.015±0.009
102.089	C ₄ H ₆ O ₃	C4 oxo-carboxylic acids	CIMS	4.7±1.2	3.8±0.7	2.3±0.2	0.74±0.3 7	0.57±0.3 0	0.92±0.4 3	0.044±0.02 0 ³	1.2±0.7	2.4±1.1
102.089	C ₄ H ₆ O ₃	acetic anhydride*	ptr	0.033± 0.016	0.022±0. 008	0.0020±0 .018	0.0075±0 .0046	0.0078±0 .0046	0.0072±0 .0045		0.017± 0.010	0.019±0.012
102.133	C ₅ H ₁₀ O ₂	valeric acid*	ptr	0.083± 0.042	0.057±0. 025	0.0037±0 .016	0.024±0. 014	0.027±0. 016	0.020±0. 012		0.059± 0.035	0.052±0.031
103.121	C ₄ H ₉ N O ₂	*	PTR	0.017± 0.0063	0.013±0. 005	0.0012±0 .0032	0.0030±0 .0020	0.0074±0 .0026	0.0064±0 .0011		0.016± 0.009	0.016±0.010
103.124	C ₇ H ₅ N	benzonitrile*	PTR	0.15±0. 08	0.11±0.0 5	0.00028± 0.0051	0.060±0. 029	0.065±0. 026	0.054±0. 031	0.021±0.00 4 ² 0.055±0.02 2 ³	0.14±0. 06	0.14±0.08
104.149	C ₅ H ₁₂ O ₂	pentanediol*	PTR	0.0073 ±0.0034	0.0052±0 .0016	- 0.00087± 0.0057	0.0029±0 .0025	0.0033±0 .0033	0.0024±0 .0013		0.0069 ±0.006 9	0.0060±0.003 2

Molecular Weight	Compound	Compound Name	Instrument	SP Average	NP Average	Background	Average EF (g kg ⁻¹)	NP EF (g kg ⁻¹)	SP EF (g kg ⁻¹)	Literature EF (g kg ⁻¹)	NP ER	SP ER
104.152	C ₈ H ₈	styrene*	PTR	0.053±0.027	0.041±0.020	0.000051±0.0092	0.039±0.021	0.056±0.026	0.022±0.013	0.088±0.056 ² 0.018±0.012 ³	0.12±0.06	0.058±0.033
106.121	C ₄ H ₁₀ O ₃	Diethylene glycol*	PTR	0.014±0.0035		0.0016±0.011	0.0036±0.0026		0.0036±0.0026			0.0088±0.0061
106.124	C ₇ H ₆ O	benzaldehyde*	PTR	0.10±0.05	0.079±0.037	0.011±0.015	0.036±0.019	0.042±0.018	0.030±0.019	0.095±0.053 ² 0.084±0.026 ³	0.087±0.038	0.077±0.047
106.168	C ₈ H ₁₀	C8 aromatic s	PTR	0.19±0.09	0.13±0.06	0.0082±0.020	0.075±0.012	0.082±0.012	0.068±0.013	0.21±0.08 ³	0.17±0.02	0.17±0.03
107.112	C ₆ H ₅ NO	pyridine aldehyde*	PTR	0.0035±0.0021		0.00051±0.0036	0.0015±0.0008		0.0015±0.0008			0.0038±0.0020
107.156	C ₇ H ₉ N	dimethyl pyridine/heptyl nitriles*	PTR	0.0048±0.0014		0.000012±0.0040	0.0018±0.001		0.0018±0.0010	0.0050±0.0033 ²		0.0043±0.0024
108.096	C ₆ H ₄ O ₂	benzoquinone*	PTR	0.093±0.043	0.061±0.023	0.0025±0.019	0.025±0.013	0.024±0.011	0.025±0.015	0.084±0.024 ² 0.077±0.020 ³	0.049±0.022	0.062±0.035
108.14	C ₇ H ₈ O	methyl phenol/anisol/cresol*	PTR	0.13±0.07	0.083±0.043	0.00068±0.0094	0.040±0.020	0.040±0.017	0.040±0.023	0.41±0.17 ² 0.23±0.11 ³	0.083±0.035	0.099±0.057
108.184	C ₈ H ₁₂	cyclooctadiene*	PTR	0.036±0.016	0.029±0.013	0.0038±0.017	0.015±0.0089	0.017±0.010	0.013±0.008		0.034±0.020	0.032±0.020
109.104	C ₆ H ₅ O ₂	*	PTR	0.019±0.0095	0.013±0.005	0.0012±0.0058	0.0030±0.0020	0.0055±0.0026	0.0055±0.0011		0.011±0.007	0.014±0.008
110.112	C ₆ H ₆ O ₂	benzene diol/methyl furfural*	PTR	0.34±0.17	0.22±0.11	0.00028±0.016	0.11±0.05	0.11±0.04	0.11±0.06	0.68±0.29 ² 0.25±0.12 ³	0.21±0.08	0.27±0.15
110.156	C ₇ H ₁₀ O	norcamphor/C3 furan*	PTR	0.096±0.049	0.062±0.030	0.0014±0.016	0.032±0.018	0.030±0.015	0.034±0.020	0.079±0.032 ² 0.046±0.024 ³	0.059±0.029	0.083±0.048
110.2	C ₈ H ₁₄	cyclooctene*	PTR	0.017±0.0083	0.012±0.004	0.0011±0.0085	0.0088±0.0071	0.012±0.009	0.0053±0.0034		0.024±0.019	0.014±0.009
111.1	C ₅ H ₅ NO ₂	dihydroxypyridine/methyl maleimide*	PTR	0.0074±0.0031	0.0062±0.0021	0.00025±0.0040	0.0026±0.0018	0.0031±0.0022	0.0022±0.0015	0.024±0.008 ³	0.0061±0.0043	0.0051±0.0034
112.084	C ₅ H ₄ O ₃	furoic acid/hydroxy furfural*	PTR	0.18±0.06	0.14±0.04	0.071±0.058	0.041±0.036	0.044±0.038	0.038±0.035	0.12±0.03 ³	0.087±0.074	0.089±0.080
112.128	C ₆ H ₈ O ₂	cyclohexanedione*	PTR	0.057±0.027	0.044±0.021	0.0017±0.017	0.014±0.0072	0.014±0.007	0.014±0.007	0.12±0.06 ³	0.028±0.014	0.033±0.018
112.172	C ₇ H ₁₂ O	ethylcycloheptanone*	PTR	0.019±0.0074		0.0019±0.0087	0.0070±0.0045		0.0070±0.0045	0.014±0.007 ³		0.016±0.010
114.144	C ₆ H ₁₀ O ₂	sum of cyclic saturated	CIMS		0.19±0.07	0.074±0.086	0.12±0.04	0.12±0.044		0.039±0.017 ³	0.11±0.04	

Molecular Weight	Compound	Compound Name	Instrument	SP Average	NP Average	Background	Average EF (g kg ⁻¹)	NP EF (g kg ⁻¹)	SP EF (g kg ⁻¹)	Literature EF (g kg ⁻¹)	NP ER	SP ER
		and n-unsaturated C5 carboxylic acids										
114.144	C ₆ H ₁₀ O ₂	Caprolactone/c6 esters/c6 diketone isomers*	ptr	0.033±0.011	0.029±0.011	0.0065±0.019	0.0068±0.0048	0.0082±0.0057	0.0053±0.0037		0.016±0.011	0.013±0.009
114.188	C ₇ H ₁₄ O	heptanone/heptanal/isomers*	PTR	0.010±0.006		0.00080±0.0078	0.0039±0.0025		0.0039±0.0025	0.0072±0.025 ³		0.0090±0.0057
116.116	C ₅ H ₈ O ₃	C5 oxo-carboxylic acids	CIMS	0.18±0.04	0.15±0.03	0.10±0.01	0.031±0.017	0.026±0.013	0.037±0.020	0.034±0.019 ³	0.050±0.025	0.083±0.045
116.16	C ₆ H ₁₂ O ₂	butyl acetate/c6 esters*	ptr	0.023±0.010	0.019±0.009	0.00086±0.0081	0.0073±0.0045	0.0094±0.0054	0.0052±0.0033		0.018±0.010	0.012±0.007
116.222	C ₆ H ₁₂ S	cyclohexanethiol*	PTR	0.0094±0.0037	0.0073±0.0017	0.00048±0.0064	0.0032±0.0028	0.0040±0.0037	0.0025±0.0016		0.0075±0.0069	0.0056±0.0036
118.088	C ₄ H ₆ O ₄	succinic acid*	PTR	0.0026±0.0011	0.0025±0.0011	0.0012±0.0031	0.0017±0.0007	0.0026±0.0009	0.00081±0.00034		0.0048±0.0016	0.0018±0.0007
118.135	C ₈ H ₆ O	benzofuran*	PTR	0.039±0.022	0.025±0.016	0.0018±0.0060	0.017±0.009	0.018±0.010	0.017±0.009	0.037±0.020 ² 0.041±0.015 ³	0.034±0.018	0.038±0.021
118.179	C ₉ H ₁₀	methylstyrene/propenyl benzenes*	PTR	0.022±0.010	0.016±0.007	0.0021±0.0079	0.018±0.012	0.024±0.016	0.011±0.007	0.037±0.020 ³	0.046±0.030	0.025±0.015
119.167	C ₈ H ₉ N	*	PTR	0.0039±0.0022		0.0012±0.0017	0.0016±0.0015		0.0016±0.0015			0.0035±0.0029
120.151	C ₈ H ₈ O	methylbenzaldehyde/tolualdehyde*	PTR	0.064±0.031	0.039±0.019	0.0026±0.013	0.025±0.014	0.024±0.012	0.026±0.016	0.13±0.08 ² 0.082±0.030 ³	0.044±0.022	0.058±0.034
120.195	C ₉ H ₁₂	trimethylbenzene/C9 aromatic s*	PTR	0.070±0.031	0.056±0.022	0.0078±0.017	0.052±0.029	0.075±0.037	0.029±0.018	0.051 ¹ 0.051±0.022 ² 0.069±0.031 ³	0.14±0.07	0.064±0.039
122.123	C ₇ H ₆ O ₂	benzoic acid/hydroxybenzaldehyde*	PTR	0.068±0.025	0.053±0.016	0.0092±0.018	0.020±0.011	0.021±0.010	0.019±0.012	0.079±0.035 ² 0.065±0.023 ³	0.037±0.018	0.040±0.026
122.167	C ₈ H ₁₀ O	xyleneol/C2 phenol/methylanisole*	PTR	0.033±0.019	0.025±0.014	0.00069±0.0081	0.015±0.0082	0.016±0.009	0.013±0.008	0.11±0.04 ² 0.10±0.06 ³	0.029±0.015	0.029±0.017
122.211	C ₉ H ₁₄	cyclohexylallene*	PTR	0.019±0.0074	0.014±0.005	0.0027±0.0083	0.0076±0.0051	0.0083±0.0059	0.0068±0.0043		0.015±0.011	0.015±0.009

Molecular Weight	Compound	Compound Name	Instrument	SP Average	NP Average	Background	Average EF (g kg ⁻¹)	NP EF (g kg ⁻¹)	SP EF (g kg ⁻¹)	Literature EF (g kg ⁻¹)	NP ER	SP ER
124.095	C ₆ H ₄ O ₃	hydroxy benzoquinone*	PTR	0.014±0.008	0.011±0.005	- 0.00040±0.0051	0.0032±0.0022	0.0029±0.0021	0.0035±0.0023	0.073±0.018 ² 0.045±0.026 ³	0.0051±0.0037	0.0075±0.0047
124.139	C ₇ H ₈ O ₂	guaiacol*	PTR	0.15±0.09	0.093±0.054	- 0.0013±0.0073	0.052±0.026	0.051±0.020	0.053±0.031	0.37±0.12 ² 0.27±0.17 ³	0.091±0.037	0.12±0.07
124.183	C ₈ H ₁₂ O	acetylcyclohexene*	PTR	0.018±0.009	0.013±0.005	0.00032±0.0056	0.0078±0.0045	0.0087±0.0051	0.0068±0.0039		0.015±0.009	0.015±0.008
126.111	C ₆ H ₆ O ₃	hydroxy methylfurfural*	PTR	0.033±0.014	0.025±0.010	0.00066±0.0087	0.0096±0.0053	0.0094±0.0049	0.0098±0.0056	0.27±0.10 ² 0.064±0.026 ³	0.016±0.009	0.021±0.012
126.155	C ₇ H ₁₀ O ₂	unsaturated C6 cyclic carboxylic acid*	CIMS	0.052±0.005	0.043±0.011	0.0088±0.0096	0.012±0.005	0.015±0.0057	0.0087±0.0044		0.026±0.010	0.019±0.009
126.155	C ₇ H ₁₀ O ₂	cyclohexene carboxylic acid*	ptr	0.015±0.006	0.013±0.003	0.0026±0.0091	0.0064±0.0045	0.0080±0.0056	0.0048±0.0032		0.014±0.010	0.010±0.007
126.199	C ₈ H ₁₄ O	octenone*	PTR	0.064±0.0029		0.00012±0.0051	0.0027±0.0016		0.0027±0.0016			0.0057±0.0033
126.217	C ₇ H ₁₀ S	trimethyl thiophene*	PTR	0.013±0.004	0.011±0.005	0.00044±0.0084	0.011±0.011	0.016±0.015	0.0054±0.0030		0.028±0.026	0.012±0.007
128.127	C ₆ H ₈ O ₃	di hydroxy methyl furan*	PTR	0.024±0.013	0.020±0.007	- 0.0017±0.0087	0.0044±0.0026	0.0059±0.0032	0.0029±0.0017		0.010±0.006	0.0063±0.0036
128.171	C ₇ H ₁₂ O ₂	cyclohexanoic acid*	ptr	0.014±0.004		0.0028±0.011	0.0050±0.0034		0.0050±0.0034			0.010±0.007
128.174	C ₁₀ H ₈	naphthalene*	PTR	0.033±0.013	0.025±0.011	0.00075±0.0086	0.017±0.011	0.018±0.012	0.015±0.009	0.078±0.056 ²	0.031±0.021	0.031±0.018
128.215	C ₈ H ₁₆ O	octanone*	PTR	0.0072±0.0035		0.0014±0.0055	0.0028±0.0020		0.0028±0.0020			0.006±0.0042
130.187	C ₇ H ₁₄ O ₂	amyl acetate*	ptr	0.0074±0.0046	0.0056±0.0021	0.00025±0.0046	0.0031±0.0019	0.0034±0.0020	0.0028±0.0018		0.0056±0.0033	0.0058±0.0036
132.159	C ₆ H ₁₂ O ₃	C6 hydroxy-carboxylic acids	CIMS	0.0090±0.0006	0.010±0.002	0.0062±0.0014	0.0017±0.0008	0.0027±0.0011	0.00075±0.00034		0.0045±0.0018	0.0016±0.0010
132.162	C ₉ H ₈ O	methyl benzo furans*	PTR	0.023±0.012	0.016±0.0085	0.00018±0.0050	0.010±0.006	0.010±0.006	0.011±0.006	0.055±0.030 ² 0.046±0.021 ³	0.017±0.009	0.021±0.012
132.206	C ₁₀ H ₁₂	ethyl styrene/methyl propenyl benzene*	PTR	0.019±0.009	0.014±0.007	0.0013±0.0063	0.0083±0.0050	0.0083±0.0050	0.0083±0.0050	0.041±0.019 ² 0.040±0.026 ³	0.014±0.008	0.017±0.010
134.134	C ₈ H ₆ O ₂	phthalic acid*	PTR	0.0074±0.0028	0.0071±0.0025	0.0011±0.0051	0.0039±0.0029	0.0044±0.0035	0.0033±0.0022		0.0071±0.0057	0.0065±0.0042

Molecular Weight	Compound	Compound Name	Instrument	SP Average	NP Average	Background	Average EF (g kg ⁻¹)	NP EF (g kg ⁻¹)	SP EF (g kg ⁻¹)	Literature EF (g kg ⁻¹)	NP ER	SP ER
134.178	C ₉ H ₁₀ O	methylacetophenone*	PTR	0.012±0.007	0.0085±0.0041	- 0.00032±0.004	0.0059±0.0035	0.0062±0.0036	0.0056±0.0033	0.053±0.031 ² 0.045±0.019 ³	0.010±0.006	0.011±0.006
134.222	C ₁₀ H ₁₄	C10 Aromatic s*	PTR	0.030±0.013	0.024±0.010	0.0024±0.0095	0.024±0.014	0.035±0.019	0.013±0.008	0.040±0.021 ³	0.058±0.031	0.026±0.016
136.15	C ₈ H ₈ O ₂	methylbenzoic acid*	PTR	0.027±0.015	0.018±0.009	0.00058±0.007	0.013±0.007	0.014±0.0069	0.012±0.007	0.081±0.030 ² 0.066±0.029 ³	0.022±0.011	0.023±0.014
136.238	C ₁₀ H ₁₆	monoterpenes*	PTR	0.68±0.28	0.65±0.31	0.057±0.055	0.41±0.19	0.49±0.20	0.33±0.17	0.41±0.06 ¹ 0.87±0.72 ² 0.21±0.15 ³	0.80±0.32	0.65±0.38
138.122	C ₇ H ₆ O ₃	hydroxybenzoic acid*	PTR	0.0080±0.0030	0.0076±0.0033	- 0.000093±0.0050	0.0026±0.0017	0.0039±0.0023	0.0014±0.0008		0.0061±0.0036	0.0028±0.0015
138.166	C ₈ H ₁₀ O ₂	creosol/methylguaiacol*	PTR	0.016±0.0093	0.012±0.006	0.0000038±0.0069	0.0073±0.0046	0.0077±0.0049	0.0069±0.0042	0.14±0.11 ³	0.012±0.008	0.013±0.008
138.21	C ₉ H ₁₄ O	isophorone*	PTR	0.027±0.0075	0.025±0.009	0.0079±0.01	0.0092±0.0064	0.0086±0.0053	0.0098±0.0074		0.014±0.009	0.019±0.014
146.189	C ₁₀ H ₁₀ O	dimethylbenzofuran/ethylbenzofuran*	PTR	0.0098±0.0044	0.0072±0.0033	- 0.00041±0.0037	0.0048±0.0029	0.0052±0.0034	0.0045±0.0024	0.043±0.018 ² 0.051±0.028 ³	0.0078±0.0051	0.0083±0.0044
146.233	C ₁₁ H ₁₄	*	PTR	0.0064±0.0035		0.0012±0.0041	0.0034±0.0013		0.0034±0.0013			0.0061±0.0044
148.161	C ₉ H ₈ O ₂	cinnamic acid*	PTR	0.0040±0.0033		- 0.00094±0.0048	0.0021±0.0013		0.0021±0.0013			0.0037±0.0022
148.205	C ₁₀ H ₁₂ O	benzylacetone/estragole*	PTR	0.0047±0.0021	0.0043±0.0019	0.00045±0.0030	0.0023±0.0016	0.0022±0.0017	0.0024±0.0015	0.027±0.012 ² 0.025±0.015 ³	0.0033±0.0026	0.0044±0.0027
148.249	C ₁₁ H ₁₆	C11 aromatic s/pentamethylbenzene*	PTR	0.0074±0.0032	0.0054±0.0027	0.00054±0.0047	0.0041±0.0028	0.0043±0.0032	0.0038±0.0023	0.014±0.008 ² 0.014±0.007 ³	0.0064±0.0048	0.0069±0.0041
150.177	C ₉ H ₁₀ O ₂	ethylbenzoate/vinylguaiacol*	PTR	0.0059±0.0029	0.0044±0.0020	0.00039±0.0034	0.0028±0.0020	0.0029±0.0023	0.0028±0.0017	0.14±0.08 ² 0.036±0.025 ³	0.0043±0.0034	0.0049±0.0030
150.221	C ₁₀ H ₁₄ O	carvone*	PTR	0.0040±0.0022	0.0039±0.0017	0.00055±0.0028	0.0021±0.0016	0.0027±0.0021	0.0015±0.0009		0.0039±0.0030	0.0027±0.0016
152.237	C ₁₀ H ₁₆ O	camphor/isomers*	PTR	0.022±0.0074	0.023±0.010	0.0063±0.0086	0.011±0.007	0.013±0.008	0.0087±0.0066	0.027±0.017 ² 0.025±0.014 ³	0.020±0.011	0.015±0.011
154.209	C ₉ H ₁₄ O ₂	norbornaneacetic acid*	PTR	0.0036±0.0015		- 0.00050±0.0041	0.0022±0.0012		0.0022±0.0012			0.0038±0.0020
154.212	C ₁₂ H ₁₀	acenaphthene*	PTR	0.0054±0.0020	0.0040±0.0015	- 0.00026±0.0031	0.0029±0.0022	0.0033±0.0028	0.0025±0.0013		0.0046±0.0040	0.0042±0.0023

Molecular Weight	Compound	Compound Name	Instrument	SP Average	NP Average	Background	Average EF (g kg ⁻¹)	NP EF (g kg ⁻¹)	SP EF (g kg ⁻¹)	Literature EF (g kg ⁻¹)	NP ER	SP ER
154.253	C ₁₀ H ₁₈ O	terpine-4-ol/cineole/isomers*	PTR	0.0024 ±0.0009	0.0020±0.00068	- 0.00044±0.0022	0.0018±0.0014	0.0019±0.0018	0.0017±0.0009	0.0056±0.0021 ² 0.0027±0.0017 ³	0.0029 ±0.0028	0.0028±0.0015
204.357	C ₁₅ H ₂₄	sesquiterpenes*	PTR	0.0027 ±0.0011		0.00030±0.0021	0.0017±0.0011		0.0017±0.0011	0.15±0.07 ² 0.029±0.028 ³		0.0022±0.0014
239±61	C ₁₁ to C ₂₅	I/SVOCs - CH	cartridge			5.2	1.4±0.037 to 2.4±0.063					
255±61	C ₁₁ to C ₂₅	I/SVOCs - CHO ₁	cartridge			4.6	0.81±0.078 to 0.81±0.079					
271±61	C ₁₁ to C ₂₅	I/SVOCs - CHS ₁	cartridge			0.2	0.21±0.033 to 0.22±0.060					

1529